Physical Influences on Phytoplankton Ecology: Models and Observations.

by

Sophie Anne Clayton

Submitted in partial fulfillment of the requirements for the degree of

Doctor of Philosophy

at the

MASSACHUSETTS INSTITUTE OF TECHNOLOGY
and the
WOODS HOLE OCEANOGRAPHIC INSTITUTION

June 2013

Signature of Author .....
Joint Program in Oceanography – Massachusetts Institute of Technology / Woods Hole Oceanographic Institution
April 5th 2013

Certified by ... .
Michael J. Follows
Senior Research Scientist
Massachusetts Institute of Technology
Thesis Supervisor

Accepted by ....
Glenn R. Flierl
Professor of Oceanography
Massachusetts Institute of Technology
Chair, Joint Committee for Physical Oceanography

Physical Influences on Phytoplankton Ecology: Models and Observations.

by

Sophie Anne Clayton

Submitted to the Joint Program in Oceanography,
Massachusetts Institute of Technology and the Woods Hole Oceanographic Institution
on April 5th 2013, in partial fulfillment of the
requirements for the degree of
Doctor of Philosophy

Abstract

The physical environment in the oceans dictates not only how phytoplankton cells are dispersed and their populations intermingled, but also mediates the supply of nutrients to the surface mixed layer. In this thesis I explore both of these aspects of the interaction between phytoplankton ecology and ocean physics, and have approached this topic in two distinct but complementary ways, working with a global ocean ecosystem model, and collecting data at sea.

In the first half of the thesis, I examine the role of mesoscale physical features in shaping phytoplankton community structure and influencing rates of primary production. I compare the output of a complex marine ecosystem model coupled to coarse resolution and eddy-permitting physical models. Explicitly resolving eddies resulted in marked regional variations in primary production, zooplankton and phytoplankton biomass. The same phytoplankton phenotypes persisted in both cases, and were dominant in the same regions. Global phytoplankton diversity was unchanged. However, levels of local phytoplankton diversity were markedly different, with a large increase in local diversity in the higher resolution model. Increased diversity could be attributed to a combination of enhanced dispersal, environmental variability and nutrient supply in the higher resolution model. Diversity "hotspots" associated with western boundary currents and coastal upwelling zones are sustained through a combination of all of these factors.

In the second half of the thesis I describe the results of a fine scale ecological and biogeochemical survey of the Kuroshio Extension Front. I found fine scale patterns in physical, chemical and biological properties that can be linked back to both the large scale horizontal and smaller scale vertical physical dynamics of the study region. A targeted genomic analysis of samples focused on the ecology of the picoeukaryote *Ostreococcus* clade distributions strongly supports the model derived hypotheses about the mechanisms supporting diversity hotspots. Strikingly, two distinct clades of *Ostreococcus* co-occur in

more than half of the samples. A "hotspot" of *Ostreococcus* diversity appears to be supported by a confluence of water masses containing either clade, as well as a local nutrient supply at the front and the mesoscale variability of the region.

Thesis Supervisor: Michael J. Follows
Title: Senior Research Scientist
Massachusetts Institute of Technology

Acknowledgments

First and foremost, I thank Mick Follows, my advisor. Mick has been incredibly supportive and has allowed me to approach my research interests with a wide range of methods. He has a great knack for identifying the essence of a problem.

I would also like to thank my thesis committee. Amala Mahadevan, Heidi Sosik, Raffaele Ferrari and Scott Gallagher who provided useful comments and guidance throughout the process. Glen Gawarkiewicz kindly agreed to serve as the Chair of my thesis defense.

I have been lucky to collaborate with lots of great people while conducting my thesis research. Stephanie Dutkiewicz has been generous with her time and always willing to discuss a new idea. I am eternally grateful to Oliver Jahn for all of his help with dealing with computing challenges. Thanks also to Patrick Heimbach and Chris Hill for their assistance and helpful discussions about ECCO-GODAE and ECCO2. I am particularly grateful to Takeyoshi Nagai and Hidekatsu Yamazaki for inviting me to join their 2009 cruise to the Kuroshio Extension and assisting me with so many aspects of the logistics of shipping equipment and samples between the USA and Japan. Without all of their help I would have been lost (quite literally!). I am also incredibly grateful to Alexandra Worden for being interested in the potential of my data and to Yun-Chi Lin for spending part of her summer performing the qPCR analysis on my samples.

Special thanks also go to Penny Chisholm for graciously allowing me the use of her Cytopeia Influx flow cytometer, and Ed DeLong for donating space in one of his -80^{o}C freezers to accomodate my samples from the Kuroshio. Rex Malmstrom and Anne Thompson both helped to teach me how to use and to troubleshoot inevitable problems with the Influx. Rebecca Case gave me invaluable advice on how to plan for a cruise ("don't forget to bring Sharpies!").

Finally thanks to Mike for putting up with me and the inevitable ups and downs of the PhD process.

Financial support. I gratefully acknowledge the financial support from the following sources: MIT Presidential Fellowship, Gordon and Betty Moore Foundation Marine Microbiology Initiative, NASA and NSF. Small grants for travel and equipment from the PAOC Houghton Fund, EAPS Student Research Fund and MISTI Hayashi Fund allowed me to pursue my research collaboration with Prof Takeyoshi Nagai at the Tokyo University of Marine Science and Technology.

Abbreviated Contents

Contents

List of Figures

Chapter 1

Introduction

1.1 Overview: Physical Transport and Phytoplankton

Phytoplankton play an important role in the cycling of many climatically active elements such as carbon, sulphur and nitrogen. Marine production and export of organic matter by phytoplankton ultimately reduces the atmospheric carbon dioxide concentration to about half what it would be were the oceans dead [Falkowski, 1994]. As a group, phytoplankton account for roughly half of the primary production on Earth [Field et al., 1998], forming the base of the marine food chain, fuelling organisms in the higher trophic levels which humans exploit for food. It is clear that this group of organisms plays a fundamental role not only in the Earth system, but also in providing ecosystem services that we rely on. However, the phytoplankton are a highly diverse group of organisms spanning several orders of magnitude in size, exhibiting a wide range of morphologies and highly diverse biogeochemical functions. Hence the phytoplankton community structure is as important to global biogeochemical cycles and the climate system as is total phytoplankton biomass and production.

Physical processes determine the structure of the phytoplankton community directly by mediating the rate of nutrient supply and levels of turbulence which modulate the light environment. The oceans can be readily split into biogeochemical provinces distinguished by

different physical dynamics and associated community structures [Margalef, 1978, Cullen et al., 2002, Ducklow, 2003]. However, the fluid environment of the oceans, in constant motion, transports and disperses phytoplankton over entire basins and potentially mixes communities from different provinces. Conversely, dynamical barriers may separate disparate phytoplankton communities. Thus, a greater understanding of how the physical dynamics of the oceans shape the phytoplankton community structure is important for questions about global biogeochemical cycles and climate.

The purpose of this thesis is to explore how the physical dynamics of the oceans influence phytoplankton community structure. I explore both its influence on bottom-up processes (e.g. nutrient supply) and the mixing and dispersal of communities and individual species. To this end, I use a combination of in situ data and ecological models described in more detail in the following chapters. I analyze the output of complex global ecosystem models and develop metrics to explicitly address the role of dispersal in shaping the modelled phytoplankton community. I also collected data on dissolved nutrients and phytoplankton community structure during a cruise in Kuroshio Extension Front region. I developed simple box models to explore both the global model output and the in situ data. I have attempted to focus on those processes directly related to the physical circulation, but where necessary I have also touched on top-down controls on the community. Each chapter is written in such a way that it can be read independently of the rest, but there are strong interconnections between the studies that I highlight in the text.

In this chapter, I review what is known about the linkages between phytoplankton community structure and physical dynamics, focussing particularly on the role of the mesoscale and oceanic fronts in modifying the resource environment and mixing, transporting or creating transport barriers between phytoplankton communities. Finally, I outline the main questions and goals of each of the following chapters.

1.2 Ocean Dynamics and Phytoplankton Community Structure

Phytoplankton biomass and primary production in the oceans vary over orders of magnitude from region to region. The global distribution of chlorophyll in the Northern spring observed from space is shown in figure 1-1, illustrating the spring bloom in the North Atlantic and North Pacific. There is a clear separation between regions of higher surface chlorophyll in the subpolar gyres and the equatorial upwelling, and much lower surface chlorophyll in the subtropics. These large scale patterns in phytoplankton biomass are principally driven by corresponding large scale patterns of nutrient supply, which are in turn the result of wind-driven Ekman up/downwelling [Williams and Follows, 2011]. These large scale shifts in biomass and production are also reflected in changes to the phytoplankton community. The subtropical gyres are typically dominated by smaller phytoplankton species [Marañòn et al., 2000], and the subpolar gyre, supports seasonal blooms of large phytoplankton including *Phaeocystis* colonies and diatoms [Li et al., 1993, Tarran et al., 2001].

Although globally significant, biological activity in the oceans is organized on much smaller time and space scales. Phytoplankton cells have a doubling rate on the order of a day, and phytoplankton blooms may develop over the course of a few weeks. Patches of phytoplankton range from several metres to a few kilometers, and as such are much much smaller than basin scales. In figure 1-2 I reproduce a figure first published in Dickey [1991] which illustrates the characteristic time and space scales associated with different physical and biological processes. Phytoplankton growth timescales interact with ocean physics most closely at the mesoscale and submesoscale, ranging from 10s of metres to 10s of kilometres and time scales ranging from several days to a month. The snapshot of chlorophyll concentrations in the Gulf Stream region shown in figure 1-3 illustrates this quite clearly. Patterns in chlorophyll occur on fine spatial scales formed by the action of eddies (mesoscale, 10-100km) and fronts and filaments (submesoscale, 1-10km) which

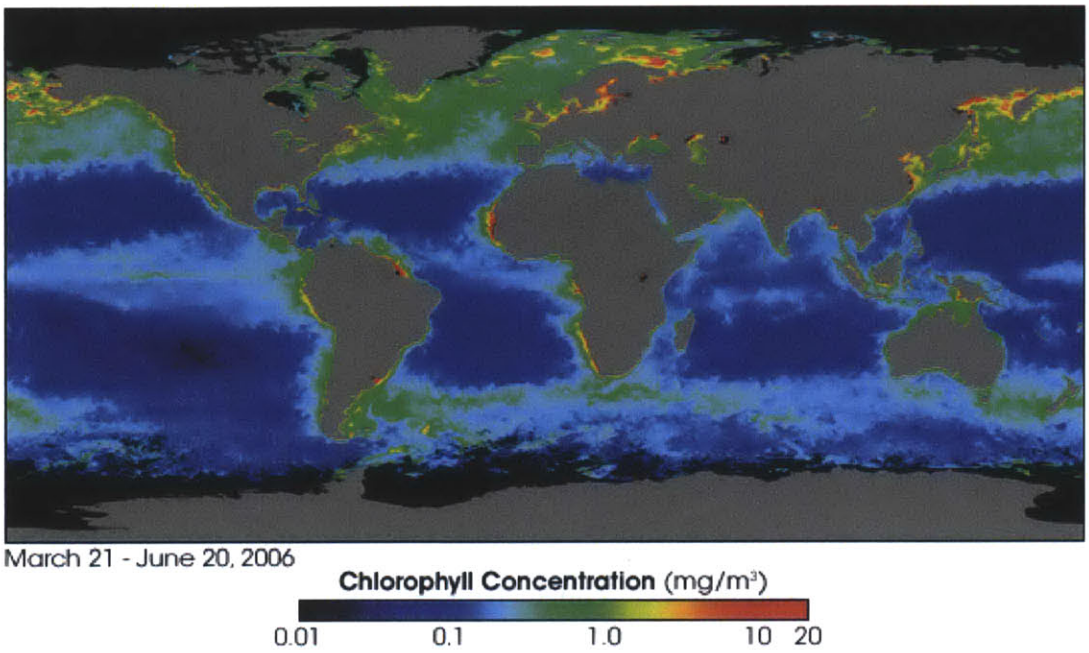

Figure 1-1: Global mean distribution of chlorophyll (March 21 to June 20, 2006), NASA.

are important and ubiquitous dynamical features in the ocean [Klein and Lapeyre, 2009]. Follows and Marshall [1994] estimated that the small-scale vertical circulations at fronts could be an important mechanism for fluid exchange between the mixed layer and the thermocline, and that an active front 1000s km long could drive a large scale subduction rate comparable to that of the mean gyre-scale circulation. In a modeling study, [Lapeyre and Klein, 2006] found that, over the whole domain, the tracer flux associated with small-scale filaments was as significant as that associated with mesoscale eddies. Similarly, Lévy et al. [2001] found that $1/3$ of the large scale new production in their model was due to nutrient injection by small-scale physical processes. So, if the fine scale circulation in eddies and frontal regions is indeed an important basin-scale driver of exchanges of properties between the thermocline and the mixed layer, then it is important to understand how this in turn affects the primary production and the phytoplankton community structure in different regions of the ocean.

Discussion of interactions between the physical circulation and phytoplankton com-

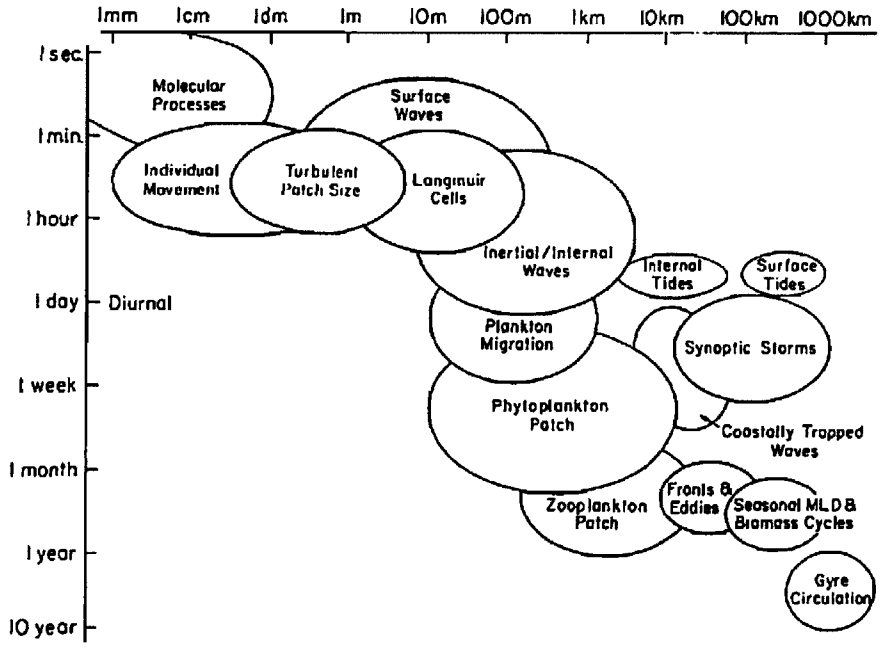

Figure 1-2: Time and space scales of physical and biological processes in the oceans, taken from Dickey [1991]. ©American Geophysical Union , 1991.

munities and their activity can be broadly split into the following themes: vertical motions which affect nutrient supply and light levels, dynamical niches delimited by physical fronts, lateral transport and dispersal. Clearly there must be a large amount of overlap and interaction between processes driven by vertical and lateral motions, acting over a range of time and space scales [Sournia, 1994]. Here I discuss each of these mechanisms in turn.

1.2.1 Vertical Motions

Vertical motions have a profound effect on both the supply of dissolved inorganic nutrients into the surface mixed layer, and on the light levels experienced by phytoplankton. The most vigorous vertical motions in the ocean are associated with mesoscale and submesoscale features. Mesoscale eddies displace isopycnal surfaces as they pass through a region, either pulling up or pushing down the nutricline bringing nutrients into the euphotic

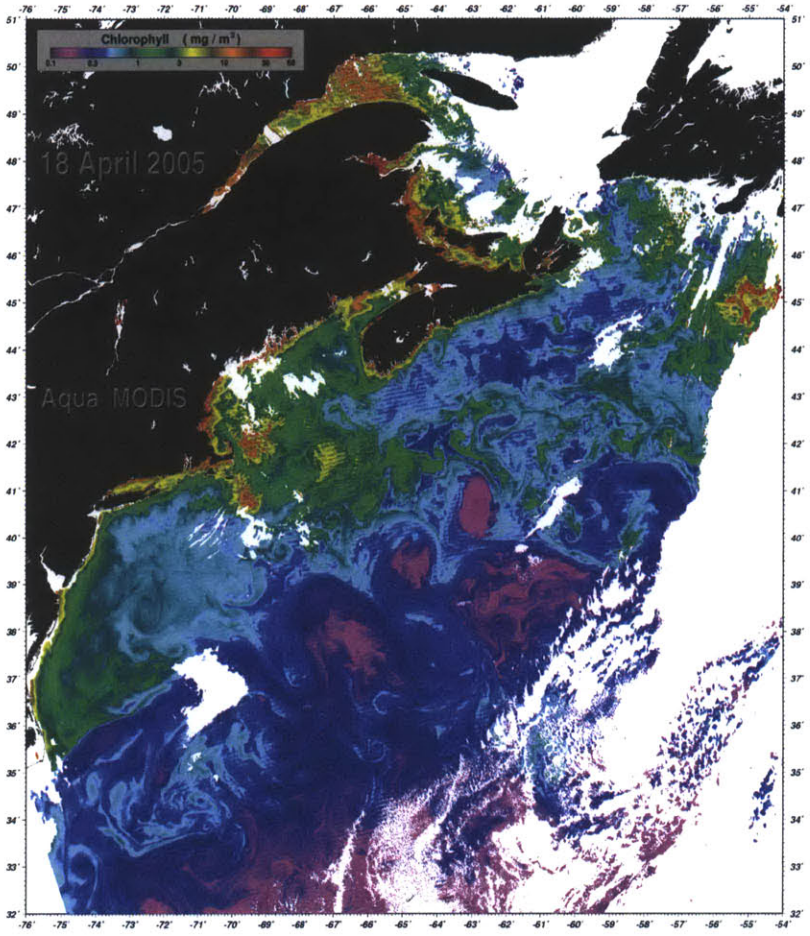

Figure 1-3: Remotely sensed chlorophyll distribution in the Gulf Stream region on 18 April 2005, NASA.

layer adiabatically [Falkowski et al., 1991, McGillicuddy et al., 1999]. Submesoscale processes, associated with fronts and filaments formed between eddies, can drive even more intense vertical circulations with velocities up to O(100 m d^{-1}) [Lévy et al., 2001, Thomas et al., 2008]. Although these are transient features which drive both upward and downward velocities, because production by phytoplankton at the surface represents a sink for upwelled nutrients, mesoscale and submesoscale vertical motions result in a net supply of nutrients to the surface and new production. In the subtropics, where the supply of inorganic nutrients limits primary production, there has been considerable interest in understanding

the role episodic inputs of nutrients by eddies [Falkowski et al., 1991, Oschlies and Garçon, 1998, McGillicuddy et al., 1999, Siegel et al., 1999, Mahadevan and Archer, 2000], submesoscale features such as filaments [Spall and Richards, 2000, Lévy et al., 2001] and Rossby waves [Sakamoto, 2004] in stimulating primary production. In situ observational studies of oceanic eddies have shown increased rates of primary production and phytoplankton biomass [Falkowski et al., 1991, McGillicuddy et al., 2007], and in some cases increased export [Benitez-Nelson et al., 2007] compared to the surrounding waters. Basin-scale modeling studies [Oschlies and Garçon, 1998, McGillicuddy et al., 2003] as well as more idealised models [Flierl and Davis, 1993, Lévy et al., 1998, Martin et al., 2002] have shown that incorporating mesoscale dynamics can result in large increases in integrated primary production in oligotrophic regions [Oschlies and Garçon, 1998, McGillicuddy et al., 2003]. Modeling studies have shown that submesoscale dynamics can drive large increases in primary production [Spall and Richards, 2000, Lévy et al., 2001]. However, the vast majority of these studies have focussed on how nutrient fluxes, phytoplankton biomass and rates of primary production are modified by these fine scale dynamics, and have not incorporated any ecological dimension.

In the subpolar gyres, light is most commonly the limiting factor for phytoplankton growth. Studies have shown that both mesoscale McGillicuddy et al. [2003] and submesoscale dynamics Mahadevan et al. [2012] can drive restratification of the mixed layer. This mechanism has been shown to be a crucial factor in the inititation of the spring bloom in the North Atlantic [Mahadevan et al., 2012]. Frontal dynamics may also play a critical role in controlling the magnitude and variability in the light levels experienced by phytoplankton. Strass et al. [2002] showed in data collected at the Antarctic Polar Front that mesoscale frontal dynamics which increase stratification created a favourable light environment which sustained higher chlorophyll abundances than the surrounding regions.

The magnitude and rate of supply of nutrients, as well as mixing, can play a role in determining the phytoplankton community structure [Margalef, 1968]. Tozzi et al. [2004] found with a simple box model that a more intermittent nutrient supply could result in di-

atoms outcompeting coccolithophores, and vice versa. Similarly, Dutkiewicz et al. [2009] showed in a diverse global biogeochemical model that the seasonal dynamics of the higher latitudes favoured large, r-adapted phytoplankton phenotypes over the small K-adapted types. On smaller scales, observations from the Pacific subtropical gyre have shown that eddies stimulate transient blooms of opportunistic diatoms [Benitez-Nelson et al., 2007, Brown et al., 2008] and shifts in community structure [Dickey et al., 2008], as well as a community response towards more opportunist phytoplankton species with the passage of a Rossby wave [Sakamoto, 2004]. In the Kuroshio Extension Front, Yamamoto et al. [1988] found that large coastal diatoms with higher growth rates, were able to outcompete smaller oceanic phytoplankton at the core of the front where nutrient inputs where highest. However, there are few studies that have collected phytoplankton community structure data as well as physical data at high enough resolution across mesoscale or submesoscale features to clearly interpret relationships between the physical dynamics and the community structure. This is further complicated by the fact that the observed community is not only the result of "local" vertical dynamics, but will also have been influenced by upstream processes. These issues have not, as yet, been addressed.

Despite the shortage of observational studies of phytoplankton communities at eddy and frontal scales, a few modeling studies have begun to explore the effect of frontal dynamics on phytoplankton community structure (e.g. Lima et al. [2002], Rivière and Pondaven [2006]). Rather than simply resolving one phytoplankton variable, these studies have used simple ecological models with two phytoplankton and at least one zooplankton. It is somewhat difficult to distinguish a community effect of the physical regime in these studies. However, the small and large phytoplankton species represented in the simple ecological models have different physiological requirements more or less analogous to picophytoplankton and microphytoplankton. Typically picophytoplankton are relatively slow growing and thrive in low nutrient conditions, whereas the microphytoplankton are faster growing and require higher nutrient levels. Thus we can think of the picophytoplankton as gleaners and the microphytplankton as opportunists, or K- and r- strategists, respec-

tively [MacArthur and Wilson, 1967, Kilham and Hecky, 1988]. Rather than concentrating on the mixing of different populations by a front, these studies concentrate on how spatially variable nutrient inputs and trapping of different populations by the physics shape the community. It is important to note that the physical models used are typically re-entrant channels, periodic in the along-front direction, and as such do not consider the along-front transport and its effect on phytoplankton ecology. A distinct spatial segregation is observed in the model results of Rivière and Pondaven [2006], with larger, r-adapted, phytoplankton dominating in filamentary structures, regions of increased nutrient flux, and the smaller, K-adapted, phytoplankton dominating outside of these regions. Beyond the effect of nutrient inputs on the phytoplankton community structure, Rivière and Pondaven [2006] also find that interactions between the fine scale frontal dynamics and grazing in their model can result in switches in the dominant phytoplankton species.

It is clear that mesoscale and submesoscale dynamics can play an important role in driving nutrient supply to the surface mixed layer, and in mediating the light environment experienced by phytoplankton. However, it is still unclear what the globally integrated contribution of these small scale dynamics is on primary production and export. In an idealized basin-scale model Lévy et al. [2010] showed that submesoscale (and mesoscale) processes play an important role in the mean circulation and transports at the basin scale. As a result we should expect that mesoscale and submesoscale processes will also have an impact on biological and ecological processes at the basin scale. This is still very much an open question. On a more local scale, might we find that incorporating mesoscale and submescale processes into ecological models would result in ecological shifts? Would opportunist phenotypes be preferentially selected for with the addition of more fine scale variability? There is also very little observational data available right now at appropriate spatial and temporal resolution to resolve fine scale physics, as well as including a high level of ecological resolution (e.g. phytoplankton functional groups and species identified). Clearly there are large gaps in our understanding of the links between meso- and submesoscale physical dynamics and phytoplankton ecology.

1.2.2 Dynamical Niches and Mixing

Oceanic fronts and eddies are thought of both as dynamical barriers and agents of lateral mixing. The Gulf Stream has been shown to be an effective for tracer transfer in the upper ocean, but a blender for tracers in the deeper thermocline [Bower et al., 1985]. Do these features also act as ecological barriers between populations, or as regions where populations from different source regions are actively mixed? Could fronts and eddies support distinct populations from those either side of or outside of them? Either way, understanding how these features affect community structure is fundamentally important for understanding patterns of biodiversity in the phytoplankton, as they can act to either limit or enhance the dispersal of individual species and populations. Although few observational studies have addressed the community structure of phytoplankton across fronts and in and around eddies, those that do exist are not conclusive [Sournia, 1994]. Yamamoto et al. [1988] and Taylor et al. [2012] found in observations of the Kuroshio Front and the California Current Front, that they could identify distinct frontal populations in their data. Similarly, Ribalet et al. [2010] inferred high levels of phytoplankton diversity at the core of a coastal front in the North Pacific, but it is unclear whether this represented a distinct population at the front or was due to mixing of populations from either side of the front, or along-front transport of an upstream population. Conversely, studies of ocean rings have shown that they trap and transport populations away from their source region to eventually die off and be replaced by the local community [Wiebe et al., 1976, Ring Group, 1981, Ewart et al., 2008]. Finally, a study using estimates of the dominant phytoplankton functional group (based on ocean colour) in the Brazil-Malvinas Confluence zone paired with geostrophic velocities showed that small scale filaments and eddies did seem to support distinct populations [d'Ovidio et al., 2010]. Although this method gives good spatial and temporal coverage, it is limited in that it can't really diagnose community separation or mixing as it does not have enough ecological resolution (i.e. only the dominant species can be determined, not the assemblage).

A few modelling studies have examined the effect of the physical structure of the flow

on the plankton community structure. Bracco et al. [2000] found that physical refuges within a turbulent mesoscale flow field allowed two phytoplankton species competing for the same resource to coexist. They attribute this result to the trapping action of the eddies and filaments present in the flow, and suggest that this may help to explain the 'Paradox of the Plankton" [Hutchinson, 1961]. Hewson et al. [2006] suggest in their study of variations in microbial diversity over the global oceans, that the characteristic length of variation between communities, i.e. the size of a patch containing a distinct community, coincides with the characteristic scale for mesoscale eddies. However, their study does not include many open ocean sites, and the result does not seem to be conclusive. A study of the scales of separation between distinct plankton assemblages may help to understand whether this process of physical segregation by coherent structures is important or not for the community, and for larger scale patterns of phytoplankton diversity.

Clearly the questions of how eddies and fronts act to shape patterns of phytoplankton diversity, if at all, is wide open. It is unclear whether we will find that fronts are regions of enhanced diversity, where populations are brought together and mixed, or that they simply act as a barrier between distinct populations which do not interact. It seems more likely, however, that eddies, as agents of cross-front exchange, also act to disperse populations away from their origin.

1.2.3 Large Scale Lateral Transport and Dispersal

Previous studies addressing the controls on phytoplankton community structure and diversity in global ecosystem models have focused predominantly on biological processes: resource competition [Dutkiewicz et al., 2009, Barton et al., 2010], grazing [Prowe et al., 2011] and nutrient supply [Prowe et al., 2012]. Ecological studies aimed at understanding the distributions of marine phytoplankton species and ecotypes have also tended to approach the question as a local one [e.g. Johnson et al. [2006]]. By that I mean that species are assumed to inhabit regions where they are best adapted to the environmental conditions. This, by definition, assumes that no dispersal has taken place, as dispersal can

transport organims well outside of their "comfort zone". However, the ocean is a highly dynamic and connected environment, where water parcels can be transported over large distances in a matter of days, and mixing across sharp environmental gradients is common. In such a dynamic environment, local community structure and species diversity must be controlled not only by local environmental conditions and species interactions, but also by larger scale regional processes such as dispersal [Ricklefs, 1987]. Fronts, particularly those associated with western boundary currents, are regions of strong horizontal velocities. These swift currents, O(2 m/s) can act to transport phytoplankton species, and their habitat, large distances outside of their expected range. This has been observed in both the Gulf Stream [Lillibridge et al., 1990, Cavender-Bares et al., 2001] and the Kuroshio Extension [Yamamoto et al., 1988]. This large scale physical forcing may be just as important as the smaller scale local input of nutrients in shaping the planktonic community structure, and thus impacting local production and export rates. As mentioned above, eddies may also be agents of lateral transport, as has been observed with warm-core and cold-core Gulf Stream rings [Wiebe et al., 1976, Ring Group, 1981]. Although these populations do not persist indefinitely in their new environment, they will contribute to local rates of production and levels of biodiversity. The role of circulation in structuring coastal plankton communities, determining larval transport and its implications for fisheries and marine protected areas has received considerable attention [Palmer and Strathman, 1981, Cowen et al., 2000, 2006, Aiken et al., 2007, Aiken and Navarrete, 2011]. In contrast, there have been very few studies, either observational or theoretical, addressing the role of physical transport in structuring phytoplankton diversity in the open ocean. Barton et al. [2010] invoked lateral mixing as a driving mechanism for the generation of diversity "hotspots" associated with highly dynamic regions of their global ecosystem model. They also suggested that coupled with long exclusion time scales, lateral mixing contributed to high diversity in the lower latitudes. Adjou et al. [2012], using a highly idealized box model, illustrated how immigration can enhance local diversity. However, to date, no studies have explicitly addressed the role of dispersal in shaping either observed or modelled phytoplankton communities at

the basin or global scale.

Although physical-biological interactions in the ocean have been the subject of much study, there is still a large gap in our understanding of physical-ecological interactions. The oceanic environment is characterized by its high degree of connectivity and dynamics occuring over a large range of space and time scales. As a result, there are clearly complex interactions between the planktonic ecosystem, the physical and resource environment. However, these can be largely split into "local" processes, such as nutrient supply, modulation of the light environment and transport barriers, and "remote" processes which occur over larger scales, such as lateral dispersal. Building up an understanding of how these local and remote processes interact to shape the ecology of phytoplankton in the oceans is a necessary next step in refining our understanding of the ecology and biogeochemistry of the oceans.

1.3 Thesis Goals and Outline

In this thesis I use both models and observations to explore how phytoplankton ecology is shaped by the physical dynamics of the oceanic environment. The thesis is split roughly into two parts, the first is made up of work I have done exploring how the physical environment shapes patterns in bulk biogeochemistry and phytoplankton ecology. I focus on the role of physical dispersal in setting patterns of phytoplankton diversity, and present what is arguably the first study to explicitly address the role of ocean physics in setting global patterns of phytoplankton diversity. In the second half of the thesis, I present a unique high resolution data set of the phytoplankton community structure across the Kuroshio Extension Front that I planned and collected in October 2009. Currently, this is the only existing data set which combines data on the concentrations of dissolved nutrients, phytoplankton accessory pigments, abundances of phytoplankton species and functional groups determined by flow cytometry, microscopy and qPCR, and 18S rRNA clone libraries across an oceanic western boundary current front. Along with this wealth of chemical, biological

and ecological data, a concurrent high resolution survey of the hydrographic and dynamical properties of the study site was also undertaken by Professor Takeyoshi Nagai, the Chief Scientist of the cruise [Nagai et al., 2012]. I have used this data set to address some of the hypotheses generated through my modelling work. The contributions and remaining challenges of both aspects of this work are described in the following chapters of the thesis, which is structure as follows.

In Chapter 2, I explore the sensitivity of a diverse self-assembling marine ecosystem model to the physical resolution of the model physics. I compare the results of the same global ecological model run at either 1^o (coarse) or $1/6^o$ (high) resolution, and address the following questions:

- **Does increasing model resolution result in an increase in primary production in oligotrophic regions through an increased, eddy-driven nutrient supply?**
- **Does an increase in model resolution result in decreased light limitation of phytoplankton in the subpolar gyres through eddy-driven restratification of the water column?**
- **Does a different phytoplankton community emerge when the model is run at different resolution?**

Chapter 3 follows on from the previous chapter with a much more focussed study of the role of ocean physics in setting patterns of phytoplankton diversity in the same diverse marine ecosystem model. I introduce a conceptual framework for separating out the contributions of dispersal and local growth to local diversity, and address the following questions:

- **What is the effect of model resolution on global (γ) and local (α) phytoplankton diversity?**
- **What proportion of local diversity can attributed to local adaptation or dispersal? Does this vary spatially?**

- **Are the diversity hotspots associated with energetic regions seen in a previous study [Barton et al., 2010] driven entirely by dispersal?**

Chapters 4 and 5 describe the results of the high resoltuion biological and ecological survey of the phytoplankton community at the Kuroshio Front. In Chapter 4, I outline the details of the cruise and sample collection, and present the data on the distribution of dissolved inorganic nutrients, phytoplankton accessory pigments and the abundance of phytoplankton functional groups across the front. In Chapter 5, I focus on describing the distribution of two distinct ecotypes of the photosynthetic picoeukaryote *Ostreococcus*. In both of these chapters, I examine the data to explore the following questions:

- **Can we identify clear linkages between the vertical circulation of the front and phytoplankton biomass and community structure?**
- **Does the Kuroshio Front act as an ecological barrier or blender?**
- **Do the observations support the hypothesis that this region is a diversity hotspot? Can we identify the local or large scale controls on diversity here? Do they agree with the hypotheses set out in Chapter 3?**

Finally, in Chapter 6 I highlight the novel contributions of this thesis, and highlight connections between the observational and modelling work. What I believe is one of the most exciting aspects of the thesis, is the incorporation of a detailed understanding of the physical oceanographic processes with state-of-the-art methods in marine ecology. Building on this, I outline plans for future work building on this strongly interdisciplinary theme.

Chapter 2

Biogeochemical and Ecological Consequences of Eddies and Fronts

The work described in this chapter was done in collaboration with Stephanie Dutkiewicz, Oliver Jahn and Mick Follows. SD and OJ ran the ecological model coupled to ECCO2 and ECCO-Godae physics (respectively). I have completed all of the subsequent data analysis and interpretation.

2.1 Abstract

Mesoscale physical processes in the ocean are known to stimulate primary production but are not typically resolved in global ocean models. Recent studies comparing highly idealized models run at differing resolutions show that, in some cases, increasing model resolution can have a dramatic effect on rates of production and biomass in simple NPZ type models. However very few of these studies have sought to explore the effect on community structure, or to evaluate the effects in a realistic global context. In this study we compare the output from a biogeochemical model representing a diverse plankton ecosystem, overlain on the MITgcm at coarse (1^o) and eddy-permitting ($\frac{1}{6}^o$) resolution. We assess the global effect of (partially) resolving mesoscale eddy dynamics on bulk biogeochemi-

cal properties and phytoplankton community strcuture. We find that bulk biogeochemical properties (primary production, phytoplankton and zooplankton biomass) are globally similar between the two models, but with marked regional differences in phytoplankton and zooplankton biomass and primary production. Primary production is enhanced at higher resolution in the lower latitudes by enhanced nutrient supply, and decreased in the higher latitudes where deeper mixed layer depths increase light limitation. The modeled plankton ecosystem is robust between models, with the same phytoplankton functional groups and phenotypes dominating in similar regions in both runs.

2.2 Introduction

Ocean general circulation models have proved an invaluable tool for studying the role of phytoplankton in the global biogeochemical cycles of climatically important elements. Recent advances have resulted in ever higher resolution physical models of the ocean circulation [e.g. Menemenlis et al., 2008], and more complex ecological models incorporating larger numbers of phytoplankton functional groups, and even individual phytoplankton phenotypes [Follows and Dutkiewicz, 2011]. This trend for increasing resolution and complexity is aimed at creating model systems which incorporate some of the complexity seen in reality, with the hope of better resolving biogeochemical processes.

The physical framework of an ocean model is fundamental to accurately modelling biogeochemical cycles and phytoplankton ecology [Doney, 1999, Anderson, 2005]. However, most global ocean models incorporating biogeochemical and ecological processes are run at coarse resolution. In the ocean, the characteristic temporal and spatial scales of biology coincide with those of mesoscale and submesoscale physical dynamics. Spall and Richards [2000] showed in a high resolution model of an unstable frontal jet that spatial heterogeneity in primary production occured on scales of a few to 10s of kms, and that primary production could increase locally by up to 100%. Coarse resolution global biogeochemical models do not resolve these dynamics, and Lévy [2008] reviews the consequences

of this for biogeochemical models. Previous studies found that neglecting to resolve the mesoscale could result in errors of up to 30% in the estimates of primary production [Lévy et al., 1998, Oschlies and Garçon, 1998, Mahadevan and Archer, 2000, McGillicuddy et al., 2003]. Furthermore, Lévy et al. [2001] found discrepencies of up to 50% in integrated primary production comparing a coarse resolution model with one that resolved submesoscale dynamics. These studies found that, in the oligotrophic subtropical gyres, mesoscale (and submesoscale) dynamics drove an increased nutrient supply to the surface mixed layer, which enhanced rates of primary production. In the subpolar gyres, eddies may have a different effect, McGillicuddy et al. [2003] found in a 0.1^o resolution model of the North Atlantic that mesoscale processes drove a geostrophic adjustment to deep winter convection, which reduced nutrient supply. However, nutrients are less likely to be limiting than light in the subpolar gyres, so this may also have a positive effect on rates of primary production.

The studies mentioned above, although they may resolve higher resolution physics, typically employed rather simple biogeochemical models incorporating only one or two phytoplankton functional types. However, marine microbial communities are known to be incredibly diverse, and this diversity plays an important role in mediating global biogeochemical cycles. Thanks to the continuing expansion of computing resources, diversity has been included in global biogeochemical models which resolve several phytoplankton functional groups [Chai et al., 2002, Gregg et al., 2003, Quéré et al., 2005]. More recently, ecological models which resolve several tens of phytoplankton within several functional groups have been developed [Follows et al., 2007, Ward et al., 2012]. It is unknown whether a change in physical resolution will result in any changes in the emergent community structure of one of these diverse models. Sinha et al. [2010] found that an intermediate-complexity ecosystem model which resolved 5 phytoplankton functional types, run with two different physical models at similar (coarse) resolution, could produce quite different regional phytoplankton communities in each case. However, it is unclear whether a more complex ecosystem model will be more or less robust to changes in the physics.

Here we present a process study that explores the effect of refining the physical resolution on a global diverse ecosystem model which incorporates 78 distinct phytoplankton types. We explore both the effect on the bulk biogeochemical properties and the ecological structure of the model solutions. We expect that, as in previous studies, we will see increases in nutrient supply in the subtropical gyres leading to higher rates of primary production and biomass in these regions. However, we cannot predict how these changes in resolution may affect the modelled phytoplankton community. In the following section, we describe the study in more detail and introduce the biogeochemical and physical models employed. We then describe the model results in section 3 and discuss the differences and similarities between the two solutions in section 4. We conclude and propose related future research in section 5.

2.3 Method

This study was performed by coupling an ecosystem model which resolves diverse phytoplankton communities to both a high resolution and a coarse resolution physical model and comparing the two solutions. We forced the ecosystem model with initial conditions, light forcing (PAR), sea ice fields and dust inputs all set to be identical within the confines of the interpolation between the two model grids. The models were run with forcing for the same 8 year period from 1992 to 1999 and the model solutions were compared for the final year of integration. The objective of this study is not to assess which model run performs best with respect to reality, but to examine how changes in the resolution of the model domain may alter the emergent biogeochemical and ecological properties of this complex ecosystem model.

2.3.1 Physical Models

The two physical model configurations used in this study are both ECCO ocean state estimates based on the MITgcm [Marshall et al., 1997], constrained to be consistent with

altimetric and hydrographic observations (Wunsch & Heimbach, 2007). The coarse resolution model (CR) is the ECCO-GODAE state estimate, with 1^o x 1^o horizontal resolution and 23 levels. The high resolution model (HR) is the ECCO2 state estimate, with an effective $\frac{1}{6}^o$ horizontal resolution yielding a mean grid spacing of 18km, and 50 levels [Menemenlis et al., 2008]. We chose these two models as they should be so close in terms of the physical structure and forcing that we aim to ensure that the major differences between the models are dominated by differences in spatial resolution.

2.3.2 Ecological and Biogeochemical Model

We briefly describe the ecological model discussed previously by Follows et al. [2007] and Dutkiewicz et al. [2009]. We transport inorganic and organic forms of nitrogen, phosphorous, iron and silica, and resolve 78 phytoplankton types and two simple grazers. The biogeochemical and biological tracers interact through the formation, transformation and remineralization of organic matter. Excretion and mortality transfer living organic material into sinking particulate and dissolved organic detritus which are transpired back to inorganic form. The time rate of change in the biomass of each of the modeled phytoplankton types, P_j, is described in terms of a light, temperature and nutrient dependent growth, sinking, grazing, mortality and transport by the fluid flow.

All 78 phytoplankton types are initialized with a broad range of physiological attributes. The phytoplankton are assigned to one of two broad classes by random draw at the initialization of the model and a set of physiological trade-offs that reflect empirical observations are imposed accordingly. We stochastically assign nutrient half-saturation constants (κ_N), light and temperature sensitivities from ranges of plausible values for these classes. We initialize both model configurations with an identical set of phytoplankton traits and identical initial conditions for all phytoplankton types. Interactions with the environment, competition with other phytoplankton, and grazing determine the composition of the phytoplankton communities that persist in the model solutions. We then compare the output from both configurations to test the sensitivity of the modelled ecosystem to the model resolution.

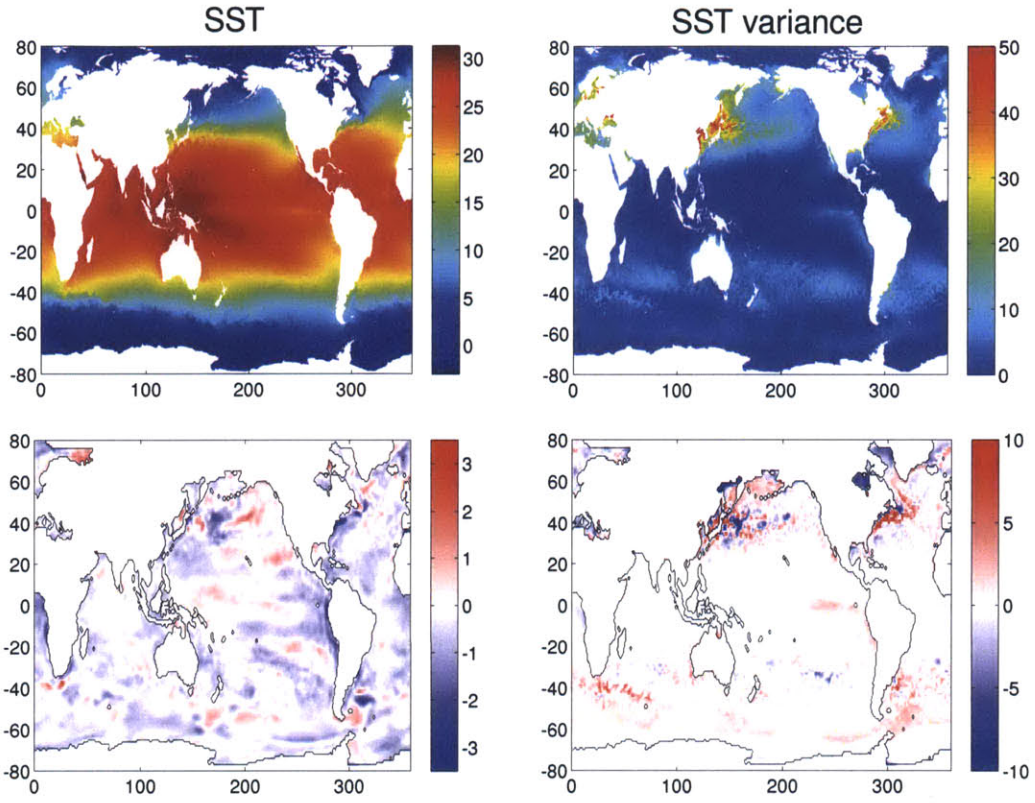

Figure 2-1: Top panels: Annual average SST (left) and SST variance (right) in the HR model for 1999. Bottom panels: the difference between those properties for both model runs (HR - CR).

2.4 Results

In this section we compare the model solution from the HR and CR runs. In order to compare the results, we interpolate the results of the HR run onto the 1^o lat/lon grid used in the CR run. In all cases, we compare the results from the final year of the integration (1999), and the difference between the model solutions (HR - CR).

2.4.1 Physics

A full assessment of the physical differences between ECCO-GODAE and ECCO2 is beyond the scope of this paper, but we briefly describe differences in some of the physical

properties most directly relevant to biogeochemical processes. We concentrate on sea surface temperature (SST), SST variance, mixed layer depth (MLD) and eddy kinetic energy (EKE). Annual average SST fields are compared between models in figure 2-1. There are differences of up to 3^oC in some regions, and the HR model appears to have a slightly cool bias relative to the CR model, which may be an indicator of enhanced upwelling/vertical mixing in the HR configuration. There are clear differences in SST in the most dynamic regions of the ocean: the Kuroshio, the Gulf Stream, the Aguhlas Retroflexion and the Brazil-Malvinas Confluence. These differences are most likely due to the those dynamical features being simulated differently in both runs, and appearing in different locations in both model solutions. This is not unexpected, as the higher resolution HR run simulates these swift, narrow currents more accurately thanks to the incorporation of finer scale physical dynamics.

The annual average mixed layer depth (MLD) is consistently deeper in the HR configuration, with large differences in the MLD in the higher latitudes, and much deeper MLD in HR north of 50^oN in the North Pacific and North Atlantic. In the Southern Ocean, we find much deeper MLD in HR south of $\sim 50^oS$, switching to a region of shallower MLD directly north of 50^oS to $\sim 40^oS$ in the regions connected to the South Atlantic and the Indian Ocean. A quick comparison to the World Ocean Atlas (WOA94) mixed layer depth climatology [Monterey and Levitus, 1997] shows that HR appears to greatly overestimate the MLD in the southern portion of the Southern Ocean, whereas in CR, MLDs are much closer to the climatology. On the other hand, in the subtropical gyres, the HR configuration produces mixed layer depths that are closer to the climatology than CR. In the higher latitudes of the northern hemisphere, the comparison is less clear, but HR appears to match the WOA94 values more closely than the CR configuration.

Sub-gridscale mixing is parameterized differently in the two models. Both configurations employ the KPP scheme [Large et al., 1994] to parameterize boundary layer turbulence. The CR model parameterizes mesoscale eddies employing the Gent & McWilliams scheme (GM) [Gent and Mcwilliams, 1990]. Although the GM scheme is tapered off in the

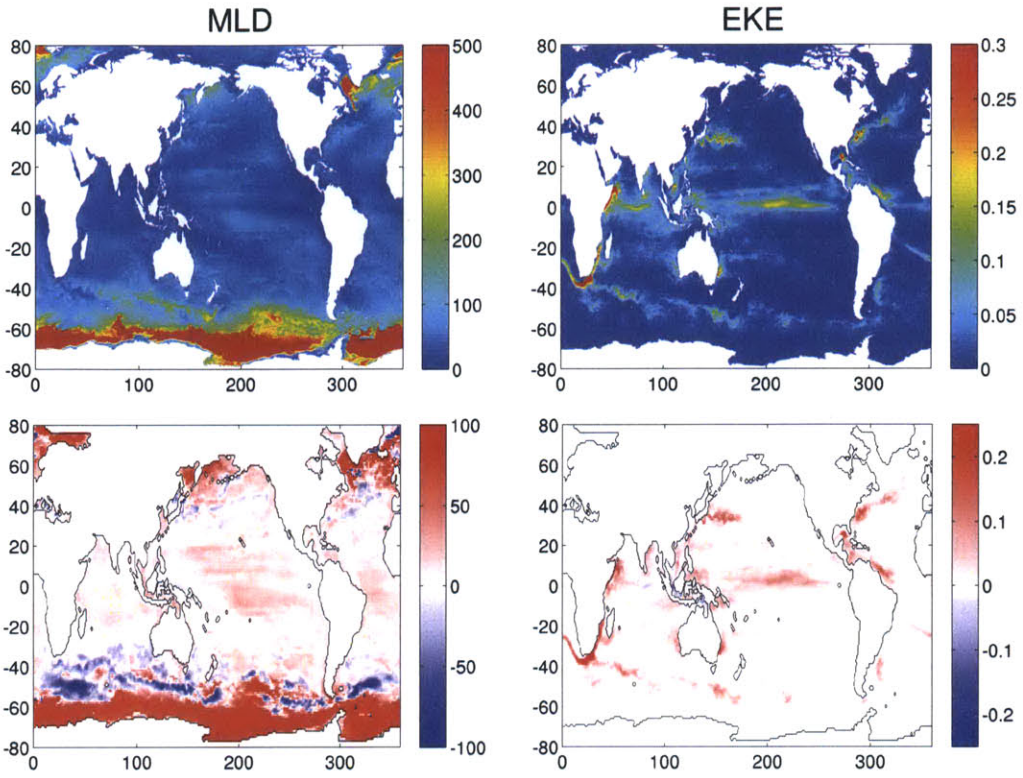

Figure 2-2: Top panels: Annual average mixed layer depth (left) and eddy kinetic energy (right) in the HR model for 1999. The mixed layer depth is determined using a σ_t criterion (0.125 kg/m^3). Bottom panels: the difference between those properties for both model runs (HR - CR). A positive value indicates a deeper MLD in the HR run, and vice versa.

mixed layer, it still has an effect on the mixed layer depth by modifying the subsurface stratification. The HR model does not employ this parameterization, assuming that mesoscale features are resolved. However, the HR run is eddy-permitting, with mesoscale dynamics most well resolved in the low latitudes, but less well represented in the subpolar gyres where the radius of deformation is smaller. As a result, it seems likely that in the HR run, MLDs may be overestimated in the higher latitudes where the mesoscale circulation is not well enough simulated to act to restratify the water column, and the GM parameterization is not applied [Danabasoglu et al., 1994].

In figures 2-1 and 2-2 we show the variance of SST and the EKE in the HR run and

the difference between both runs. Both of these quantities are indicators of the range of environmental variability in the model. It is clear that the HR model has a much more variable environment than the CR run. Differences in both of these quantities are most closely associated with the most dynamic regions of the global ocean, with much higher levels of EKE and SST variance in the HR run associated with the Gulf Stream, the Kuroshio, the Agulhas, the Brazil-Malvinas Confluence, the Equatorial Upwelling and the Southern Ocean.

These large scale differences in the physics suggest a range of possible outcomes for the biology. In particular, the deeper MLD and increased EKE in the subtropical gyres in the HR model may represent an enhanced nutrient supply to the surface mixed layer driving more primary production. Conversely, deeper MLDs in the HR model in the northern subpolar gyres and the Southern Ocean may result in a substantial decrease in primary production as light is generally limiting there. Decreased SSTs in some regions of the HR run may result in decreased primary production as the growth rate of phytoplankton is a function of temperature in the ecological model.

2.4.2 Integrated Biogeochemical Properties

In this section, we compare the model estimates of primary production and total phytoplankton biomass, shown in figure 2-3, along with the total zooplankton biomass shown in figure 2-4. Globally and regionally integrated values of these properties are listed in table 2.1. Although the globally integrated primary production is very similar between both models, there are clear regional differences, with the HR model having higher rates of production in the low latitudes and lower rates of production in the high latitudes, relative to the CR model.

There is a $\sim$ 20% increase in the standing stock of phytoplankton biomass globally in the HR model compared to the CR model, mostly accounted for by higher phytoplankton biomass between 40^{o}S and 40^{o}N in the HR solution. There is also slightly more phytoplankton biomass in the Southern Ocean and slightly less north of 40^{o}N in the HR model.

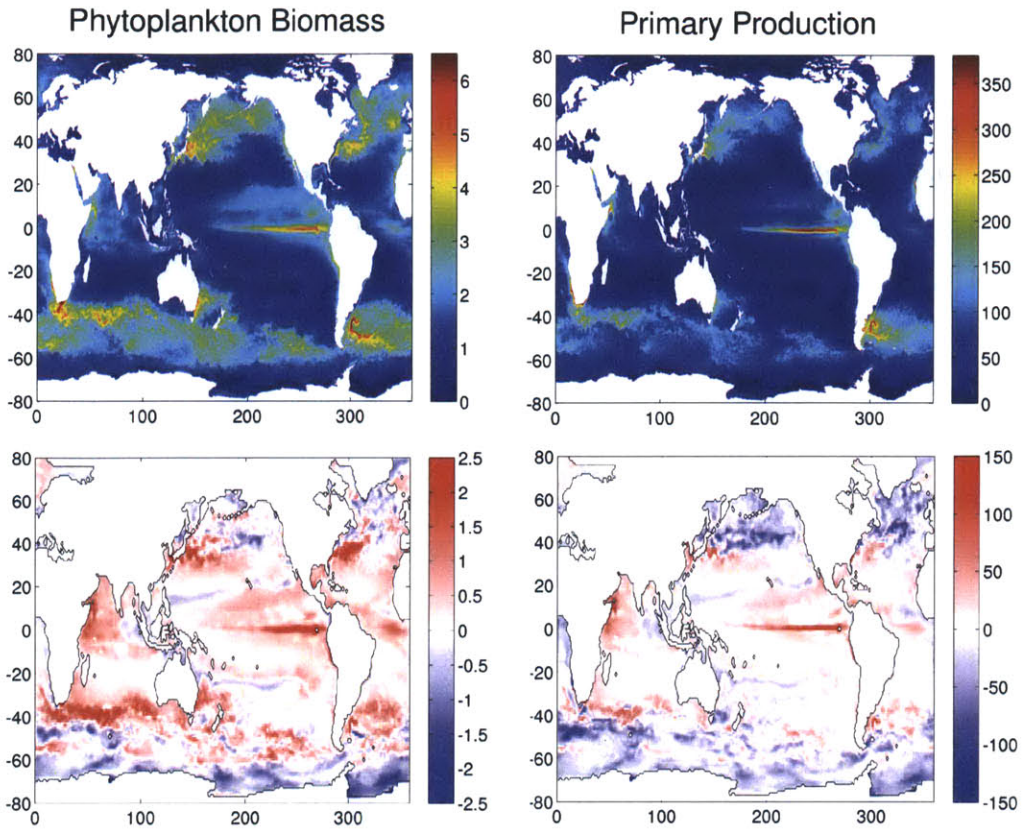

Figure 2-3: Top panel: annual average primary production in Tg C m^{-2} yr^{-1} (left), and annual average total phytoplankton biomass in Tg C m^2 (right) in the HR model solution for 1999. Bottom panels: the difference between those properties for both model runs (HR - CR).

The largest differences in both phytoplankton biomass and primary production are associated with the western boundary currents and the equatorial upwelling zone, with higher values in the HR model. Zooplankton biomass is $\sim$ 10% lower, globally, in the HR solution. That difference is in large part accounted for by much lower zooplankton biomass in the North Atlantic and North Pacific. There is slightly less zooplankton biomass in the subtropical and equatorial regions in HR, balanced by slightly higher zooplankton abundance in the Southern Ocean in the same run. This increased zooplankton biomass south of 40°S in the HR run is accounted for primarily by a much higher abundance of zooplankton

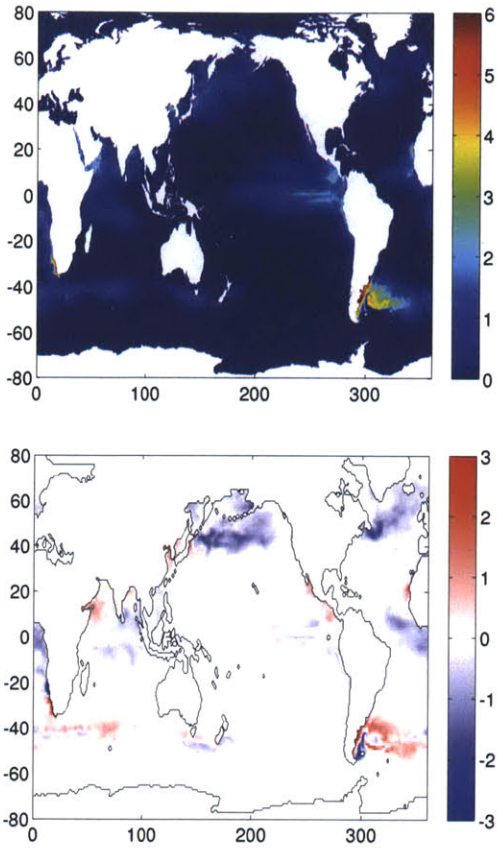

Figure 2-4: Top panel: annual average total zooplankton biomass in Tg C m^{-2} in the HR model solution for 1999. Bottom panel: the difference in total zooplankton biomass between oth models (HR - CR).

in the Brazil-Malvinas Confluence zone and downstream of it, in the HR results. In both cases, the estimates of globally integrated primary production are much lower than suggested by observations. Improvements in the ecosystem model since this study, including faster turnover of organic matter and higher zooplankton grazing have resulted in integrated primary production values closer to those observed ($\sim$ 45 Pg C yr^{-1}). Unfortunately these improvements were implemented in the model after the computationally-expensive "one-off" HR model run was completed and could not be incorporated into this study.

These results suggest that the differences in the physical models are resulting in marked

Table 2.1: Global and regional primary production, phytoplankton biomass and zooplankton biomass integrated over the top 200m of the water column. All values are annual averages for the final year of integration (1999).

	Region	HR	CR	(HR-CR)
Primary Production	Global	22.57	22.44	+0.13
(Pg C yr^{-1})	North of 40°N	2.72	3.48	-0.76
	40°S - 40°N	13.72	11.76	+1.96
	South of 40°S	6.14	7.19	-1.05
Phytoplankton Biomass	Global	568.72	479.27	+89.45
(Tg C)	North of 40°N	69.88	70.85	-0.97
	40°S - 40°N	342.85	255.43	+87.42
	South of 40°S	155.99	152.99	+3.0
Zooplankton Biomass	Global	74.27	88.12	-13.85
(Tg C)	North of 40°N	6.96	19.51	-12.55
	40°S - 40°N	49.75	54.68	-4.93
	South of 40°S	17.57	13.93	+3.64

regional differences in bulk biological properties in the model solutions. In the equatorial and subtropical region, we see an increase in both primary production and phytoplankton biomass, coupled with a slight decrease in zooplankton biomass in the HR result. In the northern subpolar regions, we see a decrease in primary production and zooplankton biomass, but little change in phytoplankton biomass in the HR solution. In the Southern Ocean, we see a slight decrease in primary production, but a slight increase in both phytoplankton and zooplankton biomass in the HR solution. We discuss these key results in light of the physics, nutrients and phytoplankton community structure in more detail in section 3.

2.4.3 Nutrients

In figures 2-5 and 2-6, we show the annual average modeled surface concentrations of nitrate, dissolved iron, phosphate and silicate found in the HR model run, and the difference between the two runs. The largest differences in the concentrations of nutrients is found in the Southern Ocean, and to a lesser extent in the subpolar Atlantic and Pacific. Concentrations of nitrate and phosphate are essentially the same in both models in the Atlantic

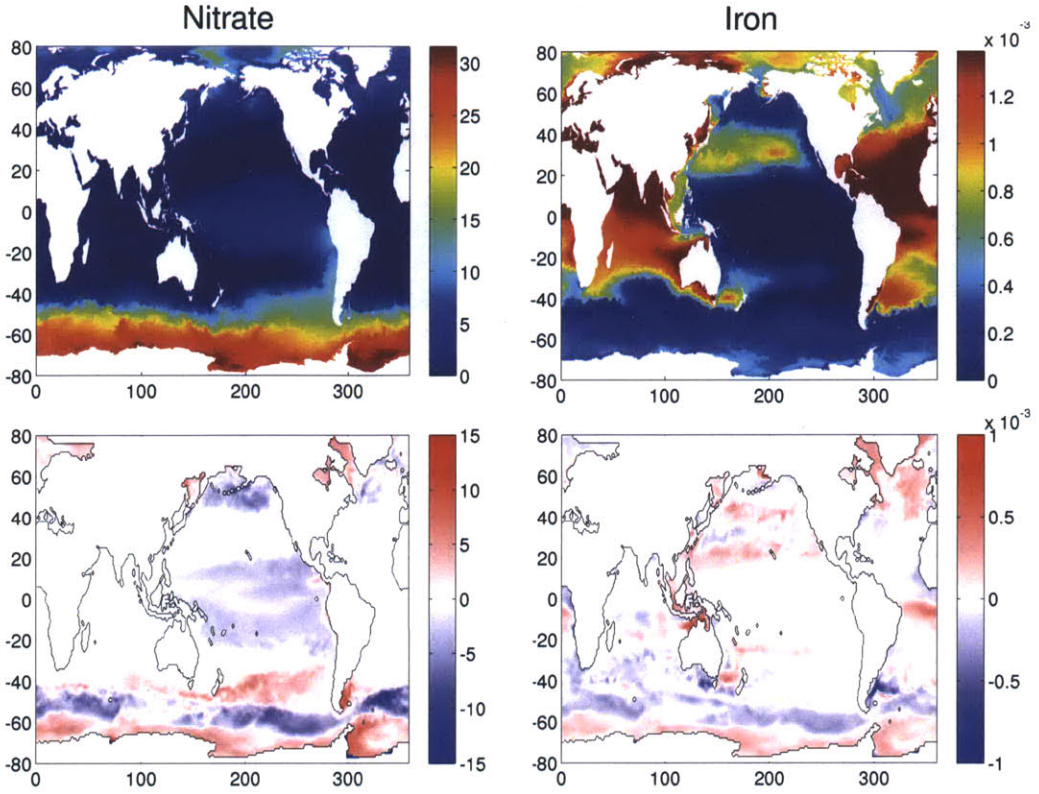

Figure 2-5: Top panel: Annual average surface concentrations of nitrate in mmol N m^3 (left) and dissolved iron in mmol Fe m^{-3} in the HR model solution for 1999. Bottom panels: the difference in these properties between both models (HR - CR).

between 40^{o}S and 50^{o}N, the Indian Ocean and in the Pacific between 10^{o}N and 50^{o}N and $\sim$ 40^{o}S and 20^{o}S. Similarly, surface concentrations of dissolved iron are the the same in both models between 40^{o}S and 20^{o}N in the Pacific. We do not see any similar patterns in the silicate distributions as both models tend to deviate from each other everywhere with respect to silicate.

We evaluate and map the annual average limiting nutrient in figure 2-7, and show that nitrate and dissolved iron are the dominant limiting nutrients. In both models, the phytoplankton are limited by nitrate in the Atlantic, the Indian Ocean, the North Pacific between $\sim$10^{o}N and 50^{o}N and in a small region the western South Pacific between 20^{o}S and 40^{o}S. Dissolved iron is the limiting nutrient in the Southern Ocean, the subtropical and equatorial

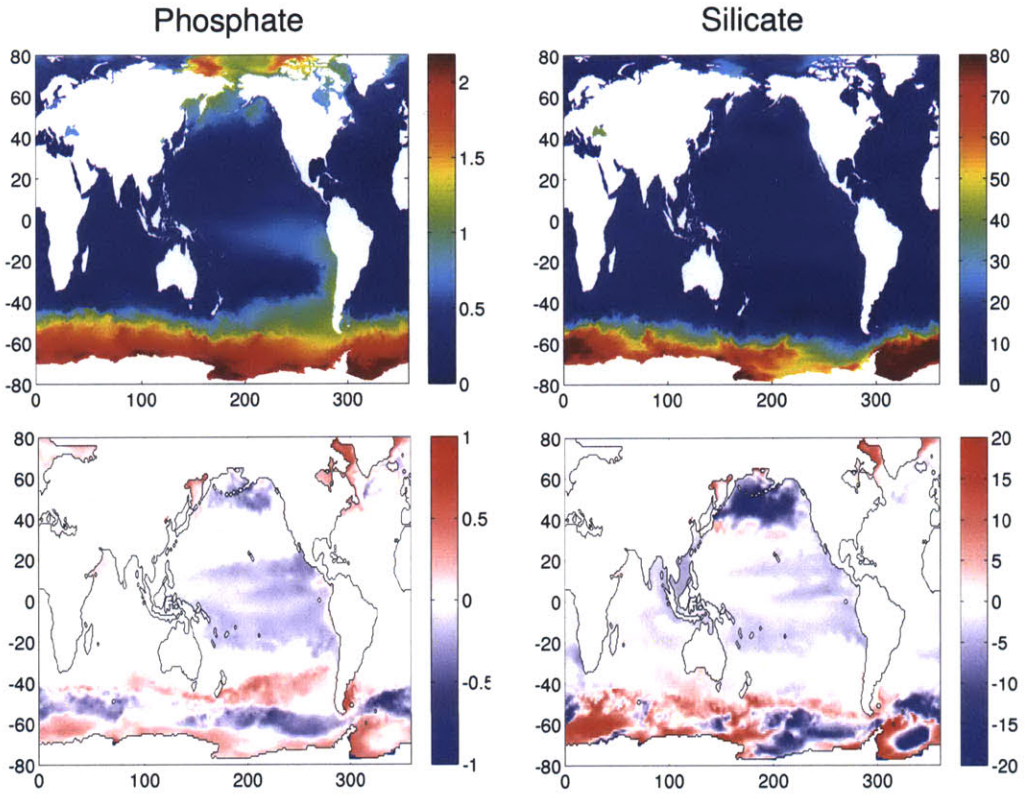

Figure 2-6: Top panel: Annual average surface concentrations of phosphate in mmol P m^3 (left) and silicate in mmol Si m^{-3} (right) in the HR model solution for 1999. Bottom panels: the difference in these properties between both models (HR - CR).

South Pacific and the North Pacific, north of 40°N. There are only limited regions of silicate limitation of diatoms found in the Southern Ocean and the northern North Atlantic, Pacific and Arctic Oceans. Phosphate is not the dominant limiting nutrient anywhere in the HR solution, but there are some very small regions of phosphate limitation present in the CR model solution. There is a very close correspondance in the patterns of nutrient limitation between models, with only small deviations at the boundaries between provinces defined by limitation to different nutrients. It is clear that the regions where nutrient concentrations are unchanged between models coincide with regions where that particular nutrient is limiting. For example, the regions where nitrate is limiting in both model solutions coincides with the regions where there is no difference in the nitrate concentration found in either

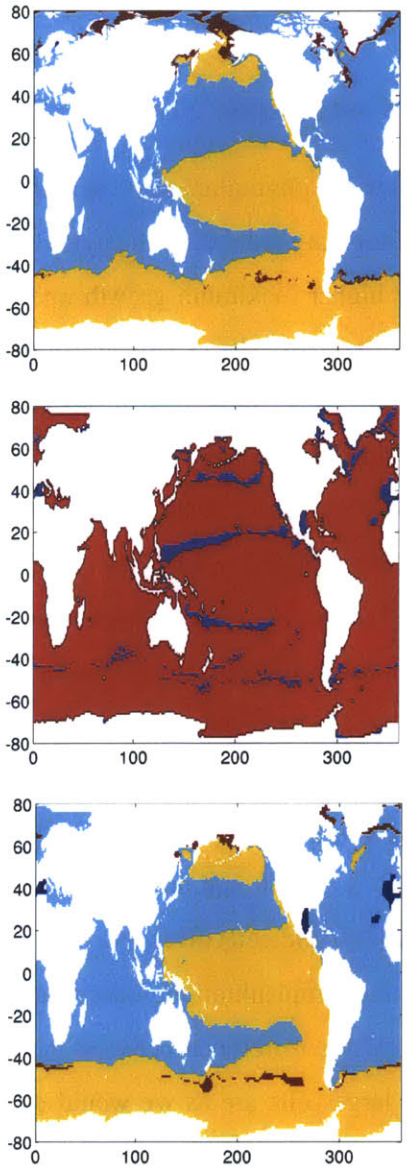

Figure 2-7: Map of limiting nutrients, based on a biomass weighted average of the most limiting nutrient for each of the 78 total phytoplankton types in the HR model (top panel) and the CR model (bottom panel), (orange = iron-limited, light blue = nitrate-limited, dark blue = phosphate-limited, dark red = silica-limited). The middle panel shows in blue the regions where the models have a different limiting nutrient, and in red where they are the same.

model solution. We see similar patterns in dissolved iron, which are discussed later.

2.4.4 Phytoplankton Community Structure

In this section, we explore how the phytoplankton community differs between the HR and CR model solutions. The ecological model divides phytoplankton first into large and small cell types. Large cells have higher maximum growth rates, nutrient half saturation constants and sinking rates than the small cells. Small and large cells are then subdivided into four functional groups: diatoms, other large phytoplankton, *Prochlorococcus*-like phytoplankton and *Synechococcus*-like phytoplankton. Diatoms require silica, whereas the other large pytoplankton do not. *Prochlorococcus*-like phytoplankton only use ammonium and nitrite as a nitrogen source, whereas the *Synechococcus*-like phytoplankton can use ammonium, nitrite and nitrate. We use these physiological subdivisions of the model in our assessment of the differences in the phytoplankton community structure. Patterns of phytoplankton diversity are another aspect of the model output that describe the ecology of the model solution. These are not discussed here, but we explore differences in the patterns of diversity in detail in the following chapter (Chapter 3). Briefly, we find that although the same set of phytoplankton types persist, and are present globally in both model runs, the HR run has higher levels of local (grid cell) diversity.

In figure 2-8, we show the phytoplankton biomass split into small "gleaner" and large "opportunistic" cell types, and the difference between the two models. The patterns in the abundance of small vs. large cells are as we would expect, with small gleaner type phytoplankton dominating in the subtropical regions, whereas larger opportunist type phytoplankton are more abundant in the seasonal higher latitudes [e.g. Dutkiewicz et al., 2009]. Small, gleaner cells with lower nutrient half saturation constants are better adapted to thrive in the stable oligotrophic subtropical gyres. Conversely, large opportunist cells with high maximum growth rates are better adapted to the subpolar gyres where nutrient inputs are seasonally intermittent. Overlain on these large scale patterns, we see regions of increased small phytoplankton biomass associated with the western boundary currents and increased

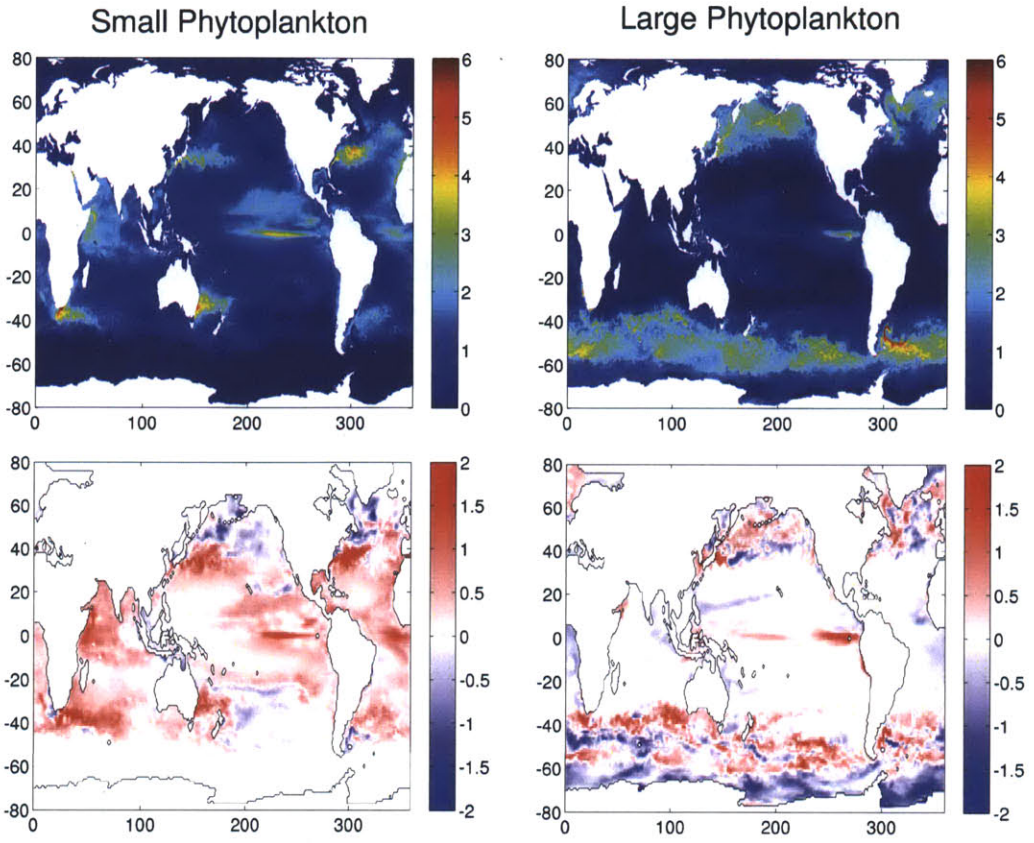

Figure 2-8: Top panel: Annual average depth integrated biomass of large, opportunist (left), and small, gleaner (right), phytoplankton in Pg C m^{-2}. Bottom panels: the difference in these properties between both models (HR - CR).

large and small phytoplankton biomass associated with the equatorial upwelling region in the HR model. These "hotposts" of phytoplankton biomass (and diversity) are discussed in detail in the following chapter (Chapter 3), but for now we note that these are regions of confluence of populations subject to enhanced nutrient inputs compared to both the subpolar and subtropical gyres.

Comparing the two models, although the large scale patterns in small and large phytoplankton are essentially the same, we see an increase in the biomass of both small and large phytoplankton in the subtropical regions of the HR solution relative to the CR solution. Although we may have expected a large increase in the biomass of large phytoplankton in

these regions thanks to more episodic eddy-driven nutrient injections to the surface mixed layer, instead we see only a modest increase in large phytoplankton. There is a much larger increase in small phytopankton biomass in the lower latitudes in the HR solution, which accounts for the larger part of the overall increase in phytoplankton biomass in the subtropics in that run. We also see a large increase in the small phytoplankton biomass associated with the western boundary currents. In the higher latitudes, the picture is somewhat less clear. In the Southern Ocean there appears to be no change in the biomass of small phytoplankton, but this is most likely due to the fact that, in this model, there is a very low abundance of small phytoplankton cells there. Generally speaking, the difference in large phytoplankton biomass is split into two bands in the Southern Ocean. There is a decrease in the abundance of large phytoplankton cells south of $\sim 60^{o}$S, but to the north of this, up to $\sim 40^{o}$S, there is an overall increase in the large phytoplankton biomass in the HR solution.

Overall the emergent ecosystem in both sets of model results is almost identical. Figure 2-9 maps the dominant phytoplankton functional groups, and the small regions where these differ between both models. The large scale patterns remain strikingly similar between both models, with diatoms and other large phytoplankton dominating the phytoplankton population in the high latitudes and *Prochlorococus*-like and *Synechococcus*-like phytoplankton dominating in the lower latitudes. Typically, diatoms are dominant at the highest latitudes, with other large phytoplankton taking over, followed by *Synechococcus*-like types and finally *Prochlorococcus*-like types are dominant at the lowest latitudes. Overlain on this latitudinal pattern, we find that in the equatorial region, there is a transition from waters dominated by *Synechococcus*-like types in the eastern parts of the Atlantic and Pacific Oceans, to waters dominated by *Prochlorococcus*-like types in the western parts of the basins. There are also some small regions in the equatorial region where large phytoplankton types dominate along and offshore of the western coast of Central America. This is presumably due to nutrient inputs associated with coastal upwelling and equatorial upwelling which are depleted moving westwards across the basins. The patterns in the dominant pytoplankton functional types are essentially the same between models, with the

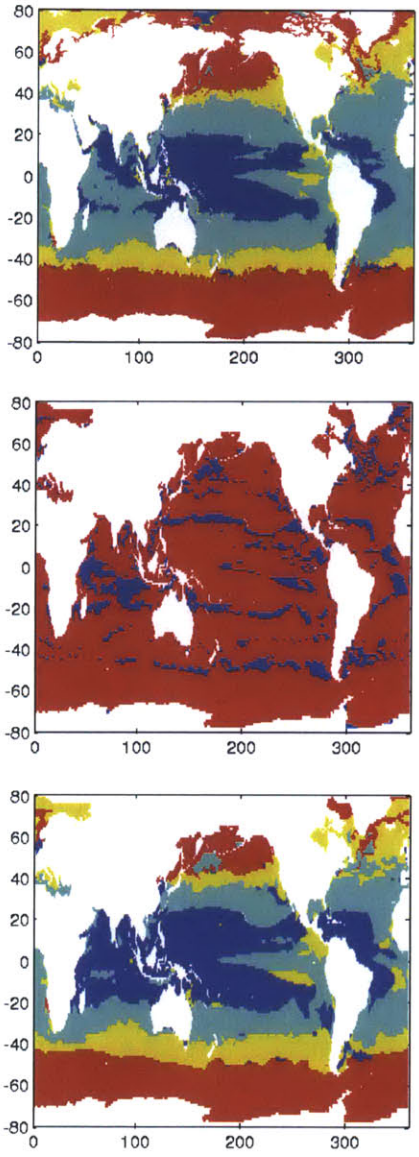

Figure 2-9: Dominant phytoplankton group in the HR model (top panel) and the CR model (bottom panel). Diatoms are shown in red, large phytoplankton in yellow, *Synechococcus*-like types in green and *Prochlorococcus*-like types in blue. The middle panel shows in blue the regions where the models have a different dominant phytoplankton functional group, and in red where they are the same.

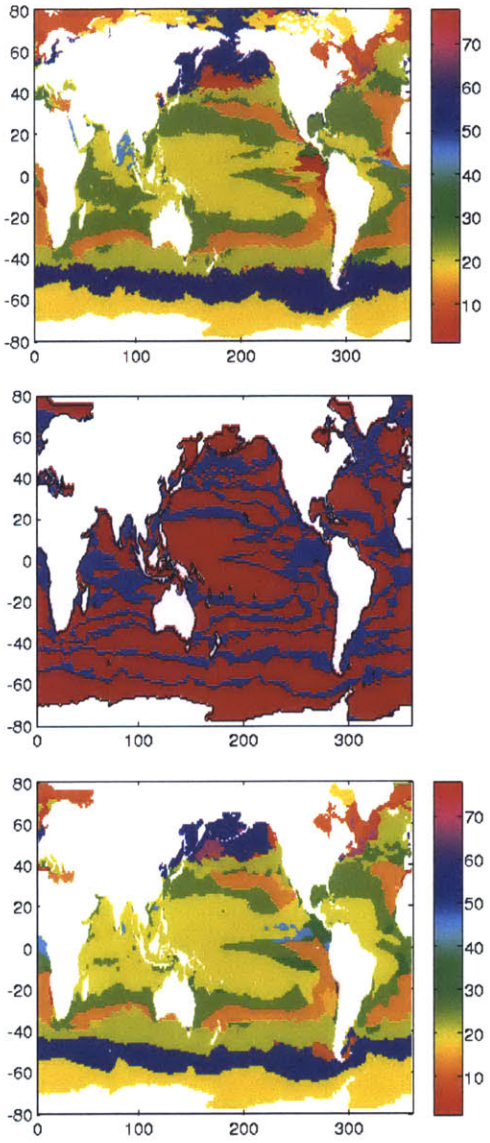

Figure 2-10: Dominant phytoplankton type in the HR model (top panel) and the CR model (bottom panel). The middle panel shows in blue the regions where the models have a different dominant phytoplankton functional type, and in red where they are the same.

exception of the Indian Ocean, where there is a switch from dominant *Prochlorococcus*-like types in the CR model to *Synechococcus*-like types in the HR model. We speculate that this may be due to a shift in the supply of nutrients to the surface mixed layer, as the

Synechococcus-like types can use nitrate, whereas *Prochlorococcus*-like types cannot utilize it (as defined here). Other regions where the models do not agree occur mainly at the borders between different biogeochemical provinces.

Exploring the phytoplankton community structure in more detail, we look at the distribution of individual phytoplankton phenotypes. In figure 2-10 we map the dominant types for both models, and again, show the regions where the dominant phenotypes differ between models. There is a strikingly close correspondance between both of the model solutions, with the same phenotypes dominating in similar geographical locations. Looking more closely at the regions where the dominant phenotype differs, we see a banded latitudinal pattern. This reflects the importance of the role of temperature in limiting the growth rates of individual phytoplankton types. The largest difference in the dominant phenotype is in the Indian Ocean reflecting the switch from *Prochlorococcus*-like phenotypes in the CR run to *Synechococcus*-like types in the HR model. Despie this, the striking similarity between both model solutions is somewhat surprising. There is only one comparable study that we know of that has compared the emergent ecosystem of a global ecological model with several phytoplankton function types [Sinha et al., 2010]. In that study, changes in the physical forcing, but not in resolution (1^o vs 2^o) resulted in large shifts in the dominant phytoplankton functional type. We do not see any such shifts despite our model asccomodating more than 10 times as many phytoplankton phenotypes overall.

2.5 Discussion

Here we interpret the physical, chemical and biological results of the model to explain some of the more striking differences and similarities between the two model solutions. As both physical models are constrained with the same data, the differences in the ecological and biogeochemical solutions are fundamentally related to the model resolution. However we can find that these differences are either the direct result of local differences in the vertical and horizontal circulation, or result from these differences being integrated

over a larger area, e.g. the gyre. "Integrated" differences would be manifest as large-scale dynamical or biogeochemical features occuring in different geographical locations in either model. An example would be the offset in the location of the Gulf Stream between both models. "Local" differences, on the other hand, can be rationalised as more directly due to differences in the circulation driving different biological responses, for instance increased nutrient supply driving increased primary production in a given region in one of the runs. We find three main regions that are affected in different ways by the different model resolution: the subtropical gyres and equatorial upwelling zone, the northern subpolar gyres and the Southern Ocean. We discuss these differences and attempt to distinguish between those that are mainly due to integrated or local effects.

2.5.1 Subtropical gyres and Equatorial upwelling zone

In the subtropical gyres we see, as predicted by previous studies, an increase in both primary production and phytoplankton biomass, as well as a small decrease in zooplankton biomass in the HR model. Despite this increase in both phytoplankton biomass and primary production, we do not see a major shift in the phytoplankton community, with the dominant phenotypes remaining essentially unchanged between both model solutions. The limiting nutrient and its surface concentration also remain essentially the same in both models, but there is a slight decrease in the surface concentrations of the nutrients that aren't limiting. There is also more or less no change in the dominant phytoplankton type and functional group, with the exception of the Indian Ocean. We have also shown that the annual average mixed layer depth is consistently deeper in these regions in the HR run. Taking all of these factors together, we suggest that these differences point to a nutrient enrichment in a stable enviroment where the community is set by resource competition. If we think of the subtropical gyres as stable, steady state, regions where seasonality is low, and phytoplankton growth is nutrient-limited, we can apply the simple resource competition framework introduced by [Tilman et al., 1982] and applied to this system by [Dutkiewicz et al., 2009] to understand the simultaneous differences and similarities in the model results. If we can

assume that predation is low, which it is in this region, then we can set up a simple model phytoplankton growth model where growth is nutrient limited, and phytoplankton are removed from the system by a simple linear mortality term:

$$\frac{dR}{dt} = -\frac{\mu RP}{R+k} + S_N \tag{2.1}$$

$$\frac{dP}{dt} = \frac{\mu RP}{R+k} - mP \tag{2.2}$$

where R is the limiting resource, P is the phytoplankton biomass, k is the resource half saturation constant, m is the phytoplankton mortality rate, and S_N is the rate of resource supply into the system. The steady state solution to this simple set of equations is given by:

$$P* = \frac{S_N}{m} \tag{2.3}$$

$$R* = \frac{mk}{\mu - m} \tag{2.4}$$

In this framework, the steady state concentration of the limiting resource, $R*$, is controlled not by the magnitude of the nutrient supply, but by the physiological attributes of the dominant phytoplankton phenotype P. On the other hand, the steady state concentration of the phytoplankton, $P*$, is a function of the resource supply, S_N, as well as the mortality rate. Thus, an increase in S_N will result in increased phytoplankton biomass, but not a shift in the dominant phytoplankton type (or functional group), as $R*$ is only a function of the physiology of the fittest phytoplankton type. So, given an increase in S_N driven by the enhanced mixing in the HR model run, the overall dominant phytoplankton type will not change but its biomass, $P*$, will increase and primary production will also increase. At the same time, the concentration of the limiting nutrient, $R*$, remains unchanged as seen here. This is evident in the nitrate and dissolved iron distributions shown in figure 2-5. However, we do see a decrease in the nutrients that are not limiting (figures 2-5 and 2-6). This is driven by the increase in primary production in the HR run, which results in higher consumption of non-limiting resources. We therefore wouldn't expect to see a

big shift towards large cells in the subtropical gyres, even with an increased nutrient supply, as the conditions are stable enough to allow gleaner types to continue to dominate. We do however see a small increase in the biomass of large phytoplankton, and this must be due to the enhanced nutrient supply. This is in line with observations that show that episodic nutrient inputs associated with eddies may stimulate blooms of opportunist types in subtropical gyre regions [Benitez-Nelson et al., 2007, Brown et al., 2008], but these do not change the overall dominance of small phytoplankton cells in these stable, oligotrophic regions. Enhanced nutrient supply, surprisingly does not alter the phytoplankton community structure significantly, or the surface concentration of the limiting nutrient, but it does enhance primary production and increase the standing stock of phytoplankton biomass.

2.5.2 North Atlantic and Pacific Subpolar Gyres

We see a somewhat different picture in the North Atlantic and North Pacific subpolar gyres, where primary production and zooplankton biomass are much lower in the HR model, but phytoplankton biomass remains at similar levels in both models. These are regions where nutrients are replete and light is more typically the most limiting factor for the growth of phytoplankton. In figure 2-11, we show the monthly integrated primary production, phytoplankton and zooplankton biomass for the region north of 40^{o}N for both models. It is clear that the magnitude of the spring bloom, in terms of primary production is smaller in the HR run. Although we see large differences in primary production and somewhat smaller differences in phytoplankton biomass between the models during the spring season, for the rest of the year, their values are much closer, with only slightly higher primary production in the CR run, and roughly equal phytoplankton biomass. What happens during the spring season drives the differences in the annual average primary production and phytoplankton biomass values. In April, rates of primary production are on average 5 Tg C day^{-1} lower in the HR run than the CR run. The difference in phytoplankton biomass during the spring bloom period is less pronounced, but there is a striking difference in zooplankton biomass between the model runs. Higher production in the CR run is converted relatively quickly

into zooplankton biomass, which peaks in July for both model runs. This explains the seeming disconnect between the differences in the phytoplankton biomass and primary production between models. Looking more closely at the difference in the mixed layer depths for the spring season (March, April and May), it is clear that the HR run has deeper MLD over most of the region north of 40°N. As a result the phytoplankton community in the HR run is more light-limited than the CR community during the spring bloom season. We believe that this difference in the mixed layer depths may be driven by differences in the parametrizations of sub-gridscale mixing discussed earlier in this paper.

We also note a decrease in the surface concentrations of most nutrients in the HR solution. This is somewhat counter-intuitive since rates of primary production are lower in the HR model run, but we suggest that this may in fact be driven by the much lower zooplankton abundance in that run. In the model, zooplankton mediate the remineralization of organic matter into dissolved inorganic nutrients. If there is no real difference in the surface concentrations of nutrients during the winter, then a decrease in the remineralization due to zooplankton in the summer when their abundance peaks could result in lower annual mean nutrient concentrations.

2.5.3 Southern Ocean

Patterns in the difference between the two models in the Southern Ocean are somewhat more complicated. Overall, the differences in the regionally integrated annual average phytoplankton biomass and primary production are small, and we see a slight increase in zooplankton biomass in the HR model run. However, it appears that a decrease in primary production and phytoplankton biomass in the southern half of the region in the HR solution is balanced by a corresponding increase in these properties in the northern half of the Southern Ocean. Similar to the case in the nothern subpolar gyres, we see deeper mixed layer depths in the southern part of the Southern Ocean in the HR run. Phytoplankton in this region are more light limited in the HR run due to the deeper mixed layers, and thus less productive. As a result, nutrients are consumed less efficiently in this region.

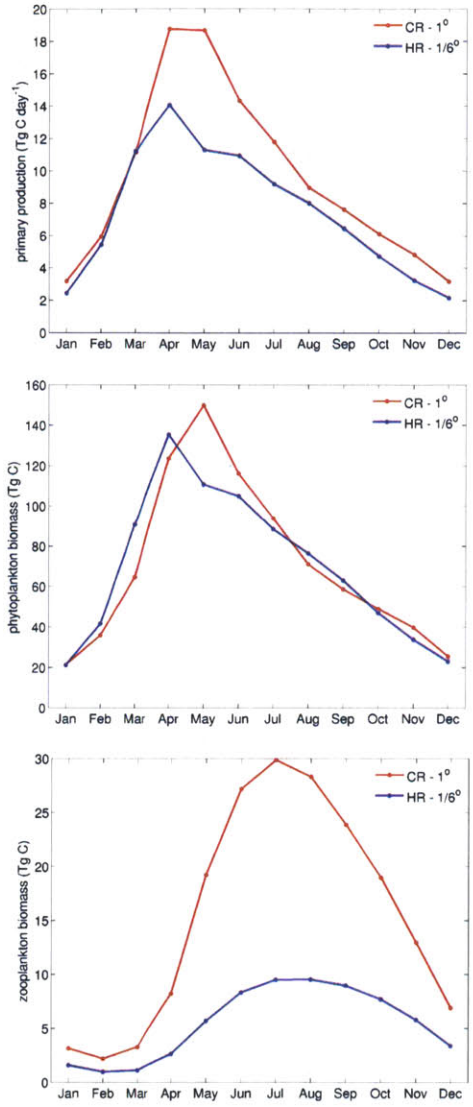

Figure 2-11: Monthly integrated primary production, phytoplankton biomass and zooplankton biomass for ocean regions north of 40^{o}N.

This is reflected in the surface nutrient fields, with higher surface concentrations of nitrate, phosphate, silicate and dissolved iron in the HR run. However, in the northern half of the Southern Ocean, the pattern is reversed. Phytoplankton biomass and primary production in this case are higher in the HR model run, and the surface concentration of dissolved

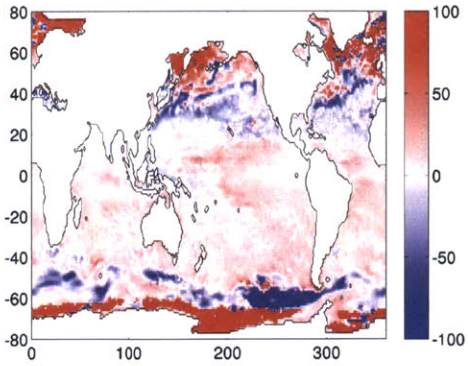

Figure 2-12: Average difference in MLD for March, April and May.

nutrients is lower than in the CR run. It appears that the higher production in the HR run is supported by shallower MLDs, relative to CR, in the northern half of the Southern Ocean, resulting in decreased light limitation.

2.5.4 Boundaries between biogeographical provinces

We have dicussed large scale differences in primary production and phytoplankton biomass that can largely be explained by local 1-D (vertical) differences between the models. However, we have also identified marked differences in the biological fields which appear to be due to more complex spatial interactions. These appear to be predominantly due to differences in the geographical extent of biogeographical provinces. In figure 2-13 we show the difference in phyoplankton biomass and primary production again, this time plotted with contours showing the regions where the limiting nutrients in the models are not the same. In essence, these contour lines delineate regions of the model domain where biogeochemical provinces in both models do not coincide spatially. Within the northern and southern Pacific subtropical gyres, we see two bands characterised by a decrease in both primary production and phytoplankton biomass in the HR model. These differences coincide with geographical differences in the extent of biogeochemical provinces in the models. More specifically, the shift between iron-limited and nitrate-limited regions in the Pacific

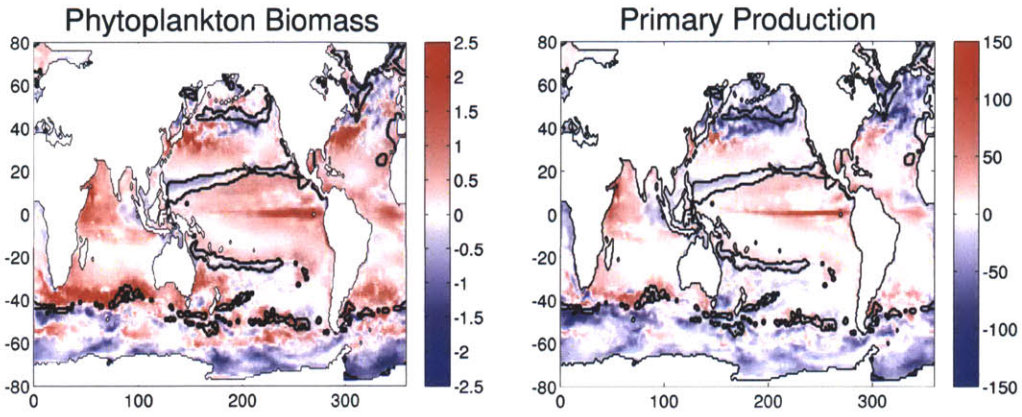

Figure 2-13: Differences in phytoplankton biomass (top) and primary production (bottom) between models. Black contour lines delineate the regions where the limiting nutrients differ between both models.

subtropical gyres, and to a lesser extent between the Southern Ocean and the basins bounding it to the north. In the subtropical Pacific, we attribute this decrease in production and biomass to a decrease in the supply of nutrients from the equatorial region. An increase in the dissolved iron supplied by stronger upwelling in the equatorial region in the HR model drives both higher productivity and a higher abundance of large phytoplankton types. As iron is limiting in this region, an increase in the dissolved iron supply will result in increased depletion of other dissolved nutrients, such as nitrate. If more nitrate is consumed in the equatorial Pacific, then it follows that less will be transported out to the edges of the subtropical gyres where it is the limiting nutrient, shifting the boundary between provinces.

Although the modelled phytoplankton community is largely the same between runs, suggesting some level of convergence on a stable ecosystem structure, there are large regional differences in biogeochemical properties. This suggests the possibility that, even at this eddy-permitting resolution, our biogeochemical model has not converged to a stable solution, and further refining the physical model resolution may drive more changes in these properties. However, Levy (pers. comm.) found in a similar study that there was little change in bulk properties in a biogeochemical model run at $\frac{1}{9}^o$ and finer. This would point to the possibility that our eddy-permitting model configuration is close to convergence).

Further work would be needed to confirm this.

2.6 Conclusions

We have explored the sensitivity of a diverse marine ecosystem model to the resolution of the coupled physical model. In particular, we have tried to understand what drives differences and similarities in the both bulk biogeochemical properties of the model results such as primary production and phytoplankton biomass, as well as the modelled phytoplankton community structure. We find that some globally integrated values are similar between runs, but that others differ strongly. In fact, there are marked regional differences in the model results for phytoplankton and zooplankton biomass and primary production. These differences are primarily driven by changes in the mixed layer depth, resulting from differences in resoltuion in the model configurations, which in turn affect either the nutrient supply to the surface mixed layer or the light experienced by phytoplankton. Without exploring the regional differences, the globally integrated values may be somewhat misleading. In most cases these regional differences are not unexpected, such as the increase in primary production and phytoplankton biomass in the subtropical gyres already seen in several previous studies [Oschlies and Garçon, 1998, Lévy et al., 2001, McGillicuddy et al., 2003]. However, it is possible that some differences in model results could be due to underlying differences in the structure of the physical models. Deeper mixed layer depths in the high latitudes in the HR model appear to be the result of the way the physical model is parameterized, rather than the increase in resolution. Although ECCO2 is eddy permitting, its grid spacing is only $\sim$ 18km, which may not be enough to effectively resolve mesoscale processes in the high latitudes.

In the higher latitudes, deeper mixed layers in the HR configuration result in increased light limitation. We have shown that in the Northern Hemisphere, this results in a decrease in the magnitude of the spring bloom. This in turn results in reduced zooplankton biomass, and a reduction in surface nutrients as remineralisation by zooplankton is in turn reduced.

One of the most striking results of this study is the robustness of the emergent phytoplankton community. Unlike a previous study comparing complex ecosystem models run with different physics [Sinha et al., 2010], we find that the dominant phytoplankton functional groups and phenotypes remain unchanged between model runs, despite differences in SST and mixed layer depths. By applying concepts from resource competition theory [Tilman et al., 1982, Dutkiewicz et al., 2009], we can explain why in the subtropical gyres, despite increased primary production, the dominant phytoplankton phenotype and the surface concentration of the limiting nutrient remain the same in both configurations. The combination of low seasonality and low grazing pressure means that despite an increased nutrient supply, phytoplankton with the lowest R* will always be selected for in this region.

Given the complexity of our ecosystem model, which incorporates 78 individual phytoplankton types, it may seem surprising that our modelled phytoplankton community structure is so similar in both cases. This presents interesting implications for marine biogeochemical and ecological modelling. It is clear that accuracy in the representation of the physical dynamics of the environment is necessary for effectively modelling ocean biogeochemistry. However, where possible, employing a complex, self-assembling model of the phytoplankton community may avoid some of the pitfalls that have been identified in intermediate complexity ecosystem models which resolve only functional groups and not individual phenotypes. Our higher resoltuion ecological model allows for subtler gradations of change in the community when the environment is changed, whereas in coarser ecological models, regime shifts could easily result. We do not advocate simply tuning parameters to get the "right" result, but rather increasing the physiological parameter space constrained by laboratory and observational work in order to create a more robust phytoplankton community.

Chapter 3

Dispersal, Eddies and the Diversity of Marine Phytoplankton

I co-authoured this draft manuscript with Stephanie Dutkiewicz, Oliver Jahn and Mick Follows, and it will be submitted to Limonology & Oceanography: Fluids and Environments. SD and OJ ran the ecosystem models used here, but I planned and undertook all of the analysis of the results. SD and MF contributed to the writing of this manuscript.

3.1 Abstract

Using a global ocean ecosystem model we examine the role of physical dispersal in regulating patterns of diversity of marine phytoplankton. In a comparison of the same model with different physical resolution, total global diversity, and global patterns of diversity are similar, but swifter current speeds, faster dispersal and increased environmental variability in the higher resolution model enhance local diversity almost everywhere. We explore how diversity is made up of phytoplankton that are either locally viable ("locally-adapted"), or those whose populations are maintained by transport ("immigrants"). Immigrant populations account for a higher proportion of the local diversity in the equatorial and subtropical regions: similar fitness and long exclusion timescales allow intermingling of types from dif-

ferent regions to maintain species richness. In the higher latitudes, diversity is controlled more by locally adpated types. We find significant hotspots of diversity associated with western boundary currents and coastal upwelling regions. The former have high locally-adapted diversity within the core of the current system: though immigration provides a diverse seed population, it is the increased nutrient supplies and the high eddy-induced environmental variability which stimulates the high diversity. Downstream of these regions, once nutrient supplies are used up, we find higher proportion of immigrant-dominated diversity.

3.2 Introduction

Phytoplankton diversity is important for the stability and functioning of the oceanic ecosystem, and by extension, for the ocean carbon cycle. However, the mechanisms regulating phytoplankton biodiversity and its regional patterns are still poorly understood.

3.2.1 Dispersal and Diversity in the Ocean

Dispersal has long been recognised as a population-structuring mechanism in ecology [MacArthur and Wilson, 1967, Chesson, 2000] and several recent studies have pointed to dispersal as a mechanism for sustaining and enhancing regional biodiversity for many types of organisms in a diverse range of aquatic and terrestrial environments [Loreau and Mouquet, 1999, Cadotte, 2006, Gilbert, 2012]. Recent mesocosm studies focused on dispersal and phytoplankton diversity, reveal a range of possibilities, depending on the specific circumstances. Small scale experimental studies have found that, depending on the local environment, dispersal may or may not influence the local community structure [Matthiessen and Hillebrand, 2006, Vanormelingen et al., 2008]. The impact of dispersal is, no doubt, complex depending upon the relative timescales of immigration and exclusion (assuming that speciation acts on much longer timescales than either of these). With respect to more applied studies of in situ oceanic plankton communities the role of transport and connec-

tivity has been most studied in the shelf and coastal environments [Palmer and Strathman, 1981, Cowen et al., 2006, Aiken and Navarrete, 2011]. In contrast, there have been fewer studies addressing the role of physical transport in structuring phytoplankton diversity in the open ocean, but the idealized model of Adjou et al. [2012] provides support for the inference that transport is an important factor in the open-ocean marine system.

Large-scale surveys of marine microbial diversity are still relatively scarce. Microscopic taxonomic analysis of phytoplankton in transects of the Atlantic basin [Cermeño et al., 2008] and North Pacific [Honjo and Okada, 1974] suggest hotspots of high diversity associated with productive regions off the west coast of North Africa, in the Patagonian shelf region, and the Kuroshio Extension. These hotspots, identified from in situ data, are consistent with interpretation of phytoplankton functional groups from remote observations [d'Ovidio et al., 2010]. The hotspots thus appeared to be maintained by immigration, which occurs more rapidly than exclusion in these dynamic regions.

Hotspots of phytoplankton diversity identified in simulations [Barton et al., 2010] and interpreted from remote observations [d'Ovidio et al., 2010] are associated with confluence regions, but these are also typically regimes of instability and enhanced eddy kinetic energy. Fine-scale features of ocean circulation may also play a role in modulating diversity. Several recent modeling studies have focused on the role of mesoscale eddies with horizontal scales on the order of 10-100km and submesoscale features (O($<$1km)), in organizing phytoplankton communities and production [Lévy et al., 2001, Rivière and Pondaven, 2006]. Several have also considered their role in organizing the phytoplankton communities [Bracco et al., 2000, Lima et al., 2002, Perruche et al., 2011]. Bracco et al. [2000] found that two competing phytoplankton types were able to co-exist in an eddying domain, where ring-like eddy structures provided an isolated refuge for the weaker competitor. Observations of plankton communities in a cold-core ring near the Gulf Stream [Ring Group, 1981] are consistent with this notion, as are the interpretations of remote observations of ocean colour by d'Ovidio et al. [2010]. Mesoscale and submesoscale features are also associated with narrower and swifter currents, as well as strong shear, which can increase

the efficiency of dispersal which could also enhance the mingling of populations and local diversity. Thus fine scale features may enhance regional or local diversity by enhancing the niche space and/or by enhancing the mixing of populations. In contrast, the intermittent nutrient supplies which are associated with such features might also drive down diversity by strongly selecting for the fastest-growing opportunist [Levin and Paine, 1974, Barton et al., 2010]. The net influence of the mesoscale and submesoscale is not clear.

To investigate the role of transport and mesoscale motions in regulating patterns of diversity in the phytoplankton we employ global simulations of ocean circulation, nutrient cycles and phytoplankton communities. We quantify the contribution of biological processes and physical transport in maintaining patterns of diversity in the simulations. By comparing simulations which are identical in all respects except for the physical resolution of the ocean circulation, we examine how mesoscale features affect global patterns of diversity.

3.3 Methods

The main tool of this study is a numerical model of global ocean circulation, biogeochemical cycles and plankton populations. We use two physical configurations of the MITgcm ocean model [Marshall et al., 1997] which drives biogeochemical and ecological components as detailed in Dutkiewicz et al. [2009].

3.3.1 Physical Configurations

Two physical configurations of the ocean model are applied in this study, both from the Estimating the Circulation and Climate of the Oceans (ECCO) project. Firstly, we utilize a fine-resolution configuration, ECCO2, which has a cubed-sphere grid with relatively uniform horizontal grid dimensions of about 18km on a side [Menemenlis et al., 2008]. This fine-scale grid resolves mesoscale features (eddies) in the tropics, where the radius of deformation is hundreds of kilometers. It permits, but does not truly resolve such features in

the polar regions, where the radius of deformation is comparable to the grid-scale. In order to elucidate the role of the mesoscale we also use the circulation from a coarser, 1^ox1^o resolution configuration (ECCO-GODAE) [Wunsch and Heimbach, 2007]. Both physical configurations have been integrated from 1992 to 1999, and are constrained to be consistent with observed hydrography and altimetry. We will refer to the ECCO2 high resolution simulation as HR, and the coarse resolution ECCO-GODAE simulation as CR.

3.3.2 Biogeochemical and Ecological Model

As described in Dutkiewicz et al. [2009], we transport inorganic and organic forms of nitrogen, phosphorous, iron and silica, and resolve 78 phytoplankton types and two simple grazers. The biogeochemical and biological tracers interact through the formation, transformation and remineralization of organic matter. Excretion and mortality transfer living organic material into sinking particulate and dissolved organic detritus which are transpired back to inorganic form. The time rate of change in the biomass of each of the modeled phytoplankton types, P_j, is described in terms of a light, temperature and nutrient dependent growth, sinking, grazing, mortality and transport by the fluid flow.

78 phytoplankton types are initialized with a broad range of physiological attributes. The phytoplankton are randomly assigned to one of two broad size classes. Larger cells are assumed to be "opportunists" with higher maximum growth rates but lower nutrient affinities in oligotrophic conditions. Small size class cells are assumed to be "gleaners" with the opposite characteristics. Additional characteristics are assigned stochastically, and include light and temperature sensitivities of growth. Each of the 78 types are initialized at very low, identical biomass in the physical-biogeochemical model and explicit competition selects for the regionally varying community structure over the course of a few years of simulation. To ensure that the ecological components of the fine- and coarse-resolution calculations are identical, we initialize the populations and biogeochemical forcing (incident PAR, aerial iron dust inputs) identically. The physiological parameters of the 78 seeded phytoplankton types are also set to be identical in both integrations. In both cases,

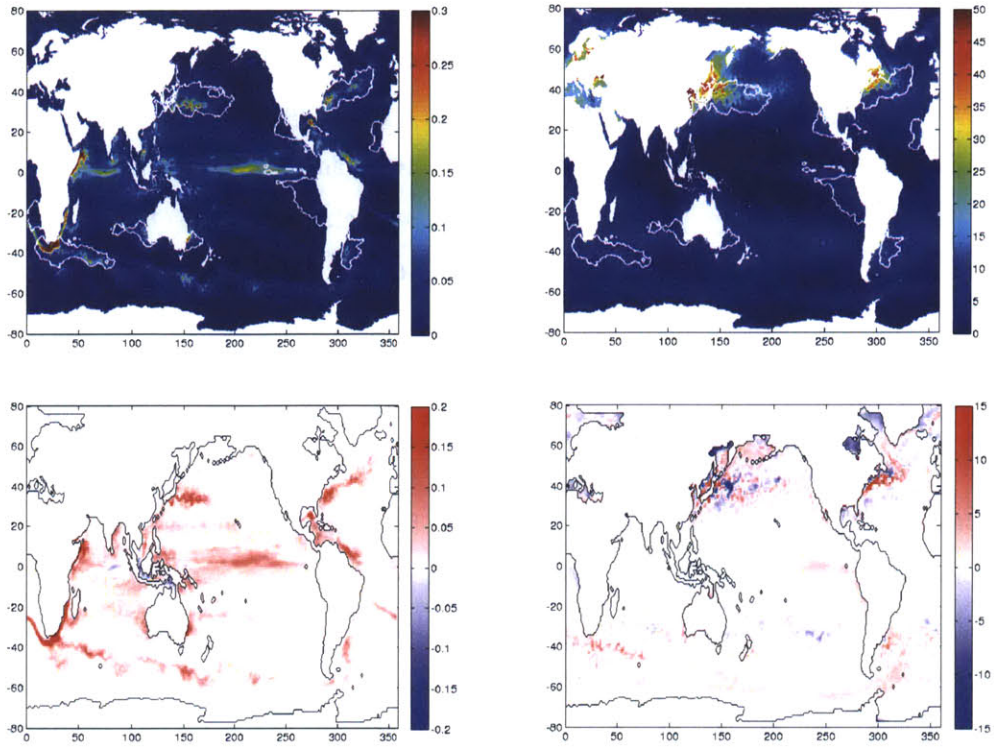

Figure 3-1: Annual EKE ($m^2 s^{-2}$) (top left) and SST variance ($^oC^2$) (top right) in the HR model. White contour lines indicate phytoplankton diversity hotspots. The bottom panels show the difference in EKE (bottom left) and SST (bottom right) variance between the two models (HR-CR).

the model was integrated for 8 years from 1992 to 1999.

3.4 Results

We present and interpret the results from the high-resolution (HR) simulation, comparing and contrasing it with the coarse-resolution (CR) integration. In our analysis we focus on the annually averaged charateristics of the surface layer from the final year of each integrations. Figure 1 shows the eddy kinetic energy (EKE) and the variance of SST in the HR model, and a comparison to the CR run. The higher resolution of the HR run results in much higher levels of EKE than in the CR run. The western boundary currents are more

dynamic, as is the equatorial upwelling region in the Pacific. The variance of SST, also shown in Figure 1, can be seen as a measure of the levels of environmental variability in the surface layer of the oceans. Differences in the levels of SST variance between models closely follow the differences in EKE and show that the environment in the surface ocean of the HR model is far more variable than in the CR model. The largest differences in both SST variance and EKE are found in the temperate higher latitudes, but the lower latitudes in the HR run are also subject to more environmental variability than the CR run.

3.4.1 Modelled phytoplankton diversity

Our basic measure of diversity within each model grid cell is the total number of distinct phytoplankton types persisting with an annual-average biomass that exceeds 0.001% of the total phytoplankton biomass within that grid cell [Barton et al., 2010]. We will use the term diversity throughout to refer to this measure of "model type richness" above the given threshold. Though this measure of local, or α, diversity depends upon a threshold, the inferred patterns and subsequent interpretations are robust provided the threshold remains below $\sim 0.1\%$ of total phytoplankton biomass. Annual-average phytoplankton diversity of both HR and CR simulations is illustrated in Figure 2. There is a strong qualitative agreement between the large-scale patterns, suggesting that, for this system, resolving mesoscale motions has not changed the first-order, large-scale controls on patterns of diversity relative to the coarse-resolution simulations of Barton et al. [2010] and Prowe et al. [2011]. There is a background, meridional gradient of very low diversity in the highly seasonal, subpolar oceans and intermediate diversity in the very stable, sub-tropical and tropical regimes, as discussed in Barton et al. [2010]. Overlain on this background gradient are hotspots of very high relative diversity associated with the Gulf Stream and the Kuroshio, upwelling regions off the west coasts of Africa, South America and North America, and the Agulhas Retroflection and Brazil-Malvinas Confluence zones.

While qualitatively consistent, there are indeed significant differences between the HR and CR simulations, illustrated in figure 2, reflecting the role of physical dynamics not

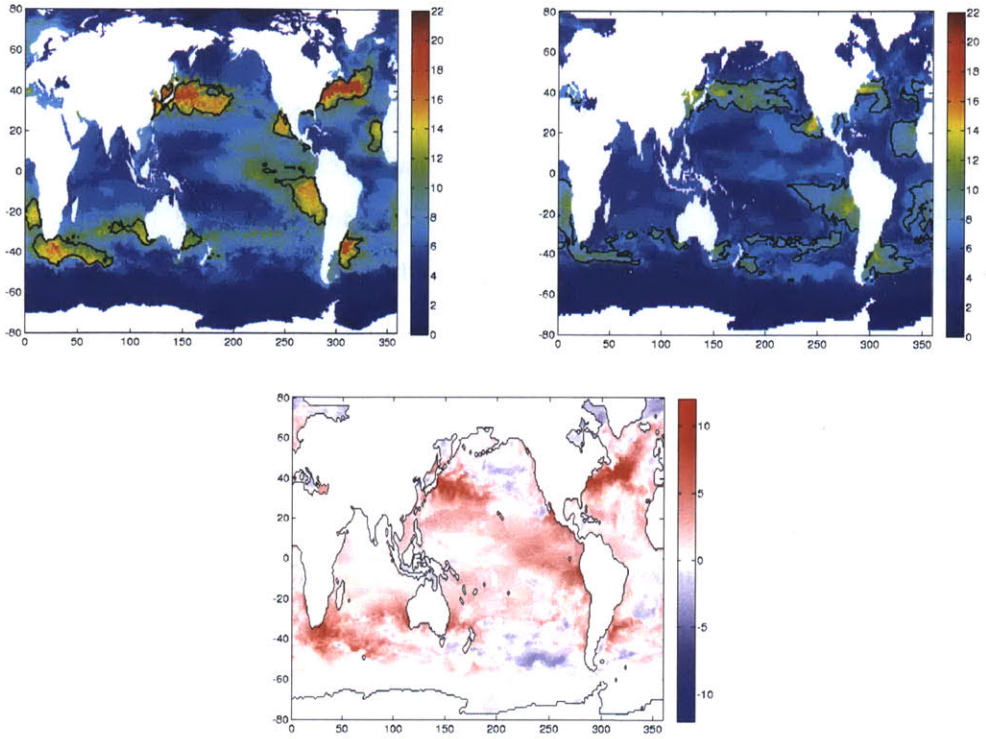

Figure 3-2: Annual average diversity in the surface layer of the HR (left panel) and CR (right panel) simulations, and the difference between the two (HR-CR, lower panel). Diversity here is defined as the total number of phytoplankton types with biomass greater than 0.001% of the total phytoplankton biomass. Black contour lines indicate phytoplankton diversity hotspots in both cases, ($\alpha > 10.2$ for HR and $\alpha > 7.5$ for CR).

resolved in the latter. Notably, local diversity (α) is significantly enhanced almost everywhere in the case where mesoscale motions are resolved. The global mean and standard deviation of diversity in the HR run are both higher, at 6.9 and 3.4 respectively, than in the CR run which has a mean of 5.3 and a standard deviation of 2.3. The largest enhancement is found in the regions where both solutions show their highest diversity: the hotspots. Here diversity, as we have defined it in this study, is increased by as much as a factor of two in the higher resolution integration. The diversity maxima are 22 and 15 in the HR and CR runs, respectively. In this case, we define diversity hotspots as regions where the local diversity (α) is greater than the mean diversity plus one standard deviation. This is somewhat

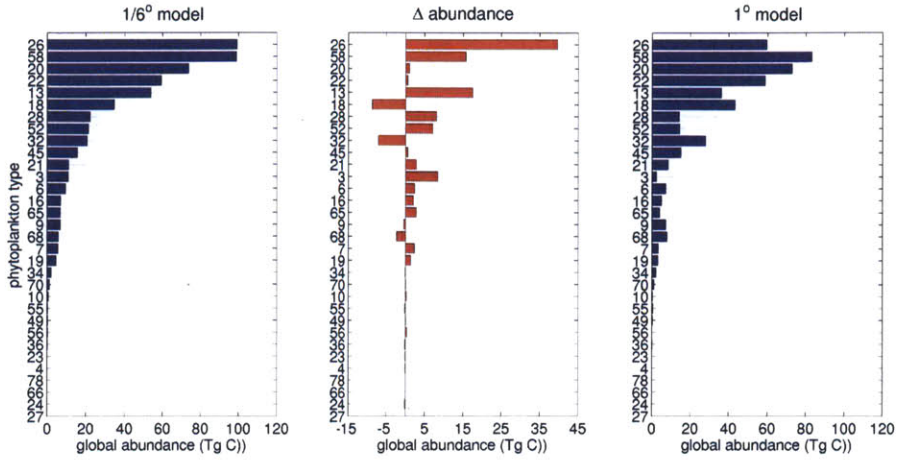

Figure 3-3: The ranking of globally integrated, annual average abundance of phytoplankton types in the high-resolution (HR, left panel) and coarse-resoulution (CR, right panel) simulations, and the difference between the two (HR-CR, bottom panel).

arbitrary, but defines regions with significantly higher levels of diversity than the global mean. Using this convention, we define diversity hotspots in the HR model as regions with $\alpha > 10.2$ and in the CR model as regions with $\alpha > 7.5$. Contours delineating these diversity hotspots are indicated in Figure 2 and occupy similar regions in both models. The area of the hotpots in the HR model are noticeably smaller than in the CR model, but this is the result of the more sharply defined physical features in that model run.

The enhanced diversity in the HR simulation is not because it supports more, or different, phytoplankton types globally. Figure 3 shows the rank of global, annually-averaged abundance of phytoplankton types in the two simulations. Although the key players do not have the same ranking of global abundance in both cases, the global phytoplankton community which contributes to biomass above the chosen threshold criterion is comprised of exactly the same subset of 32 types (of a possible 78). By this criterion, the global richness, or γ-diversity, appears unaffected by the enhanced resolution. Using additive partitioning [Lande, 1996, Veech et al., 2002], we define the β-diversity, $\beta = \gamma - \alpha$, as a measure of the relative local and global diversity; how many types present in the global diversity that are not represented locally. We have shown that increasing the model's physical resolution did

not change γ diversity while α diversity increases over most of the simulated ocean. Hence, β must decrease locally and the local communities from grid-cell to grid-cell will become more similar. Our virtual ocean system behaves consistently with expectations from ecological theory that predict that, as rates of dispersal increase, α diversity will increase while β diversity decreases [Cadotte, 2006]. Here, the increase in physical resolution enhances dispersal rates by narrowing and swiftening boundary currents, and by introducing explicit eddy stirring.

3.4.2 Dynamics and Diversity

We use the ocean simulations, which can be comprehensively and quantitatively analyzed, to ask whether rapid immigration, overpowering exclusion, is the cause of the hot-spots of richness. This framework makes it possible to compare the characteristic time scales of growth and dispersal of the modelled phytoplankton. Within a chosen control area (for the sake of this paper, that area will be a model grid cell) diversity can broadly be influenced in 2 ways: either organisms will actively grow in the grid cell, or will be transported there from outside. The rate of change of phytoplankton biomass of type j, P_j in a grid cell is described by the following prognostic equation:

$$\frac{\partial P_j}{\partial t} = \underbrace{\mu_{NET_j}(I,T,N,Z)P_j}_{\text{LOCAL GROWTH}} - \underbrace{\mathbf{u}.\bigtriangledown P_j + \bigtriangledown.(K \bigtriangledown P_j)}_{\text{TRANSPORT \& MIXING}} \tag{3.1}$$

where $\mu_{NET_j}(I,T,N,Z)$ represents the net local growth rate of phytoplankton j, which is a function of limiting nutrients (N), light levels (I), temperature (T), grazing by zooplankton (Z), and other sources of mortality. The transport term represents the combined effects of advection by the currents, $\mathbf{u}$, and mixing parameterized as a down-gradient diffusion. Both net growth and transport can be either positive or negative, but over sufficiently long time scales (annual or longer) we assume that the system is in steady state, implying that $\frac{\partial P}{\partial t} \simeq 0$. In this case, sources/sinks of phytoplankton biomass from physical processes including transport and diffusion are balanced by sinks/sources of biomass generated by

local net growth. By quantifying the time-mean of μ_{NET_j} for each modeled phytoplankton type we can separate them into two categories at each location, or grid-cell, identified by (x, y): *immigrant* types, defined as those phytoplankton with $\mu_{NET_j}(x, y) < 0$, and *locally-adapted* types defined as those phytoplankton with $\mu_{NET_j}(x, y) > 0$. This is analogous to previous ecological models of source/sink dynamics [Holt, 1985, Pulliam, 1988]. Immigrant types are maintained by a source due to transport from elsewhere, but are not best adapted to local environmental conditions. The source is balanced by a loss due to exclusion and if transport were shut off they would disappear from the local population. Conversely, locally adapted types are thriving in the local environment, which is leading to a net population growth, balanced by an export by advection or mixing. The total, annually-averaged richness at any location, $\alpha(x, y)$ is the sum of contributions from immigrant and locally adapted types; $\alpha(x, y) = \alpha_I(x, y) + \alpha_{LA}(x, y)$. We can evaluate whether diversity at any grid cell is dominated by locally-adapted or immigrant types. This framework allows us to explore questions about the drivers of regional patterns of phytoplankton diversity and to map out regions where either dispersal or local controls are dominant in controlling diversity. This analysis is easily facilitated in the context of the numerical simulations but would be challenging to address with observations of the ocean. Here we will apply this formalism to understand what mechanisms are driving high α in the simulated hotspots. We will also use it to determine the role of mesoscale processes in influencing levels of phytoplankton diversity by comparing our model results from the both physical configurations.

3.4.3 Global distributions of α_I and α_{LA}

We evaluated the annual average μ_{NET} for each phytoplankton type meeting the biomass threshold criterion, then evaluated α_{LA} and α_I at each grid cell, shown in Figure 4. Some clear, large scale patterns emerge: α_{LA} is generally very low in the subtropics and tropics, but elevated in the temperate latitudes and high northern latitudes. α_I is generally low in the subpolar and polar oceans, but elevated over large regions of the tropics and eastern

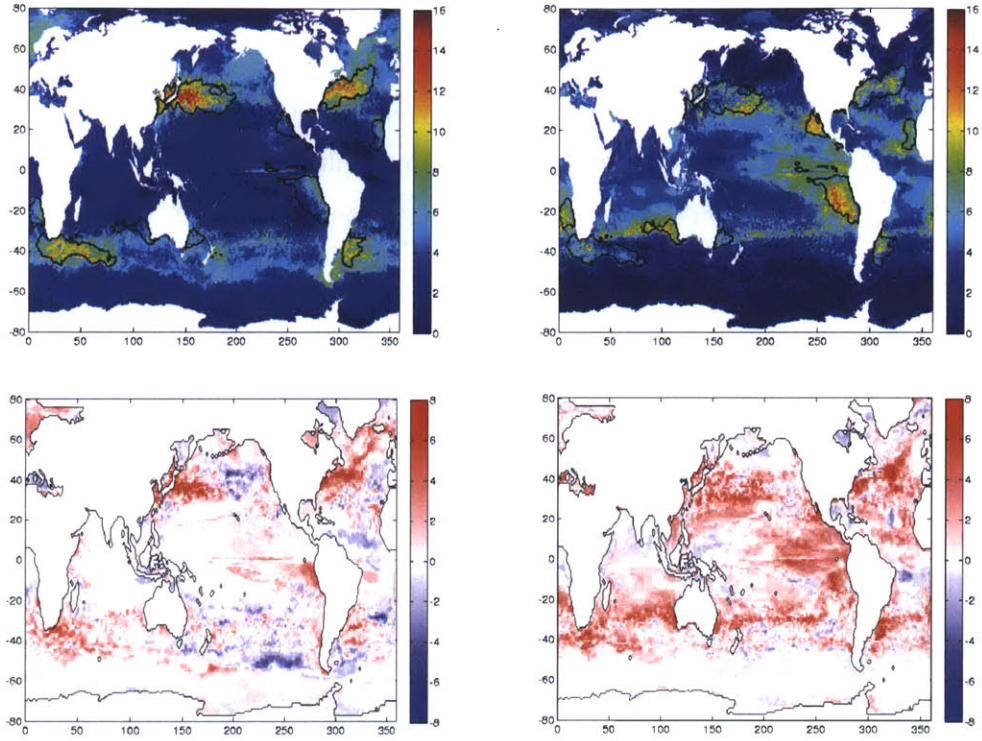

Figure 3-4: The panels in this figure show α_{LA} (top left) and α_I (top right) in the HR run and the difference between the HR and CR runs (bottom panels). Black contour lines on the upper panels indicate the phytoplankton diversity hotspots ($\alpha > 10.2$).

subtropical gyres. Interestingly the hotspots that appear in total diversity, α, are evident in both α_{LA} and α_I distributions; those associated with western boundary currents are generally high α_{LA} regimes and those associated with eastern boundaries and upwellings are mostly regions of high α_I. Comparing the HR and CR models, α_I is greater almost everywhere in the HR solution than in the CR run. There are also marked differences in α_{LA}, but these are far more localised, and strongly associated with diversity hotspots.

In Figure 5 we show the proportion of α_I to the total diversity revealing an even clearer meridional pattern: in the tropics and subtropics diversity is maintained almost entirely by dispersal, where co-occurence is facilitated by immigration and a majority of types present have negative biological population growth. In the subpolar oceans, and notably the Gulf

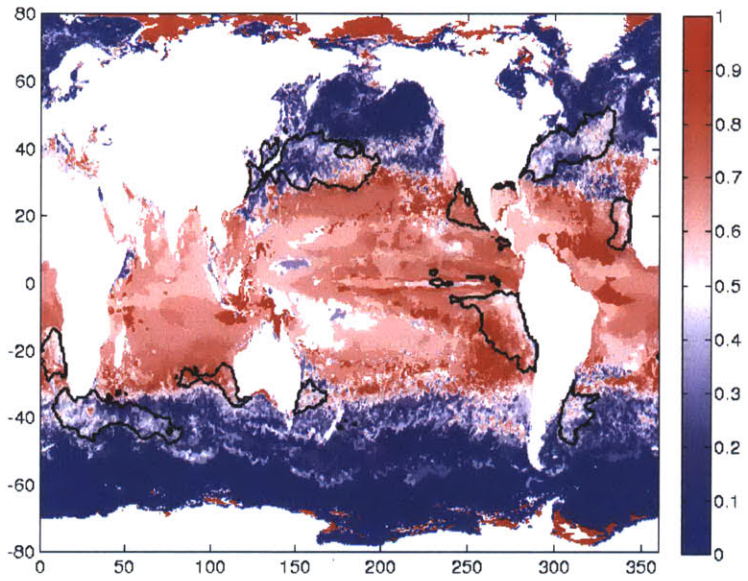

Figure 3-5: Proportion of the total diversity in the HR simulation that can be attributed to α_I. The black contour lines indicate the diversity hotspot regions where $alpha > 10.2$.

Stream and Kuroshio regimes, the opposite is true, these are regimes where most types present have net biological growth and are exported by ocean transport.

3.5 Discussion

Our analysis emphasizes the critical role of transport and dispersal in regulating patterns of biodiversity in the ocean. The simulations suggest that throughout the subtropical oceans, dispersal enhances the diversity of phytoplankton populations, while in the subpolar regions the opposite is the case. The simulations suggest that hotspots fall into two groups, one dominated by dispersal, as expected, and interestingly, another dominated by local growth. Notably, hotspots associated with the Gulf Stream, Kuroshio and the confluence region in the western South Atlantic are dominated by locally-adapted types. Why are there two different types of hotspot, and why are they not all dominated by dispersal? Additionally,

by using two physical frameworks at differing resolution, we are able to isolate the role of the mesoscale in setting patterns of α_I and α_{LA}. Do mesoscale eddies act primarily to enhance stirring and mixing of populations, or do they create environmental heterogeneity which increases the potential niches in the model domain?

3.5.1 Why does dispersal dominate diversity in the subtropics?

The deeply oligotrophic subtropical oceans are populated largely by small cell-types suited to existence at low subsistence concentrations of nutrients, with tightly-coupled losses due to rapid predation as part of the microbial loop [Pomeroy, 1974]. This is captured in the simulations, where the subtropical phytoplankton populations are dominated by the most effective gleaners which have similar fitness, as measured by R*, the subsistence concentration of the limiting nutrient [Dutkiewicz et al., 2009, Barton et al., 2010]. Due to the very similar fitness, exclusion timescales are long relative to transport. Hence, any given virtual "phenotype" in the subtropics may only thrive (have μ_{NET} positive) in a small region of the subtropics, but it will be efficiently transported away from its source region and contribute to local diversity elsewhere in the region. Hence diversity in these regions is dominated by α_I.

3.5.2 What governs the pattern and intensity of hotspots?

Diversity in some hotspots is dominated by α_I (Fig. 4), but other hotspots are instead dominated by locally adapted species, α_{LA}. We explore these two different types of hotspots below.

Locally-driven hotspots

The locally-driven hotspots are largely linked to the Western boundary currents (Gulf Stream, Kuroshio, Malvinas-Brazil, and Aghulas). We maintain that these hotspots require three ingredients to maintain high diversity: 1) confluence of seed populations of

many phytoplankton types from different water masses; 2) injection of nutrients; and 3) large local variability of the environment.

Confluence of phytoplankton types.

These four western boundary regions are indeed confluences of different water masses and their resident phytoplankton populations. The Gulf Stream and Kuroshio mix together waters of subtropical and subpolar origin. The Malvinas-Brazil current brings together Atlantic and Pacific waters. And the Aghulas brings together Atlantic, Indian, and Southern Ocean waters. The strong current systems and associated vigorous mixing brings together many immigrant seed populations from different environments. Yet here, by the metric of $\mu_{net} > 0$, the co-mingled types may originate from immigration, but all have positive net growth in this regions: conditions are favorable for all these types to grow locally.

Nutrient Injection.

The growth of the many disparate immigrant phytoplankton is enhanced as these regions all have an injection of high nutrients relative to surrounding regions. The Gulf Stream and Kuroshio Extension regimes are supplied (in the annual mean) by macro-nutrients from below due to the outcropping of the nutrient streams [Pelegri et al., 1996, Williams et al., 2006]. The Brazil-Malvinas current region brings outcropping of macro-nutrient rich waters from the Pacific basin together with essential iron deposited from the South American continent. The Aghulas hotspot region is fueled by nutrient rich Southern Ocean water. Thus all these "locally-driven" hotspot regions are defined by seed phytoplankton populations from disperse regions being brought into location with enhanced nutrient environment which fuel growth. But why do the many very disparate types (e.g. those warm and cold adapted) all survive?

Variable Enviroments.

These four regions are also associated with high eddy kinetic energy and large SST variance (Fig. 1). Here jet meandering and eddy activity (at least in the HR model where they are resolved) allow for locally variable environments. At any location there will be periods of very different temperature and light regimes. Thus at any time, one population will be favoured over another and will have a positive growth rate; and yet at another time the conditions will favour a different type. Together with the enhanced nutrients, this leads in the annual mean for many types to have a net positive growth rate and hence "locally adapted" diversity. The local diversity is in fact even further enhanced in HR relative to CR: higher eddy kinetic energy suggests even higher variability in the environment potentially leading to more disperate types that can in an annual mean sense co-exist. Eddy activity increases the "potential niche" space in the model, resulting in higher local diversity driven by locally-adapted types.

Dispersal-driven hotspots

The dispersal-driven hotspots appear (Fig. 4) further offshore of the locally-driven hotspots in the western boundary currents and also near key eastern upwelling regions (e.g. North Africa, and North and South America). We illustate two examples; one in the Kuroshio Extension, and another from an upwelling region off the coast of Peru and northern Chile (Fig 6). In both cases we find that the dispersal-driven hotspot is actually downstream (as indicated by the mean surface velocity vectors) of locally-driven diversity regions. In both cases the locally-driven diversity areas upstream are in regions of high nutrient supply. In the case of the Kuroshio, from the outcropping of nutrient streams (see previous section) and in the Peru region from upwelling of nutrient-rich deep waters. In the Kuroshio region the high diversity from the locally-driven hotspot is transported by the jet into region where there is no longer an injection of nutrients. The high diversity in this downstream region is thus maintained only by transport from futher west and the many phytoplankton types all have negative net μ_{NET}. In the Peru region (Fig 6) the locally-adapted species in the

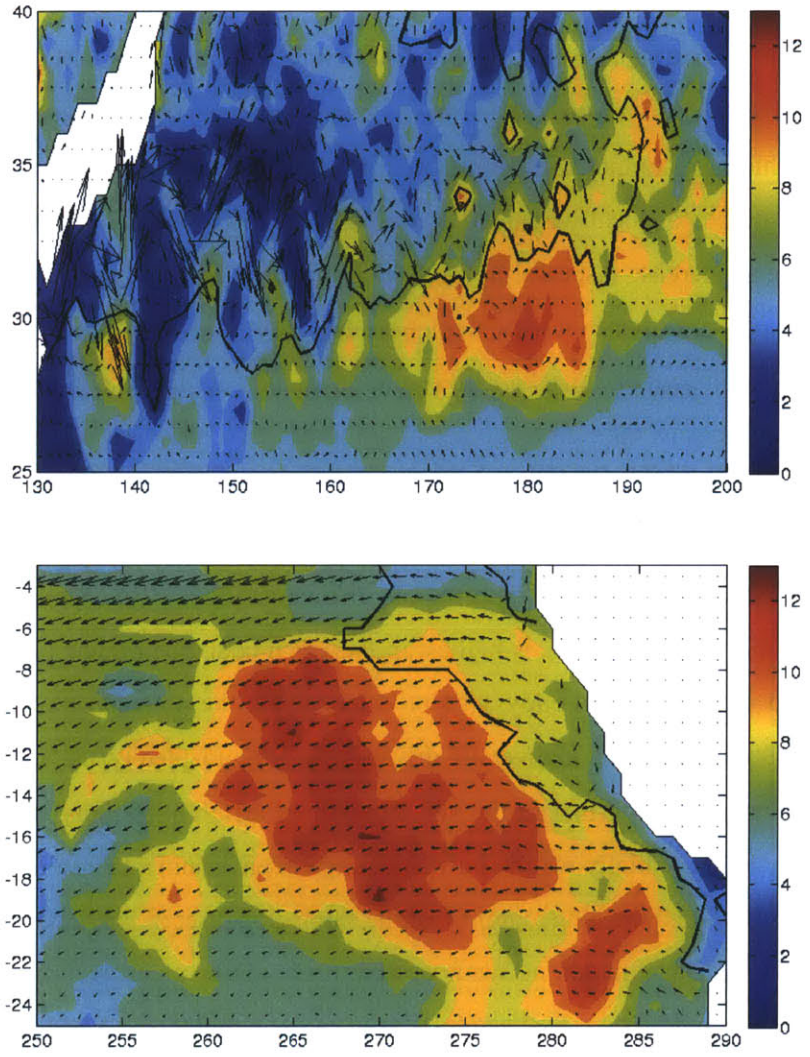

Figure 3-6: α_I (colourmap) with black contour lines at $\alpha_{LA} \geq 6$, the black arrows show the mean surface velocity. Top panel: Kuroshio Extension region. Bottom panel: Chile and Peru coastal upwelling zone.

upwelling region are transported offshore. As the nutrients are stripped out, the net growth rate shifts from positive to negative. This leads to α_I increasing and α_{LA} decreasing further downstream. The new immigrant populations mingle with background species of the subtropical gyre leading to enhanced diversity.

3.5.3 Mesoscale contributions to diversity

We consider two possible roles for mesoscale dynamics in shaping the phytoplankton community. The first is driven by the increased environmental variability (both spatial and temporal), which acts to increase the number of potential niches within a given region. As a result the number of locally-adapted phytoplankton types would increase. The second role would be to increase dispersal in the model domain, as the incorporation of mesocale dynamics results in a more realistic depiction of ocean dynamics, with swifter and narrower currents. This second mechanism results in an increase in the number of immigrant phytoplankton types as the rate of dispersal is increased. These two mechanisms are not mutually exclusive, and we see evidence that both are at play in the HR solutions. Large increases in α_{LA} in the HR model are far more localised and tend to be associated with dynamic regions of the ocean. These regions of increased α_{LA} (see Figure 4) appear to map well onto areas where EKE is highest in the HR model (see Figure 1). These results strongly support the idea that eddy activity is increasing the potential niche space in the model, resulting in higher local diversity driven by locally-adapted types.

It is perhaps surprising that in the HR simulation, different phenotypes were not selected for, since it potentially resolves a wider range of environmental regimes and niches. Instead, it has modified the biogeography of the same global set of phenotypes which were selected for in the CR simulation. We note that this could be an artifact of the somewhat simple model of phytoplankton physiology used in the simulation. Alternatively, regardless of the physiological model, our jump in resolution from 1^o to $1/6^o$ may not have been sufficient to result in a change in the global phytoplankton community.

3.6 Significance to Aquatic Environments

A long standing question in marine ecology has been why phytoplankton populations are so diverse ("The paradox of the plankton" [Hutchinson, 1961]) and what sets the spatial patterns of diversity. There are undoubtably many complementary mechanisms at play,

such as neutral theory [Barton et al., 2010], multiple limiting factors [Tilman et al., 1982], and grazer control [Armstrong, 1994, Prowe et al., 2011, Ward et al., 2012]. Here we concentrate on the role of dispersal and ocean eddies in setting global patterns of diversity in the marine environment. Dispersal allows greater mingling of diverse population, while ocean eddies provide temporally varying temperature and light environments.

We have in particular highlighted the importance of immigrants, whose populations are solely maintained by dispersal, in enhancing diversity in many regions of the ocean. The diversity of the tropics and subtropics of our numerical model simulations was largely controlled by these immigrant populations. Similar fitness and long exclusion times [Barton et al., 2010] allow intermingling of types from different regions and thus enhancing diversity. Immigrant diversity also dominates downstream of high nutrient input regions such as the western boundary currents and coastal upwelling.

Hotspots of diversity have been seen in observations [Honjo and Okada, 1974, Cermeño and Falkowski, 2009, d'Ovidio et al., 2010] associated with western boundary currents. Our model provides a laboratory to explore the mechanisms maintaining this high diversity. Though dispersal is indeed important in supplying diverse seed populations as has been hypothesised [Barton et al., 2010, d'Ovidio et al., 2010], we find here that it is the confluence of higher nutrient supplies and high eddy-induced environmental variability which stimulates the high diversity. Thus, though we emphasize the importance dispersal in mingling populations we have also highlighted the importance of variability of the environment to locally maintain many different phytoplankton types. Regions of the highest eddy kinetic energy and associated largest changes in the temperature and light environment maintain the highest diversity. In the higher resolution model, increased eddy transport and higher variability in environment allows for an increase in both local and immigrant diversity. Our analytical framework, however, does not take into account seasonal variations in diversity, which may be particularly important in the higher latitudes where there is a marked seasonal succession in the phytoplankton community. Further work is needed to address how seasonality and dispersal may interact to shape patterns of diversity on shorter than annual

time scales.

The results of our study argue for closer consideration of locally adapted and immigrant populations in controlling phytoplankton community structure and diversity. Although this may present some challenges in observational studies, we believe that advances are being made in this research area and will soon be able to test some of the predictions of this model study. We see strong potential for this modelling framework to act as a bridge between theory and observations of phytoplankton ecology in the open ocean.

Chapter 4

Fine Scale Phytoplankton Community Structure at the Kuroshio Front

I collected all of the chemical and biological data presented in this chapter during a cruise in 2009 organised by Prof Takeyoshi Nagai (Tokyo University of Marine Science and Technology). He collected all of the physical data and kindly shared it with me for this work. He has also provided many useful comments on the contents of this chapter.

4.1 Abstract

Concurrent physical, chemical and biological observations across the Kuroshio Extension Front provide a detailed view of the relationship between the physical dynamics of the front and the biological and ecological structure of the frontal phytoplankton community. In October 2009, high resolution measurements were taken along transects across the Kuroshio Front between 143°E and 145°E at around 36°N. Using a combination of flow cytometry, microscopy and HPLC pigment analysis we characterize the phytoplankton community structure across the front. We find marked spatial variability in community structure in both the vertical and across-front directions. There is a shift from large abundances of cyanobacteria to the south of the front, to a community more dominated by micro-phytoplankton to

the north. Diatoms are most closely associated with the nutricline north of the front, with dinoflagellates found predominantly near the surface. A cluster analysis of the phytoplankton community data reveals two distinct assemblages, one associated with waters found to the south of the front, and the other associated with waters found to the north. This suggests that cross-front mixing of biological properties is weak relative to local selection. Combining measurements of nitrate concentrations and estimates of the vertical velocities we calculate the advective vertical nitrate flux divergence due to the mesoscale frontal vertical circulation. We find a net upward flux of nitrate north of the front, and a net downward flux of nitrate to the south. There is a signature of lateral isopycnal transport of phytoplankton and dissolved inorganic nutrients on the southern side of the front.

4.2 Introduction

Phytoplankton community structure plays an important role in the biogeochemical cycles of many climatically important elements. Phytoplankton growth and loss processes can act on timescales of days, and can be strongly modulated by the horizontal and vertical motions associated with fronts in the oceans. Oceanic fronts are important and ubiquitous dynamical features in the ocean, with characteristic across-front length scales O(1-10km), that are known to be sites of high biological productivity [Yoder et al., 1994]. Fronts have been shown to be regions where the magnitude of vertical velocities are much larger than elsewhere in the ocean [Pollard and Regier, 1990, Rudnick and Luyten, 1996]. These large vertical velocities may be important in setting the supply of inorganic nutrients from below the mixed layer, as well as controlling the magnitude and variability in the light levels experienced by photoautotrophic cells. Although small compared to the scale of ocean basins, the effect of these features is likely to be important when integrated over the whole [Follows and Marshall, 1994], and the link between these dynamic features and phytoplankton growth and community structure deserves closer study.

The Kuroshio Extension Front is an intense front with zonal velocities O(1 m s^{-1}),

and where turbulent dissipation and mixing are enhanced in the surface boundary layer [D'Asaro et al., 2011, Nagai et al., 2012] by downfront wind stress [Thomas and Lee, 2005] and possibly in the thermocline [Nagai et al., 2009, 2012, Kaneko et al., 2012]. Recent observations in similarly dynamic regions reveal richness in biological and physical structure on lateral scales ranging from metres to kilometres [d'Ovidio et al., 2010, Ribalet et al., 2010, Taylor et al., 2012]. Most previous studies of the Kuroshio region and the Western North Pacific have concentrated on describing the diversity and distribution of microbial and planktonic species at the large scale, illustrating the shift in dominant species with latitude [Odate et al., 1990, Kataoka et al., 2009]. As part of a study of the picoplankton in this region, Odate et al. [1990] observed a shift from cyanobacteria dominated surface waters in the subtropical region of the basin, to picoeukaryote dominated surface waters of the sub-polar region. However these observations were made at intervals of more than 1^o of latitude, effectively missing the finer scale variability associated with the front itself. On the other hand, Yamamoto et al. [1988] conducted a series of three very high resolution (<2km between stations) surveys of the phytoplankton community structure across the Kuroshio, but their sampling was limited to the surface and the larger micro-phytoplankton component of the community. They did observed both the large scale shift from small to large phytoplankton moving northwards across the front, as well as smaller scale variations in diatom and dinoflagellate distributions at the core of the front. Clearly, an integrated, fine scale survey of this region is needed to start to piece together links between the physical circulation and the structure, both cross-front and vertical, of the phytoplankton community.

The phytoplankton community observed along a section across a front results from the combination of several processes, both physical and biological, operating on a wide range of length and time scales. These can be broadly split into small-scale "local" processes, acting on the shortest time and space scales, and large scale "remote" processes associated with much longer characteristic length and time scales, longer than a few days, acting over length scales of 100s km or more. The large scale biogeography of the subtropical and

subpolar gyres, which sets the composition of the phytoplankton community either side of the main stream of the Kuroshio Extension is probably the most important of the remote processes in setting the frontal biogeography. Western boundary current fronts have been shown to act as transport barriers in the surface ocean [Bower et al., 1985, Bower and Lozier, 1994], but it is inclear whether or not they also act as ecological barriers separating the communities either side of the front. Overlain on this background pattern, the stream itself can act to transport phytoplankton far from their point of origin. Coastal species have been observed within the main stream of both the Gulf Stream [Lillibridge et al., 1990] and the Kuroshio [Yamamoto et al., 1988], subtropical species have also been observed in large numbers in a region of the Gulf Stream with environmental conditions were thought to be unfavourable for their growth [Cavender-Bares et al., 2001]. Whether or not these advected and entrained species can continue to actively grow, are removed by grazing or slowly decline as they are transported away from their point of origin, largely depends on the conditions created by local processes as they are transported by the current along the front. We define local processes, as physical and biological processes acting on time scales of a few days, with a length scale set by the cross frontal distance. These include large intermittent nutrient fluxes driven by the ageostrophic vertical circulation and strong mixing events at the front, which in turn fuel primary production. This may favour opportunistic phytoplankton types with faster growth rates, which are better adapted to intermittent nutrient supplies [Margalef, 1968, Tozzi et al., 2004]. The vertical circulation will also act to modulate the light environment of the plankton as they pass through the frontal zone, with strong vertical mixing entraining phytoplankton cells more quickly than they can photo-acclimate [Falkowski and Raven, 2007, Nagai et al., 2003]. This distinction between fast-acting local processes, and slower remote processes is somewhat complicated by the fact that the biological response to physical forcing may be lagged by several days. For instance, Yamazaki et al. [2009] found that chlorophyll patches observed in the main stream of the Kuroshio were driven by inferred nutrient inputs occuring upstream, with a lag time of approximately 3 days.

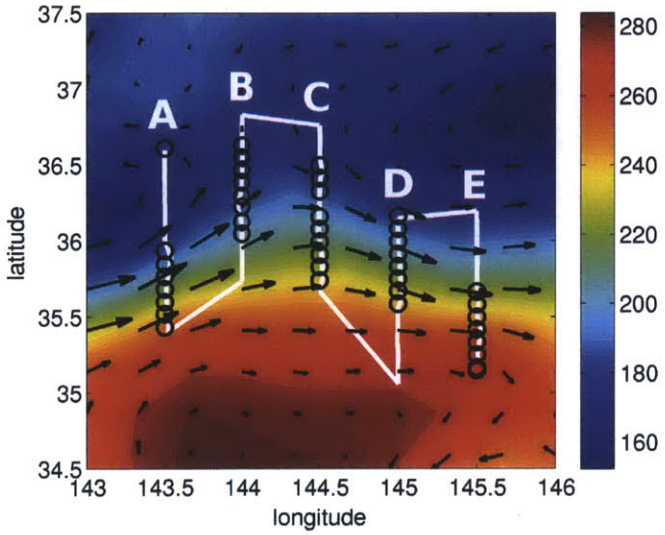

Figure 4-1: Colourmap of sea surface height (cm) for the study area on October 21st 2009, with black arrows showing the geostrophic velocity. The cruise track is overlain with a solid black line, and the open circles show the location of CTD stations.

In this study, we investigate the spatial distribution of phytoplankton along two sections across the Kuroshio Extension Front sampled in October 2009. We use a range of complementary methods to characterize the phytoplankton community: flow cytometry, microscopy and pigment analysis by high-pressure liquid chromatography (HPLC). We place these observations in context with concurrent sampling of inorganic nutrients and hydrography. The results are further analysed in order to try to identify signatures of the local and remote processes decribed above.

4.3 Method

4.3.1 Cruise Outline

Observations were made along 5 north-south transects across the Kuroshio Extension during a cruise aboard the R/V Natsushima (JAMSTEC), October 17-24th 2009. The transects were named A-E from west to east, and their location is shown in figure 4-1. Samples

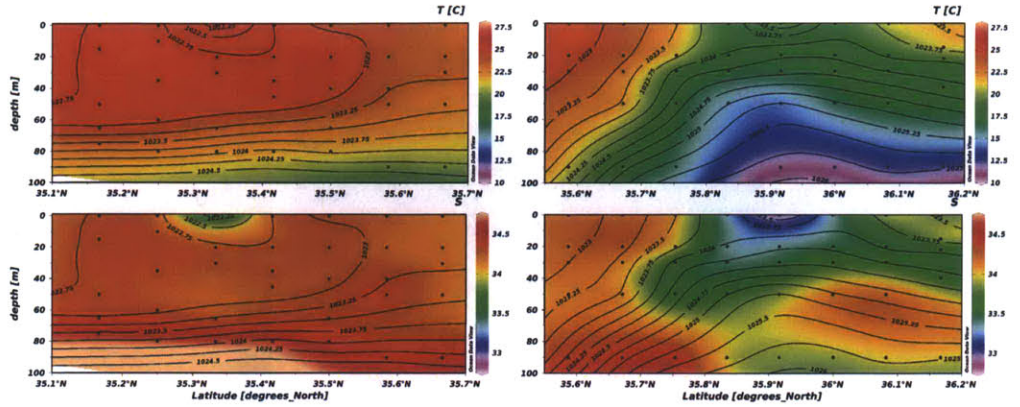

Figure 4-2: Temperature (^{o}C) and salinity sections for transects D and E, with density contours (kg/m^3) overlain in black.

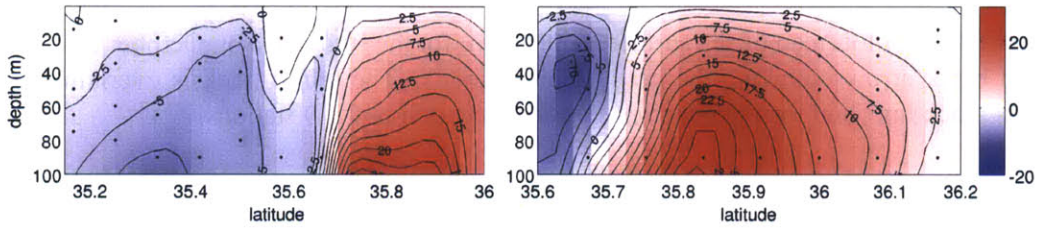

Figure 4-3: Estimates of w (m/day) using the ω-equation, taken from Nagai et al. [2012] for transects D and E.

were collected at 8 stations roughly 9 km apart along each transect. At each station, samples were recovered from 5 depth levels, including the sea surface. Watercolumn samples were obtained using 2-l Niskin bottles mounted onto a rosette sampler along with the CTD, VPR and L-ADCP. Surface samples were obtained with a clean plastic bucket. In addition, XBTs were deployed at 12 stations every 11.1 km along each transect providing temperature data north and south of the CTD stations. The physical oceanographic features of the study region during this cruise are described in detail in Nagai et al. [2012], but we give a brief description of the physical setting below.

We collected samples along all transects, but restrict our analysis to the final two sections, D and E, for which we have a complete set of chemical and biological data. Although not centered exactly on the core of the front, in both transects, we sampled part of the high

velocity core of the Kuroshio current. Transect D is offset to the north of the front, whereas transect E is offset to the south, as shown in the sea surface height shown in figure 4-1 and the respective temperature and salinity sections shown in figure 4-2. Thus we have observations from both the subtropical Kuroshio water south of the front, and the colder Oyashio water and mixed water found to the north. Kuroshio water is typically saltier with a characteristic salinity, S$>$ 34.2, whereas Oyashio water is fresher with S$<$ 33.5 [Qiu, 2001]. While it is clear from the salinity sections that transect E is dominated by Kuroshio water, transect D, on the other hand has a core of Oyashio water at the surface just north the core of the front as well as Kuroshio water coming in from the south. This input of Oyashio water to the frontal region has been observed in previous studies of this region [Yamamoto et al., 1988] and may play an important role in transporting in nutrients and plankton. Nagai et al. [2012] calculated the inferred mesoscale vertical velocities along these two sections, shown in figure 4-3, using the QG ω-equation, and found that there was an upwelling tendency north of the front, and downwelling to the south. This is as we would expect given that the front was transitioning from a meander trough to a meander crest from transect D to transect E [Nagai et al., 2012]. However, given that this is a region where the Rossby number is large, the vertical velocities obtained using the QG ω-equation should only be used to provide an indication of the patterns of up- and downwelling, rather than accurate values of the vertical velocities.

4.3.2 Picoplankton analysis by FCM

We followed the protocol outlined in Malmstrom et al. [2010] for sample collection and analysis. Whole seawater samples were collected and immediately fixed with gluteraldehyde (at a final concentration of 0.125% v/v), kept in the dark for 10 minutes, frozen in liquid nitrogen and stored at -80C until they could be analysed. We conducted the analysis using the Chisholm Lab's Cytopeia Influx flow cytometer at MIT. *Prochlorococcus*, *Synechococcus* and picoeukaryote populations were identified and quantified based on their unique autofluorescence and scatter signals [Olson et al., 1990a,b], using FlowJo software

Table 4.1: The names, abbreviations and taxonomic designations for the phytoplankton pigments measured by HPLC [Jeffrey et al., 2005].

Symbol	Pigment	Designation
Chla	Chlorophyll a	
Chlb	Chlorophyll b	Chlorophytes
DVChla	divinyl Chl a	Prochlorophytes
Allo	Alloxanthin	Cryptophytes
But	19'-butanoxyloxyfucoxanthin	Haptophytes
Caro	Carotenes	
Diad	Diadinoxanthin	
Diat	Diatoxanthin	
Fuco	Fucoxanthin	Diatoms
Hex	19'-hexanoyloxyfucoxanthin	Haptophytes
Peri	Peridinin	Dinoflagellates
Zea	Zeaxanthin	Cyanophytes and prochlorophytes
Pheoa	Pheophytin a	Copepod grazing pellets
Phidea	Pheophorbide a	Protozoan faecal pellets
TChla	Total chlorophyll a	Chla + DVChla
PPC	Photoprotective carotenoids	Allo + Caro + Diad + Diato + Zea
PSC	Photosynthetic carotenoids	But + Fuco + Hex + Peri

(Tree Star, Inc., www.flowjo.com).

4.3.3 Microscope analysis of microplankton

We collected 500ml of whole seawater from each depth level and fixed it with formaldehyde. The identification of the micro-phytoplankton by microscopy was contracted out to the Japanese firm, PlantBio (www.plantbio.com). PlantBio followed Sukhanova [1978]'s protocol for sedimenting and concentrating seawater samples prior to subsampling and microscope identification. PlantBio provided us with cell counts for each station/depth level for all of the species identified organized by group for diatoms, dinoflagellates and silicoflagellates. Total cell numbers are given for groups of smaller phytoplankton, haptophytes, prasinophytes and euglenophytes, but not identified to genus or species level.

4.3.4 HPLC analysis

Whole seawater collected from each depth level sampled and filtered onto 25mm Whatmann GF/F filters which were then frozen at -80C until they could be analysed on shore. The samples were sent to the Horn Point Marine Laboratory at the University of Maryland for HPLC analysis following standard protocols [Hooker et al., 2005]. They provided us with data on the concentrations of a full suite of accessory pigments listed in table 4.1 for each station/depth level.

4.3.5 Dissolved nutrients

Whole seawater was collected from each sample depth, filtered with 25mm Whatmann GF/F filters, collected into 50ml plastic bottles and stored frozen at -20C until it could be analysed back on shore. We subcontracted the analysis of these samples to the Water Quality Analysis Laboratory at the University of New Hampshire. They analysed the samples for nitrate + nitrite, phosphate, silicate and ammonia using standard wet chemistry methods.

4.3.6 Mapping the data

We used Ocean Data View (ODV4) [Schlitzer, 2012] to make the visualisations of the biological and chemical properties measured in our study area. The DIVA gridding option was used in order to optimally interpolate between data points spaced at variable intervals in the vertical and horizontal.

4.4 Results

In this section we present the data collected during the cruise. Given the location of transects D and E relative to the core of the front, we approach them as a southward (transect E) and northward (transect D) extension of each other. We present the data from both transects

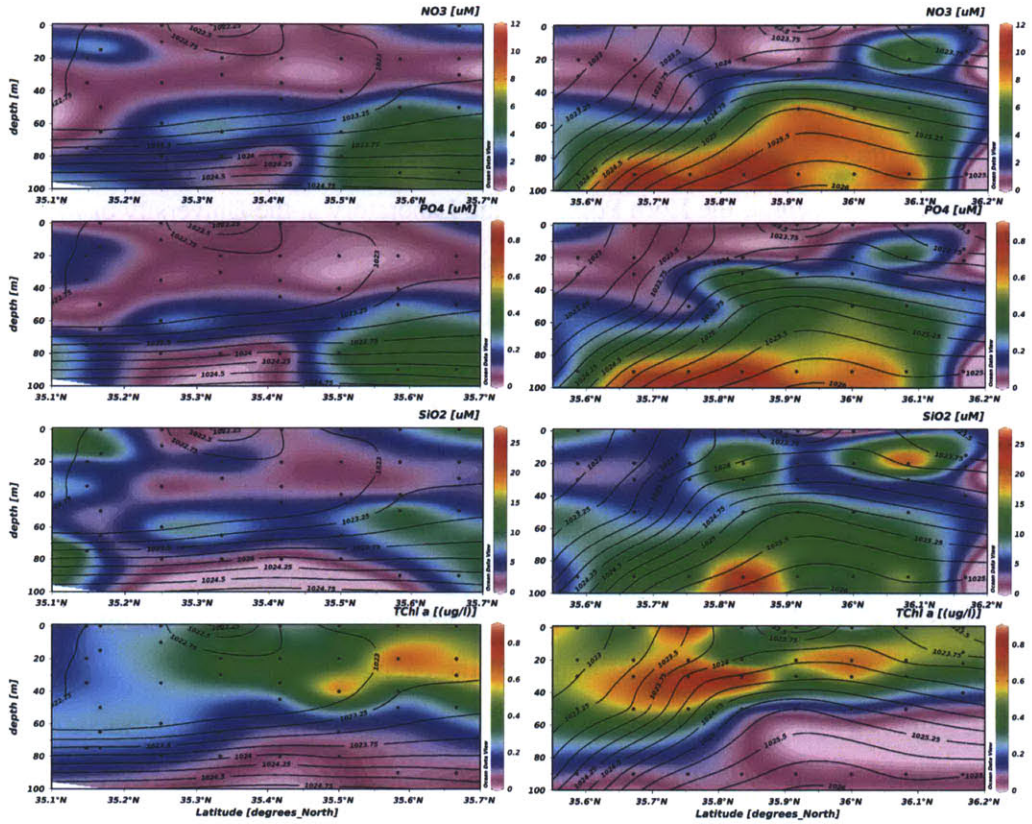

Figure 4-4: Sections of the concentration of, from top to bottom, nitrate, phosphate, silicate and chlorophyll a (TChla). Inorganic nutrients are in units of μM and chlorophyll a is in units of $\mu g/l$. Density contours are overlain as solid black lines.

together, and arrange the figures such that the data from transect E is on the left and transect D on the right, so that they can be read left to right from south to north. This provides a useful context for viewing and understanding the spatial patterns in the data.

4.4.1 Inorganic Nutrients and Chlorophyll

The distribution of nitrate, phosphate and silicate for both transects are shown in figure 4-4. In both transects, nitrate, phosphate and silicate all follow very similar distributions, as might be expected. Concentrations of nitrate, phosphate and silicate are all higher in the surface mixed layer to the north of the front (transect D) than to the south (transect E). The

nutricline is found at about 50m depth to the north of the front in transect D, and at about 80m depth to the south of the front in transect E. There is a pronounced doming upward of the nutricline at the core of the front, seen in both transects, occuring at about 35.9°N in transect D and at the northern most edge of transect E, around 35.6°N. The domed nutricline reaches to about 40m in transect D, and 70m in transect E, although it is very likely that our sampling was too far south of the core of the front on transect E to capture the feature fully.

We observe some fine structure in the nutrient distributions overlaid on the background pattern described above. Most notably, in transect E, there is an inversion in the concentrations of nitrate, phosphate and silicate at around 60m depth, extending from at least 35.25°N to 35.35°N. Nitrate concentrations in this inversion are at about $3\mu M$, whereas above and below, they are closer to 1-1.5μM. This nutrient "tongue" appears to be found between the 1023 and 1023.5 kg/m^3 density surfaces. Another, less pronounced nutrient inversion can be observed at the northern edge of transect D at about 20m depth. In this case, nitrate, phosphate and silicate are all elevated in concentration at 20m compared to the surface and the next sampled depth at 30m. This feature is only resolved by one station, so it is impossible to tell its lateral extent. We note that Baird et al. [2008] observed a similar feature in nitrate distributions in two of the transects of their high resolution survey of the Tasman Front, and that Yamamoto et al. [1988] and Ishizaka et al. [1994] also observed similar features in their respective datasets at the Kuroshio Extension, but none of these authors discussed this unusual feature in their nitrate data.

Chlorophyll (TChl a) concentrations, also shown in figure 4-4, are highest at the core of the front. Maximal chlorophyll concentrations of 0.63μg/l can be found on the southern edge of transect D, at a depth of about 30m, abutting the southern side of the domed up nutricline. The maximal chlorophyll concentration in transect E is also high at 0.55μg/l, at the northernmost edge of the section at 20m depth. High chlorophyll concentrations extend to the surface at the core of the front, where the isopycnals outcrop. Directly to the south of the front in transect E, we observe elevated chlorophyll concentrations between the surface

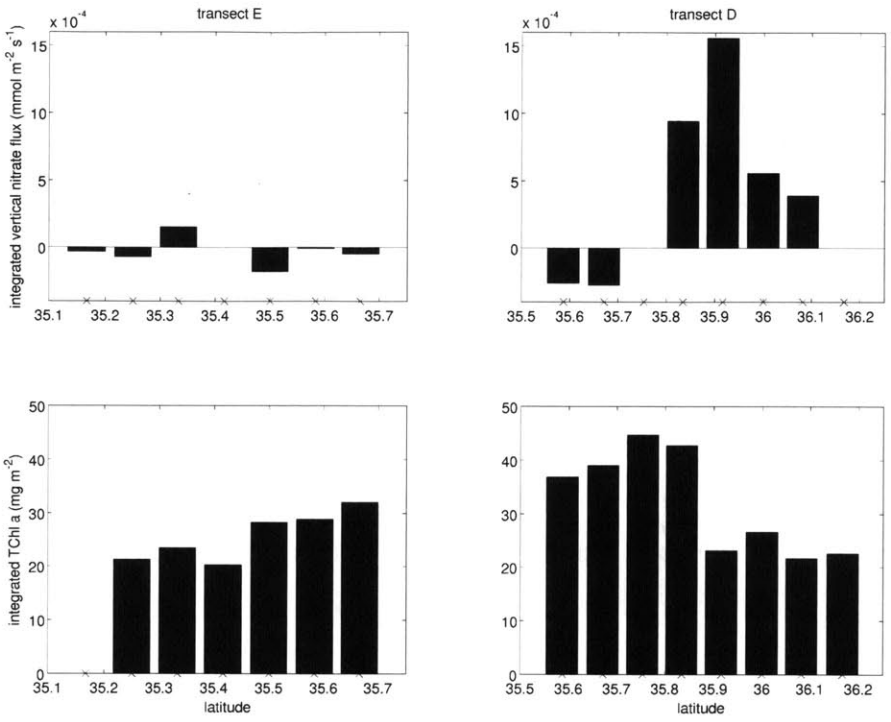

Figure 4-5: Top panel: depth integrated advective vertical nitrate flux divergence (mmol m^{-2} s^{-1}) in the top 70m of the watercolumn. Bottom panel: depth integrated chlorophyll (mg m^{-2}) in the top 90m of the water column. The location of the stations are shown as crosses along the x-axis.

and 40m, and extend southwards to at least 35.25^{o}N. At the southern end of transect E, chlorophyll concentrations are quite consistent in the top 60m of the watercolumn, declining to very low concentrations below that depth. To the north of the front, in transect D, the chlorophyll distribution appears patchier, with elevated concentrations persisting to the northernmost edge of the transect in the top 50-60m of the watercolumn. Below the 1025 kg/m^3 density surface, chlorophyll declines to very low concentrations.

Using the vertical velocities inferred by Nagai et al. [2012] using the QG ω equation, we have estimated the mesoscale advective vertical nitrate flux divergence ($w\frac{dNO_3}{dz}$) for each station with sufficient data coverage, at the mid-point between data points. We integrated

the values for $w\frac{dNO_3}{dz}$ over the uppermost 70m of the water column, as well as calculating integrated TChla for the top 90m of the water column, shown in figure 4-5. Integrated values of $w\frac{dNO_3}{dz}$ are highest just north of the front at around 35.9°N decreasing either side, and becoming negative south of 35.7°N. South of the front, along transect E, the integrated nitrate flux is much smaller and consistently negative with the exception of the station (38) at 35.3°N, which coincides with the location of the nutrient inversion. The highest integrated values of chlorophyll at 45mg m^{-2} are found just to the south of the highest nitrate fluxes, at 35.75°N. Integrated chlorophyll concentrations decrease to the north and south of this point, with the lowest integrated chlorophyll concentration found to the south of the front along at transect E at 35.4°N, with a value of 20mg m^{-2}. Similarly low values are found at the northernmost end of transect D. We note that these values should not be treated as accurate calculations of the vertical nitrate flux divergence, given the errors associated with using the QG ω equation in regions like the Kuroshio Extension, which have a high Rossby number. However, we do believe that these results can give us an indication of how the vertical nutrient fluxes relate to patterns in phytoplankton biomass.

4.4.2 Phytoplankton Community Structure

Picoplankton

The abundances of picoplankton are shown in figure 4-6. There is a high degree of spatial variability in their distributions in both the across-front and vertical directions. *Prochlorococcus* and *Synechococcus* are found at their largest abundances to the south of the front in both sections D and E. *Prochlorococcus* dominates at the extreme southern ends of the transects, with a progression to higher *Synechococcus* abundances closer to the core of the front. In section D, *Synechococcus* occurs either side of the core of the front, with abundance maxima found either side of the 1023.75 kg/m^3 density surface, in the top 40m of the watercolumn. This area of high *Synechococcus* abundance to the north of the front is located just above the domed-up nutricline where concentrations of nitrate and phos-

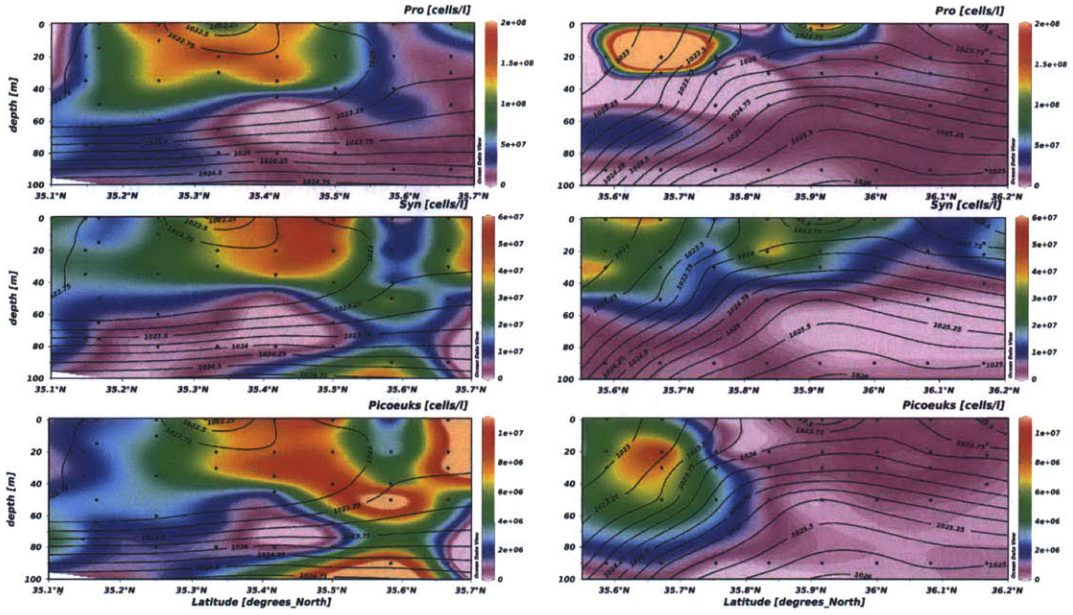

Figure 4-6: Sections of the abundance of, from top to bottom, *Prochlorococcus*, *Synechococcus* and picoeukaryotes all in units of cells/l. Density contours are overlain as solid black lines.

phate are elevated compared to the same depth either side of the front. Picoeukaryotes are also found at their largest abundances to the south of the front, although their abundance maxima appear to coincide with the core of the front in section D, rather than offest like *Synechococcus*.

Micro-phytoplankton

From the microscopy, we have abundance estimates for over 50 species of phytoplankton observed in the study region. However, in this section we present the distributions of these species by functional group: diatoms, dinoflagellates and haptophytes. We aggregate the cell counts in each group in order to get the total abundance in each case. The distributions of these three groups of micro-phytoplankton are shown in figure 4-7. The micro-phytoplankton types are found predominantly at and to the north of the core of the front. Diatoms and dinoflagellates have noticeably patchier distributions than the picoplankton

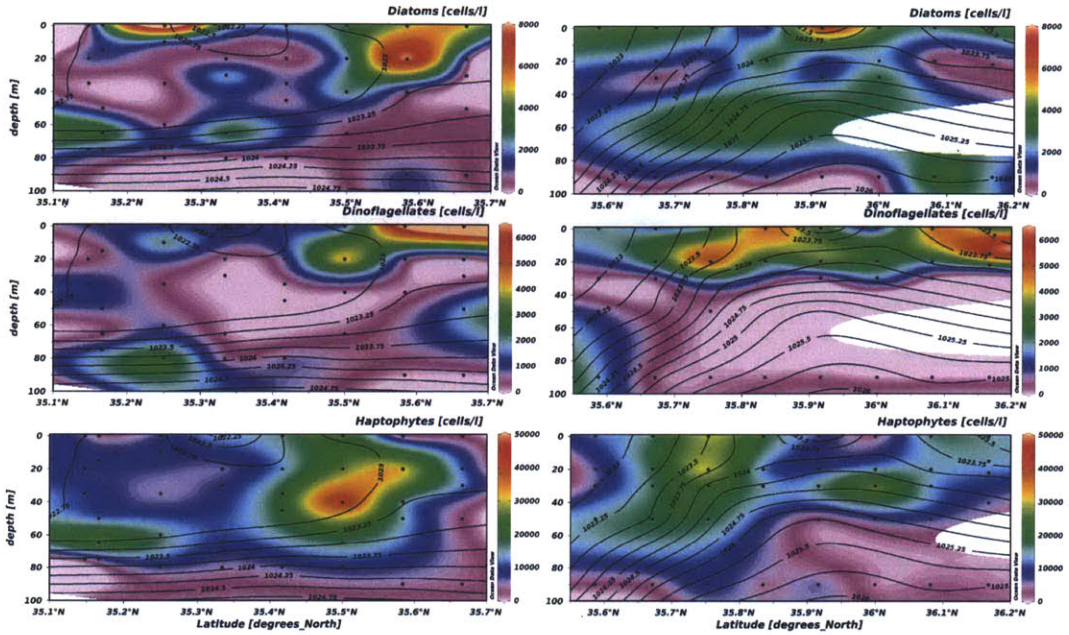

Figure 4-7: Sections of the abundance of, from top to bottom, diatoms, dinoflagellates and haptophytes all in units of cells/l. Density contours are overlain as solid black lines.

and haptopytes. The haptophytes are the most closely associated with the front itself, in transect D, their highest abundance (45600 cell/l) is found at about 35.7^{o}N at 20m depth, where the isopycnals are at their steepest. Diatoms and dinoflagellates, although present at the front, are more abundant to the north. In transect D, diatoms are predominantly found directly above the domed nutricline. There is a diatom abundance maximum at the surface at about 35.9^{o}N, associated with a lens of lower salinity water (see fig. 4-2). In transect E, diatoms are mostly confined to the surface in patches, but they are also found along the 1023.25 kg/m^3 isopycnal, where the nutrient "tongue" is also observed. Dinoflagellates are confined to the top 40m of the water column in transect D, whereas they are found mostly confined to the surface in transect E, with the exception of a patch at 80m depth on the southern edge of the transect. In the close vicinity of the front, diatoms appear to be present where dinoflagellates are absent and vice versa, however this is not the case along transect E, where diatom and dinoflagellate maxima co-occur near the surface at the northern edge of the transect. *Synechococcus* abundance is also lower where dinoflagel-

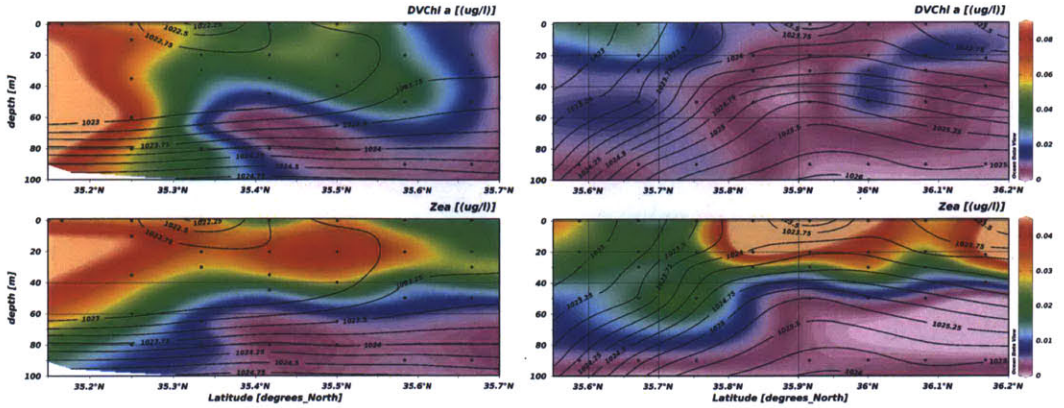

Figure 4-8: Sections of the abundance of, from top to bottom, divinyl chlorophyll a and zeaxanthin, all in units of $\mu g/l$. Density contours are overlain as solid black lines.

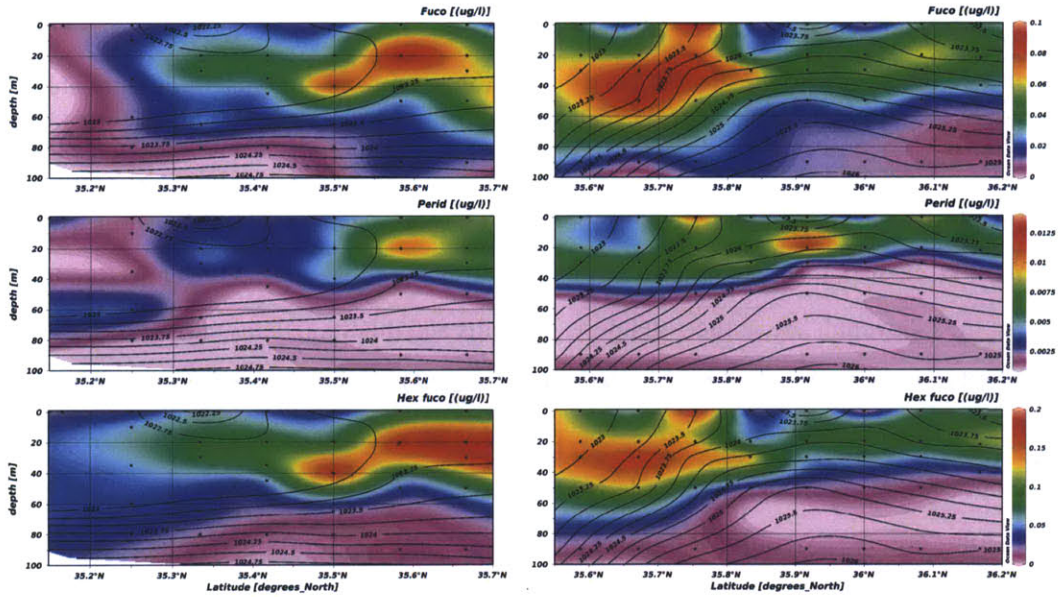

Figure 4-9: Sections of the abundance of, from top to bottom, fucoxanthin, peridinin and 19'-hexanoyloxyfucoxanthin, all in units of $\mu g/l$. Density contours are overlain as solid black lines.

lates are present at the front. In general, we see that the abundance maxima of different phytoplankton types do not tend to co-occur.

Marker pigments

In addition to the flow cytometry and microscopy data described above, we use the distributions of phytoplankton marker pigments to map the distributions of the major phytoplankton functional groups in our study region. We show the distributions of divinyl chlorophyll a and zeaxanthin in figure 4-8, and fucoxanthin (fuco), peridinin (perid), 19'-hexanoyloxyfucoxanthin (hex) in figure 4-9.

DVChla, the marker pigment for *Prochlorococcus*, corresponds well to the distribution of *Prochlorococcus* derived from the flow cytometry. The highest concentrations of DVChla are found at the southern end of transect E at around 60m depth, although the southernmost two stations along that transect have high DVChla concentrations extending from the surface down to about 80m depth. DVChla concentrations decrease northwards along transect E, and are mostly low along transect D, with the exception of a patch of higher concentrations between 35.6^{o}N and 35.75^{o}N in the top 20m, which corresponds to a patch of high *Prochlorococcus* abundance. We also see a patch of higher DVChla levels at the northern end of transect D that coincides with a region where *Prochlorococcus* abundance is lower than in the vicinity of the front, but with cell counts still O(10^6 - 10^7 cells/l). This patch of higher DVChla appears to coincide somewhat with a part of the section D influenced by the warm filament north of the front observed during the cruise.

Zeaxanthin, a marker pigment for cyanobacteria, which should reflect the distributions of both *Synechococcus* and *Prochlorococcus* appears to correspond well to their distributions. Maximum concentrations of zea are found along transecct D in the top 20m of the water column between 35.84^{o}N and 36^{o}N. This coincides with high abundances of *Prochlorococcus* and *Synechococcus*, right at the core of the front. High concentrations of zea can also be found in the top 20m at the northern end of section D, where we graze the edge of a warm filament extending north of the front. This feature is associated with higher abundances of *Synechococcus*. Zea is also very high at the southern edge of transect D, throughout the water column, with the highest concentrations confined to the top 40m of the water column as you move northwards along trasenct E. This pattern corresponds well

to the *Prochlorococcus* distribution at the southern end of transect E, moving into a more *Synechococcus* dominated area found further to the north along that transect.

Hex is the characteristic marker pigment for haptophytes. It's highest concentrations are found in the top 60m of the water column at the core of the front, at around 35.7^{o}N along transect D. It extends northwards to the end of transect D, but it mostly confined to the top 40m, with the exception of a surface patch centered around 36^{o}N where it is altogether absent, in line with the microscopy data on haptophyte distributions. South of the front, the highest concentrations of hex found in the top 50m of the water column between 35.4^{o}N and 35.7^{o}N, correspond to the region with the highest concentration of haptophyte cells observed during the cruise. Concentrations of hex fuco decrease southwards and with depth from this concentration maximum along the remainder of transect E.

Fucoxanthin, the marker pigment for diatoms, although broadly consistent, shows some marked inconsistencies with the microscopy-derived distributions. The highest concentrations of fuco are found in the top 50m at the southern end of transect D, and in the top 20m of the northern end of transect E. This is generally consistent with the observations showing large abundances of diatoms in the same area, close to the core of the front. We do see a patch of lower diatom abundance at 30m depth at 35.67^{o}N along transect D, which coincides with high fuco concentrations. Fuco concentrations decrease northwards away from the front along transect D, and southwards away from the front along section E. High diatom concentrations associated with the lens of lighter water at 35.91^{o}N are not associated with a high fuco concentration, although this is most likely due to the fact that the population of diatoms found within this feature are confined to a shallow well-lit surface layer of water and do not require high levels of fuco for photosynthesis. Similarly, a patch of high diatom abundance at the surface at 35.25^{o}N along transect E is not associated with a high concentration of fuco. The deeper patches of diatoms at the southern end of transect E at around 60m, and at 36.1^{o}N at the northern end of transect D at 90m, are also associated with quite low concentrations of of fuco (0.01-0.02 μg/l).

Dinoflagellates are generally difficult to identify using marker pigments [Roy et al.,

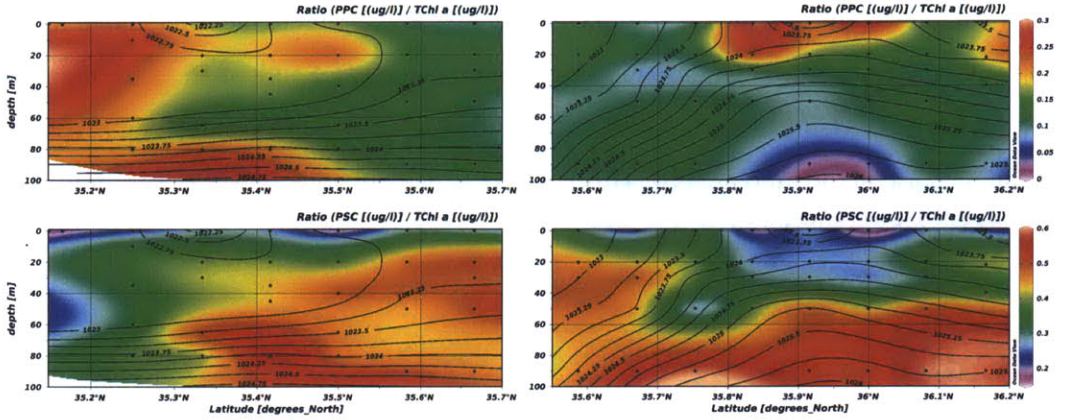

Figure 4-10: The top panels show PPC:TChl a, and the bottom panels show PSC:TChl a for setions D (left) and E (right). Density contours are overlain as solid black lines.

2011], but peridinin is a characteristic marker pigment for some autotrophic dinoflagellates. We find that like the dinoflagellate distributions, peridinin is found predominantly in the top 40m of the water column across both transects. The maximum concentration of peridinin is found to the north of the front at 35.9^{o}N at 20m along transect D, but this does not coincide with the maximal abundance of dinoflagellate cells. This is most likely due to the fact that peridinin is a marker for only a portion of dinoflagellates, whereas the cell abundances are an aggregate of all dinoflagellates. There is a patch of peridinin at 35.25^{o}N at 60m at the southern end of transect E, which corresponds to a patch of dinoflagellate cells found there.

Photosynthetic and photoprotective pigments

We calculate the ratios of the photoprotective carotenoids (PPC) and photosynthetic carotenoids (PSC) to chlorophyll, shown in figure 4-10. We observe vertical and horizontal variations in both of these pigment ratios in both transects. The stations closest to the front show little vertical variation in PPC:TChla, although PSC:TChla shows slightly more vertical variation, with a lower of values of PSC:TChla in the surface samples. To the north of the front, along transect D, both ratios vary much more markedly in the vertical. The stations with the most pronounced vertical structure are found between 35.8^{o}N and 36^{o}N. High values of PPC:TChla, up to 0.3, are associated with a lens of fresher water at the surface. Associated

with the same feature, values of PSC:TChla are very low. South of the front, along transect E, the vertical structure is less pronounced than in transect D. South of 35.55^{o}N, there is an increase in PPC:TChla in the top 20m, with lower values found below that depth, followed by an increase in the ratio at 80m. This increase is probably due in part to very low values of TChla at the same data points.

4.5 Discussion

We discuss the data described above in the context of trying to identify features of the community that are shaped by either local or remote processes.

4.5.1 Phytoplankton frontal biogeography

Following Yamamoto et al. [1988], we compare the phytoplankton species distribution at each data point using the dissimilarity of the squared Euclidean distance between data points. The dendrogram showing the groupings within the phytoplankton community across the front (figure 4-11) was prepared using the Ward method. Due to the number of data points analysed, the leaf nodes at the base of the dendrogram represent multiple data points. The data points fall into 2 distinct groups, mapped back onto the transects, which appear to be largely separated by the front. Some data points at the northern end of transect D belong to the same grouping as the data points to the south of the front in transect E. We speculate that this is most likely due to the presence of a warm filament north of the front during the study period, and there may be some intermingling of the two water masses in this region. Although confined to the northernmost part of section D, there is an increase in surface water temperatures north of 36^{o}N, which coincide with the part of transect D where the two communities are mingled. This result appears to suggest that there is limited mixing of phytoplankton populations across the front.

Our cluster analysis of the phytoplankton abundance data, taking into account all of the phytoplankton species identified by microscopy and flow cytometry, suggests that the

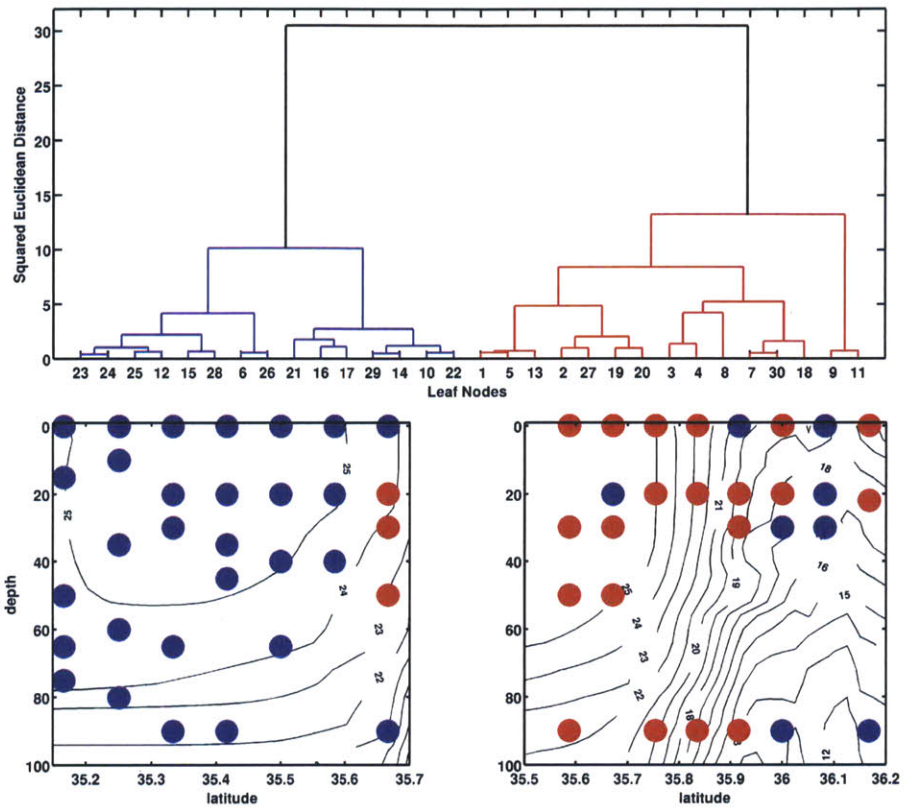

Figure 4-11: Top panel: dendrogram showing the phytoplankton community structure in the study area, using combined data from both transects D and E. Each leaf node represents several data points. Bottom panel: transects showing the grouping for each data point. Temperature contours are overlain in solid black lines.

community can be split into two distinct groups, one to the south of the front, and the other found at the front and to the north of it. This reflects our finding that the phytoplankton community to the south of the front is dominated by *Prochlorococcus*, *Synechococcus* and picoeukaryotes, whereas north of the front, diatoms and dinoflagellates are dominant. However, unlike Yamamoto et al. [1988] who used the same clustering method, we do not find a third distinct assemblage associated with the core of the front itself. Taylor et al. [2012], in their study of the California Current, also suggest that a third frontal assemblage can be distinguished in their data. Our data were collected at lower resolution than these

two other studies, with our stations roughly 9km apart, whereas Yamamoto et al. [1988] stations were <2km apart, and Taylor et al. [2012] sampled stations <3km apart. It is conceivable that this lower resolution in the across front direction may have influenced our results, especially considering the importance of submesoscale dynamics in this region, which typically occur on a scale of O(1km). However, our analysis of the phytoplankton community data differs from Yamamoto et al. [1988] in that we have included abundances of picoplankton and cyanobacteria in our data, and differs from Taylor et al. [2012] in that we have included the phytoplankton data for each identified species at each data point, rather than using depth integrated values of the biomass associated with each functional group. d'Ovidio et al. [2010] found, in their analysis of the phytoplankton community structure in the Brazil-Malvinas Confluence, that the dynamical structures in the fluid flow field acted to contain distinct populations within different water masses. We believe that the results of our study point to a similar conclusion, with the phytoplankton community being split into two distinct groups associated with subtropical waters south of the front, and colder subpolar waters found to the north. Of course this does not preclude the possibility of the intermingling of these population as their respective water masses are mixed on the small scale, but a study conducted at much finer resolution would be required to capture those features. We should also point out that the shedding of eddies and filaments from the frontal zone will act as agents of mixing between populations, and our results do show the influence of a warm filament on the phytoplankton community to the north of the front. Unlike Yamamoto et al. [1988], we did not identify the presence of coastal phytoplankton in our microscopy data, although the influence of Oyashio water was evident as a lens of lower salinity (<33.5) water found to the north of the front along transect D. Given that our study area is about 3^o further east, or roughly 3.5 days transit time, along the front from their easternmost section, it is possible that the presence of coastal phytoplankton may be less evident in our data.

4.5.2 Links between the vertical circulation and phytoplankton pigments

We found that the maximum concentration of chlorophyll was 2-fold higher at the front than at stations either side of it. This was consistent with higher values of the advective vertical nitrate flux associated with the frontal circulation, but there was a clear spatial offset between the maximum chlorophyll concentration and the highest nitrate fluxes, with the highest chlorophyll concentrations found slightly southwards of the highest vertical nitrate fluxes. Given that vertical velocities of up to 100 m/day can be generated at fronts, waters carrying high nutrient concentrations could be upwelled into the layer below the mixed layer in roughly a day. Elevated turbulent mixing measured directly by microstructure by Nagai et al. [2012] in the mixed layer along transect E, to the south of the Kuroshio, could inject nutrient-rich water from below the mixed layer supplied by mesoscale upwelling. This entrainment of nutrients into the mixed layer could be responsible for the observed high chlorophyll found in the mixed layer at the northernmost edge of transect E. With a characteristic time scale of 1 day for phytoplankton growth, it seems likely that nutrients may be supplied to the surface mixed layer in the vicinity of a front more quickly than they can be taken up. In our case, the highest vertical velocity estimated for our study area was 30 m/day just north of the front, suggesting an overturning time scale of 1.7 days for a 50m mixed layer. It is likely that this value of w is an underestimate given the limitations of using the QG ω equation for estimating vertical velocities in frontal zones characterised by a high Rossby number [Pinot et al., 1996]. ** add estimate of Rossby number from Nagai 2012 ** Similarly, our data on the ratio of photosynthetic and photoprotective carotenoids to chlorophyll also suggest a lag between the overturning time scale and the physiological response of the phytoplankton community. In the vicinity of the front, we found that the PPC:TChla ratio was more or less constant with depth, suggesting that the phytoplankton at these stations were transported vertically in the water column before they could acclimate to ambient light conditions. This contrasted particularly with the stations north of the front along transect D, where the water column was strongly stratified, and there was a

clear vertical structure in PPC:TChla values, with the highest values of the ratio found near the surface and decreasing with depth. Variations in these ratios may also be markers of the community composition at different stations, but there does not appear to be a consistent pattern linking these ratios to the distributions of any of the phytoplankton groups we observed.

Looking more closely at the distributions of different phytoplankton groups across the front, distinct patterns appear. The stations north of the front are dominated by diatoms and dinoflagellates. We note that maxima of diatom and dinoflagellate abundances do not co-occur. Diatoms are found predominantly along the nutricline, whereas dinoflagellates are more consistently confined to the surface. This would appear to reflect differences in their physiological adaptations. Dinoflagellates have been shown to have a lower Chl a to protein ratio than diatoms at similar irradiances [Chan, 1978], suggesting that diatoms better adapted for growth in lower light conditions where they can outcompete dinoflagellates. This would allow diatoms to exploit the high nutrient fluxes found at the nutricline, despite the lower light levels. South of the front, *Prochlorococcus*, *Synechococcus* and picoeukaryotes dominate the phytoplankton community. We observe a shift from *Prochlorococcus* dominating the community at the extreme southern end of transect E, transitioning to *Synechococcus*, and then picoeukaryotes approaching the front at the northern end of transect D. It seems possible that a higher nutrient supply at the front may select for picoeukaryotes, wheareas at the southern end of transect E we are approaching the more stable subropical regime, that *Prochlorococcus* is more well adapted to. At the core of the front, where the isopycnals are at their steepest, we see contributions to the phytoplanton community from all of the phytoplankton functional groups, with high abundances of all of the picophytoplankton types. The highest abundances of diatoms and dinoflagellates, however, are not located at the core of the front, but above the region of the nutricline that is domed up furthest into the photic zone.

4.5.3 Patchy nutrient distributions and frontal dynamics

Finally, we would like to highlight one of the more unusual features observed in the nutrient distributions. we observed an inversion in nitrate, phosphate and silicate at the base of the mixed layer, flanked above and below by lower concentrations. A similar feature was observed in data from the Kuroshio [Yamamoto et al., 1988, Ishizaka et al., 1994], and in sections across the East Australian Current [Baird et al., 2008], although neither of these studies proposed a mechanism to explain it. Here we highlight two possible explanations for this feature. Firstly, during the cruise, the averaged wind was aligned downfront, in the same direction as the frontal jet on the south side of the Kuroshio [Nagai et al., 2012]. A downfront wind can result in the transport of more dense waters from the northern side of the front over the lighter waters on the southern side of the front by Ekman transport. This induces a mechanical convection [Thomas and Lee, 2005], which generates elevated turbulence [D'Asaro et al., 2011, Nagai et al., 2012] which could in turn result in the subduction of well mixed water along isopycnals. This subduction could lead to the nutrient "tongue" structure we observed. A second mechanism to explain this nutrient distribution, could be the action of near-inertial internal waves. Internal waves with a sufficiently large amplitude could be subject to Stoke's drift [Thomas and Lee, 2005], driving a net southward transport of high nutrient waters. Nagai et al. [2012] showed that there was a stronger downward energy propogation in transect E, coincident with the location of the nutrient tongue. This suggests that near-inertial waves could be playing a role in the generation of this feature. We observe patches of diatoms, dinoflagellates and haptophytes all associated with the same or nearby data points as the nutrient tongue, and speculate that this could be the signature of the same process responsible for transporting nutrient-rich water away from the front. Similarly, the nutrient distributions observed along transect D are very patchy, especially in upper 40m of the northern half of the transect, with several isolated patches of higher nutrient water. Although we do not have direct measurements of the turbulent mixing along transect D, we do for transect B which was also offset to the north of the front and can be thought of as being upstream of transect D. Along transect B,

turbulent mixing was very strong [Nagai et al., 2012]. This strong mixing, coupled with the mesoscale uplifting of the nutricline, could result in the entrainment of high nutrient water from the nutricline into the surface mixed layer, where they can be consumed by primary producers.

4.6 Conclusions

We have conducted a fine scale survey of phytoplankton community structure and nutrient distributions along 2 transects across the Kuroshio Extension Front. We found fine scale variability in chlorophyll, as well as in the distributions of phytoplankton functional groups, particularly diatoms and dinoflagellates. We have also shown that there are strong variations in phytoplankton community structure across the front, and with depth. Cluster analysis of the phytoplankton abundance data shows that the frontal community can be split into two groups, one found predominantly to the north of the front and the other to the south. However, we see southern type assemblages north of the front, associated with a warm filament of Kuroshio water coiled north of the front itself. Our results show that the front acts as a barrier between two distinct assemblages of phytoplankton, which appear to be a subtropical and a subpolar assemblage. This suggests that the phytoplankton community structure at the front is strongly controlled by the physical circulation, and set by the large scale biogeography of the regions.

We observe links between the vertical nutrient supply at the front, and the community structure of the phytoplankton, with diatoms dominating at the data points where the vertical nitrate fluxes were the greatest. Using phytoplankton pigment ratios, we find evidence that the vertical circulation at the front is vigorous enough to mix the phytoplankton community more quickly than it can photo-acclimate. This view is supported by the measurement of high levels of turbulent mixing during during the same cruise by Nagai et al. [2012]. So, although the community appears to be controlled by large scale processes, the vertical circulation at the front does seem to stimulate higher levels of production by

enhancing the nutrient supply relative to the background levels either side of the front.

Highly dynamic regions such as the Kuroshio Extension Front, which integrate the effects of physical and biological processes acting over a range of time and space scales present a challenge to those wishing to understand the ecology of the phytoplankton found there. We have attempted to disentangle the influences of a range of processes, but our data only represent a very brief snapshot in the evolution of the phytoplankton community along this frontal system. However, we believe that these results do show the interplay of both large scale and finer scale controls on phytoplankton community structure in this region.

Chapter 5

Physical Dynamics Drive Co-occurence and High Abundances of *Ostreococcus* Clades at the Kuroshio Front

In Chapter 4, I described the results of a high resolution survey of the biogeochemical properties across the Kuroshio Extension Front in October 2009. I presented the distributions of phytoplankton functional groups determined by microscopy and flow cytometry. The work presented in this chapter is an extension of that ecological characterization of the frontal phytoplanton community. Here, instead of focussing on phytoplankton functional groups, I focus on one species, *Ostreococcus*, and discuss how the physical dynamics of the front shape the distributions of two genetically distinct clades of that species. This work was done in collaboration with Professor Alexandra Worden, a phytoplankton ecologist at the Monterey Bay Aquarium Reseach Institute, and her student Yun-Chi Lin. I collected the nucleic acid samples during the cruise outlined in the previous chapter and Prof Worden and Ms Lin conducted the genetic analyis on those samples. I have undertaken the subsequent analysis of the data. We are currently writing up a manuscript to be submitted to the ISME Journal which describes the genomics aspects of both the sample analysis and results in more detail. For the purposes of this chapter, I will restrict myself to describ-

ing the distributions of *Ostreococcus* clades in my study area, and my own analysis and interpretation of those distributions in the context of the corresponding enviromental data collected during the cruise and a simple theoretical model.

5.1 Introduction

Oceanic fronts are ubiquitous features, which are often associated with elevated phytoplankton biomass and primary productivity. From an ecological perspective, fronts may play several roles: separating, mixing, transporting or even acting as concentration sites for populations originating from either side of the front [Sournia, 1994]. Frontal zones can also be thought of as ecosystems in their own right, potentially supporting distinct populations adapted to that very specific environment [Yamamoto et al., 1988, Sournia, 1994, Taylor et al., 2012]. In fact, it seems more than likely that all of these processes will be acting in concert to shape the phytoplankton community within a frontal zone. Previous studies have identified the signature of population mixing reflected in the distribution of microphytoplankton species, in the Gulf Stream [Lillibridge et al., 1990], the Kuroshio Extension [Yamamoto et al., 1988] and at a coastal front of the Northeast coast of Japan [Yamamoto et al., 1981]. These studies all relied on identifying known coastal phytoplankton species, mostly diatoms, and exploring their distribution with respect to known oceanic species within the frontal zone. However, to date, there have been no studies examining the ecology of picophytoplankton in frontal zones. Given the emerging realisation of the important contribution of eukaryotic picophytoplankton to oceanic primary production [Worden et al., 2004], it is timely to explore their ecology at frontal zones. Also, with the development of molecular approaches to identify distinct phytoplankton "species" and their clades from DNA samples, this question can now be explored from a new angle. We suggest that by using molecular approaches to unambiguously identify and quantify distinct species and their clades, some of the difficulties of using microphytoplankton distributions to explore ecological controls on frontal populations (e.g. rare species, low abundances,

errors in identification and poorly known biogeography of species) can be minimized. In this study, we explore the distributions of two distinct clades of the picoeukaryote, *Ostreococcus*, across the Kuroshio Extension Front, and use the relative distributions of the two clades as a tracer of population mixing.

5.2 *Ostreococcus*

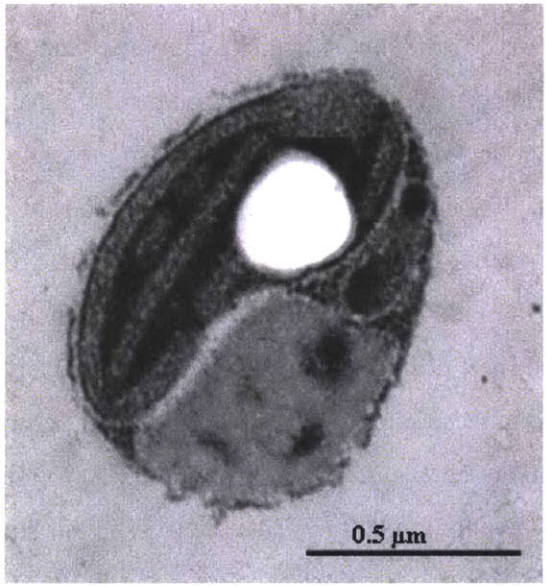

Figure 5-1: Electron microscope image of *Ostreococcus tauri*. (H. Moreau, CNRS)

Ostreococcus is the smallest known free-living eukaryote, a eukaryotic picophytoplankton species with a cell diameter of $\sim$ 0.8-1.2 μm shown in figure 5-1 [Chrétiennot-Dinet et al., 1995]. Several studies have explored its genetic diversity using the internal transcribed spacer (ITS) and found that it is clustered into four genetically distinct clades A, B, C and D [Guillou et al., 2004, Worden, 2006]. Laboratory photophysiology studies have shown that these four ITS clades fall into two differently photoadapted clades. Clades A, C and D are high-light adapted, whereas clade B is low-light adapted [Rodriguez et al., 2005, Six et al., 2008]. These distinct clades have also been termed OI and OII, where

OI represents the high-light adapted ITS clades A and C, and OII represents the low-light adapted ITS clade B [Worden and Not, 2008, Worden et al., 2009]. ITS clade D is excluded from the OI/OII designation as insufficient sequence data was available at the time of that study. *Ostreococcus* abundances have been explored in several studies using fluorescence *in situ* hybridization (FISH) and quantitive PCR (qPCR) and genus-level probes [Zhu et al., 2006, Countway and Caron, 2006]. Only one study, however, has quantitatively explored the distributions of the OI and OII clades in the field [Demir-Hilton et al., 2011]. Their systematic study of the distribution of the OI and OII clades of *Ostreococcus* (incorporating observations made in the North West Atlantic, Subtropical South East Pacific, Equatorial Atlantic, North West Pacific coastal upwelling zone and the North West Atlantic Shelf Break Front) found that the OI and OII clades were both present vertically throughout the water column. In fact, they appear to differentiate along lines of coastal vs. oligotrophic oceanic water masses, rather than by light availability as had previously been proposed. Furthermore, OI and OII clades typically did not co-occur in their data, with the exception of samples taken at the shelf break front in the North West Atlantic. It was suggested that both clades co-occured in these samples due to the mixing of oceanic and coastal waters at the front, but this could not be explored in more depth due to the small number of samples containing both clades. We focus on *Ostreococcus* clades in this study as ecological tracers of the mixing of populations at the Kuroshio Extension Front. Our fine scale sampling allows us to explore how both *Ostreococcus* clades are distributed in the frontal zone and how those distributions relate to environmental conditions there. Given the co-occurence of both the OI and OII clades at the North West Atlantic Shelf Break Front, we expect that both clades would be present in the frontal zone. Previous studies have also noted that coastal phytoplankton are often entrained into the Kuroshio [Yamamoto et al., 1988].

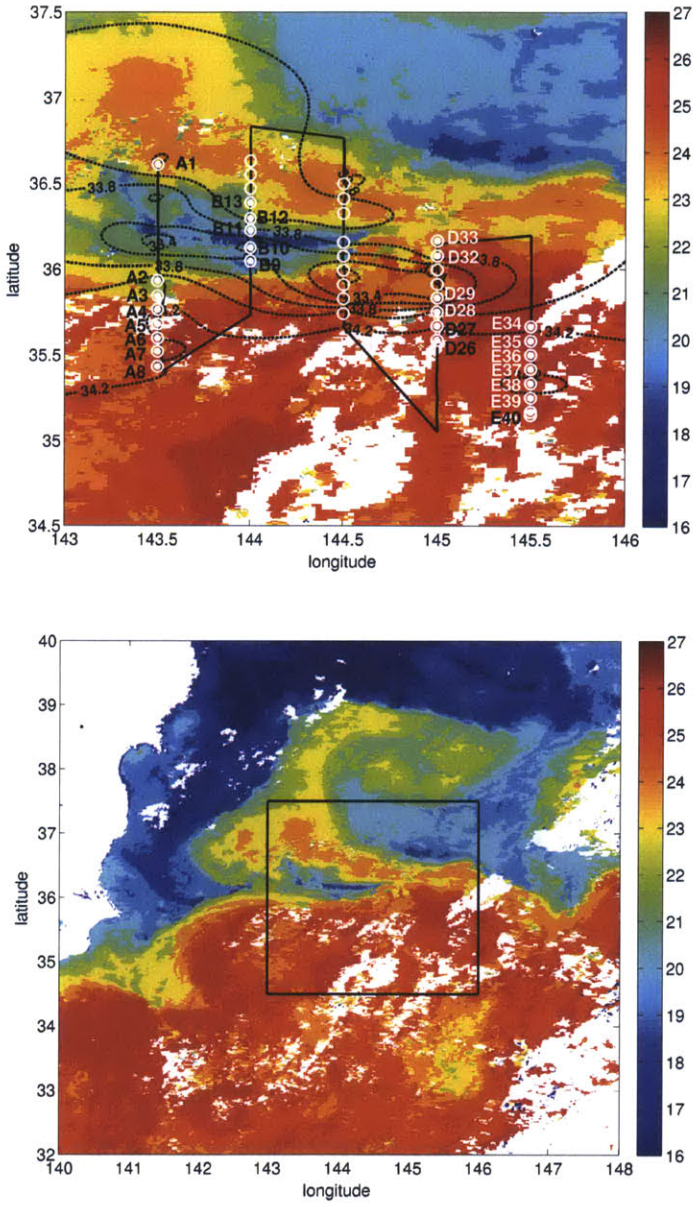

Figure 5-2: Sea surface temperature (NOAA) for the study region on 20th October 2009. The top panel shows the study region with salinity contours overlain in black. The stations where surface samples for qPCR were collected are shown as filled white circles. The lower panel shows the study area within the larger region.

5.3 Study Area and Sampling

The samples used in this study were collected during the cruise already described in detail in Chapter 4. We collected seawater ($\sim$ 1l) from the surface from stations along sections A, B, D and E (shown in figure 5-2) using a clean plastic bucket. Microbial biomass was prefiltered through a 5 μm 45mm filter and then onto a 0.8 μm 27 mm filter (Millipore durapore) for DNA extraction. The filters were placed in 1.2 ml Nalgene cryovials with 500 μl of RNAlater (Qiagen) and immediately frozen and stored at -80 ^{o}C, until DNA could be extracted. DNA extraction and subsequent genomic analyses were performed by Yun-Chi Lin and Professor Alexandra Worden at MBARI. Briefly, they constructed 18S rRNA clone libraries from samples taken at stations D28, D32, D33, E34 and E40 following Worden [2006], and initial assignment of environmental sequences to known taxa and uncultured environmental groups was performed using BLASTn to NCBI with default settings. In order to quantify the abundance of *Ostreococcus* clades, they performed qPCR on all of the samples collected using two Taqman primer-probe sets to enumerate 18S rDNA from the two Ostreococcus clades, OI and OII, following Demir-Hilton et al. [2011]. The physical setting of the study region is also outlined in the previous chapter, but here we highlight some features of the circulation most pertinent to this study. The sea surface temperature, shown in figure 5-2, reveals a cooler, lower salinity water mass entrained into the frontal region. This is bounded to the north and south by warmer, saltier subtropical waters. The warmer waters present in the northern part of the study area are part of a filament of warm Kuroshio waters pinched off from a meander a few days earlier. These warm streamers are a common feature in this region [Kawai and Saitoh, 1986]. The cooler water mass, surrounded by the warmer waters, appears to be Oyashio water, with a characteristic salinity of 33.2 and a charateristic temperature of 18^{o}C. The warmer water to the south and the north of the Oyashio water is Kuroshio water with a characteristic salinity >34.2 and charactersitic temperature of 24^{o}C.

Table 5.1: *Ostreococcus* clade abundances and measured environmental variables for each of the surface sample stations.

Station	Longitude	Latitude	OI clade (copies ml^{-1})	OII clade (copies ml^{-1})	T (^oC)	S
A1	143.48	36.61	1.2	11012.1	23.76	34.19
A2	143.53	35.93	5007.3	32942.1	22.97	34.09
A3	143.53	35.84	11.5	31110.0	24.13	33.72
A4	143.53	35.76	0	6462.3	24.87	34.19
A5	143.53	35.68	0	11402.1	25.24	34.19
A6	143.53	35.60	0	3995.8	25.38	34.14
A7	143.52	35.52	0	627.6	25.17	33.72
A8	143.53	35.43	0	155.1	25.10	34.23
B9	144.0	36.05	3406.0	839.5	20.16	33.70
B10	144.0	36.13	6825.7	192.0	18.38	33.23
B11	143.97	36.23	6349.6	4200.4	20.99	33.78
B12	143.99	36.30	224.8	50189.9	23.62	33.80
B13	144.0	36.39	0	36051.1	23.80	34.18
D26	145.08	35.59	0	10947.0	24.51	34.21
D27	145.01	35.67	166.6	4971.6	23.08	34.20
D28	145.01	35.75	85.1	7278.8	22.18	34.09
D29	145.0	35.83	958.5	47.2	18.04	33.28
D32	145.0	36.08	1514.2	4862.3	21.15	33.96
D33	145.0	36.17	3638.1	5226.7	21.32	33.80
E34	145.51	35.67	55.2	8082.3	23.95	34.16
E35	145.53	35.58	0	5716.3	24.14	34.25
E36	145.52	35.50	0	2640.7	24.14	34.29
E37	145.52	35.42	0	2395.8	25.05	34.27
E38	145.5	35.33	0	1549.7	24.51	33.43
E39	145.5	35.25	0	1613.0	24.51	34.26
E40	145.5	35.17	0	908.9	24.51	34.28

5.4 Results

5.4.1 *Ostreococcus* clade distributions

We found both *Ostreococcus* clades present in our study region. OII was present in all 26 samples and OI was present in 14 (54%) of the samples. We report the abundances of the *Ostreococcus* clades in units of copies of the 18S gene ml^{-1}, and they are listed for each station in table 5.1. The OII clade ranged in abundance from 47 copies ml^{-1} to a

maximum abundance of 50190 copies ml^{-1}, far exceeding the maximum abundances of OII previously reported in nature ($\sim$ 5000 copies ml^{-1}) in Demir-Hilton et al. [2011]. Where OI was present, its abundance ranged from 11 copies ml^{-1} to 6830 copies ml^{-1}, in line with previously reported values, with a maximum of $\sim$ 10000 copies ml^{-1} in Demir-Hilton et al. [2011]. The surface distributions of both clades are shown in figure 5-3. Broadly speaking,

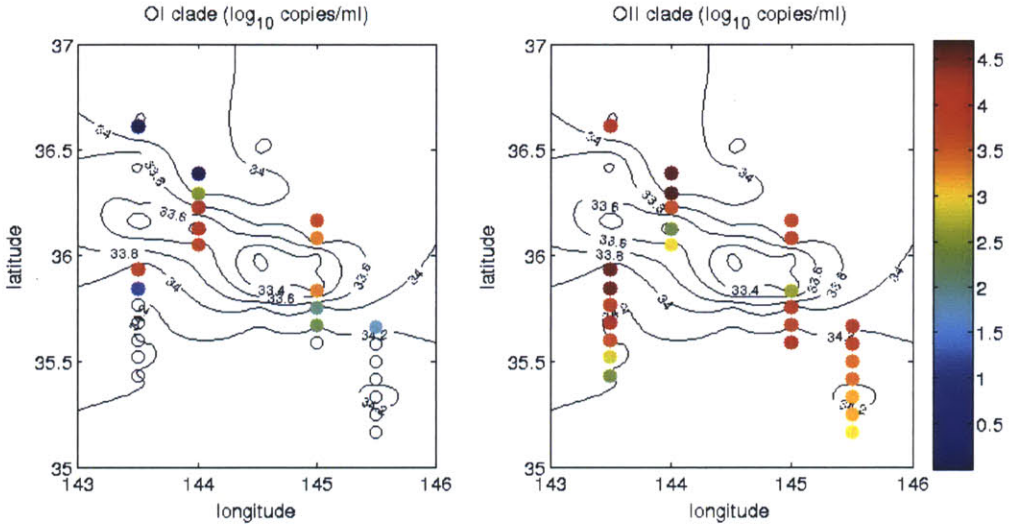

Figure 5-3: Both panels show the abundances of the *Ostreococcus* clades in $\log_{10}$ copies ml^{-1}, and the contours of surface salinity shown in black. The right panel shows OI abundance, and where the circles are empty, no OI was detected. The left hand panel shows the abundance of OII.

the highest abundances of both clades were associated with the core of the front, where temperature and salinity gradients were sharpest. Occurences of the OI clade are most closely associated with the lower salinity Oyashio waters. OII appears to be more closely associated with the higher salinity Kuroshio waters, but its abundance drops off to the south of the frontal zone. The highest abundances of OI, above 3000 copies ml^{-1}, were found at stations A2, B10, B11 and D33. These stations were all found within the Oyashio water parcel travelling along the front. With the exception of A2, all of these stations with high OI abundances were offset slightly to the north of the front itself. The highest abundances of OII, above 10000 copies ml^{-1}, were found at stations A1, A2, A3, A5, B12, B13 and

D26. These stations were all found on the more saline edge of the Oyashio water mass, and closely associated with the core of the front. Generally, we found that abundances of OII were higher everywhere than OI abundances, but at stations B11, D32 and D33, the abundances of both clades were the same order of magnitude, (O(10^4) copies ml^{-1}).

5.4.2 Relationship of *Ostreococcus* clades to environmental parameters

Unlike Demir-Hilton et al. [2011], our data all comes from a small region of the ocean. As a result, most environmental parameters are not delineated between those samples containing either OI or OII. Given that more than half of our samples contained both clades, this is not surprising. Similarly, in most cases, we do not find a significant correlation between the distributions of either clade or the environmental parameters tested (salinity, temperature, nitrate, phosphate, ammonia and fluorescence). However there were some exceptions. OI was found to have a significant negative correlation with salinity (r=-0.6461; P=0.003) and temperature (r=-0.6481; P=0.003), and OII had a positive correlation with fluorescence (r=0.5911; P=0.0012). This would seem to suggest that the distribution of OI is more influenced by the mixing of the Oyashio and Kuroshio water masses than OII. The positive correlation between OII and fluorescence suggests that the OII distribution follows the pattern of increased fluorescence in the frontal zone, which we suggest in Chapter 4 is driven by enhanced nutrient supply to the surface mixed layer, driven by both the frontal circulation and enhanced vertical mixing at the front.

5.5 Discussion

The two most striking aspects of the observed *Ostreococcus* distributions are the high proportion of samples where members of both clades co-occur, as well as the unprecedented high abundance of OII and very high abundance of OI associated with the core of the Kuroshio Front. Here we propose explanations for these features based on the correspond-

ing physical and biogeochemical data.

5.5.1 Elevated abundances of *Ostreococcus*

Our data reveals unprecedentedly high abundances of OII at stations A1, A2, A3, A5, B12, B13 and D26. These stations were all located very close to the core of the Kuroshio Front. Here we find OII abundances of over 10000 copies ml^{-1}, about an order of magnitude higher than the highest abundance of OII previously reported in Demir-Hilton et al. [2011]. These high abundances of OII are highly localized within the core of the front and drop off sharply to very low abundances at the northern and southern extensions of the sampling area. This echoes the positive correlation between OII and fluorescence, suggesting that OII abundances are enhanced in the same way as other phytoplankton species in the frontal zone. We also found high abundances of OI at stations A2, B10, B11 and D33. OI abundances within this region are also high, but appear to be in line with the highest abundances previously reported. This is intriguing because it hints at the possibility that *Ostreococcus*, in particular the OII clade, may be blooming over small scales in response to favourable environmental conditions at the front.

Nagai et al. [2012] showed that, during this cruise, some areas of the front were subject to very strong vertical mixing, and presented evidence of internal wave activity acting to drive this mixing in the frontal zone. In particular, they showed that there was a very vigorous vertical circulation at the northern end of transect A, and a very strong mesoscale vertical circulation, upwelling on the southern side of the front. Along transects D and E, the mesoscale circulation was upwelling on the northern side of the front, doming upwards the already shallower nitracline of the subpolar waters. Microstructure measurements were not taken along every transect, but high levels of turbulent dissipation were measured at the southern end of transects B and D, near the front. In figures 5-4 and 5-5 we show the *Ostreococcus* clade abundances again, this time plotted along with sections of the nitrate distribution across the front along the study transects A, B, D and E. Station A1, at the nothernmost edge of our first transect coincides with a lens of lower density water which

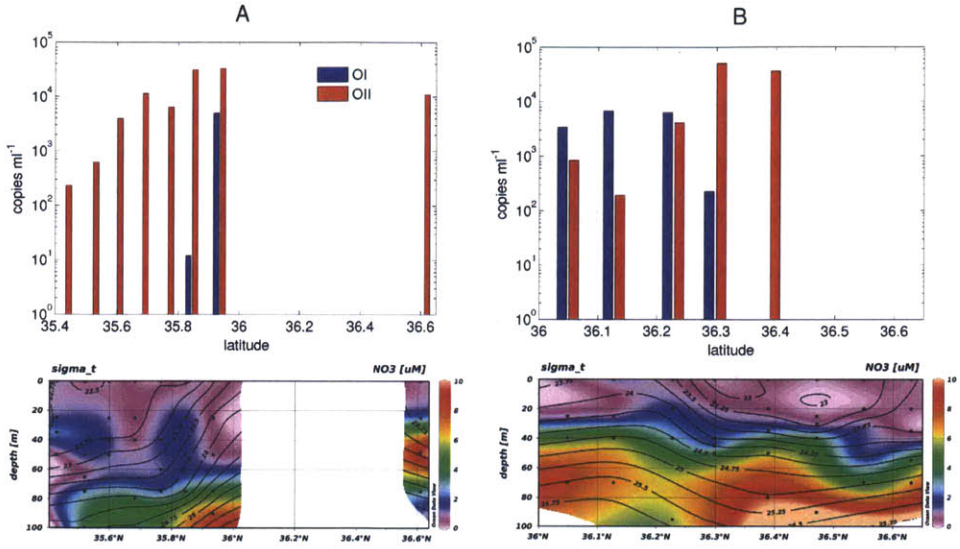

Figure 5-4: Top panels: Surface abundances of *Ostreococcus* clades OI and OII. Bottom panels: NO_3 distribution.

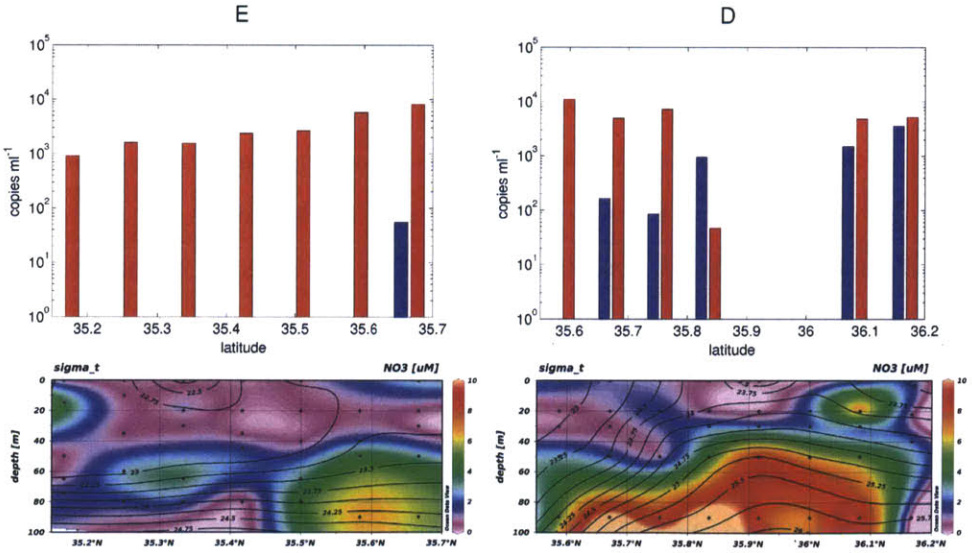

Figure 5-5: Top panels: Surface abundances of *Ostreococcus* clades OI and OII. Bottom panels: NO_3 distribution.

appears to be associated with the warm filament, but it has a rather shallow nitracline at $\sim$ 20m depth. It appears that the high abundance of OII at this station is in part due to a seed

population of OII being transported along with the subtropical waters of the filament, along with a nutrient supply enhanced by higher dissipation rates measured at $\sim$ 25 m. Stations A2 and A3, associated with a high abundance of OII, are located roughly above a "tongue" of higher nitrate abundances extending into the shallower waters from the nitracline. A similar feature in the nitrate field is also found at stations A7 and A8 at the southern end of transect with no corresponding high OII abundance at the surface, but this may just be due to our surface sampling missing variations of OII distributions with depth. OII has been found to be associated with the DCM in subtropical waters in previous work [Demir-Hilton et al., 2011], so we may be missing the bulk of the population as we move into subtropical waters to the south of the front. Station A2 also hosts a high abundance of OI cells, and we speculate that this may also be driven by an enhanced nutrient supply in the vicinity. Along transect B, stations B10 and B11 support a high abundance of OI cells and stations B12 and B13 support high OII abundances. The nitracline at all of these stations is found at $\sim$ 20 - 25 m depth, with a small intrusion of higher nitrate concentrations associated with what appears to be a small-scale secondary front between B11 and B12. Again, we see the signature of the warm filament, with a lens of less dens water associated with stations B12 and B13. It appears that the small front is separating the Oyashio water found at stations B10 and B11 from Kuroshio water advected northwards as part of the filament. A similar pattern is repeated along transect D, where we find high abundances of OI at stations D32 and D33, with OII abundances of the same order of magnitude. There are lenses of lighter water to the north and south of these stations, and relatively high nitrate concentrations found in the top 20m at these stations, presumably stimulating growth. At the southern end of section D, at station D26, we find a high abundance of OII cells, in this case coinciding with the steep pycnoclines of the front and an elevated surface nitrate abundance, overlaying waters with depleted nitrate. Taken together, these observations of correspondances between areas of increased *Ostreococcus* clade abundance and potentially enhanced nutrient supply to the surface appear to support the hypothesis that *Ostreococcus* growth may be stimulated in the frontal zone.

5.5.2 Co-occurence of *Ostreococcus* clades

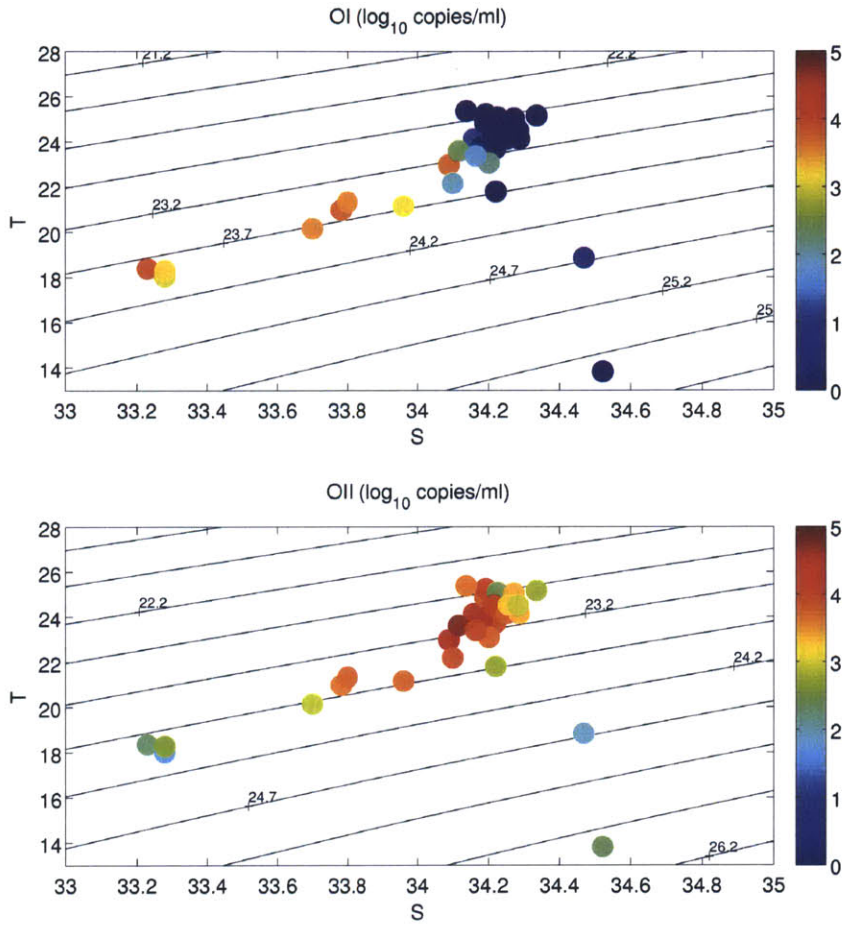

Figure 5-6: T/S plot for the Kuroshio Extension region for OI (top) and OII (bottom).

In a previous study, both *Ostreococcus* clades co-occured in only a very small number of samples all taken from continental shelf waters [Demir-Hilton et al., 2011]. Our sampling strategy was markedly different from that previous study, in that we focussed entirely on the Kuroshio frontal zone and sampled at a much higher spatial resolution ($\sim$ 9 km). The Kuroshio is a region where different water masses meet and there is a complex physical circulation. We suggest that this mixing of water masses may be responsible for

bringing these two distinct clades together. The Kuroshio is known to episodically entrain coastal Oyashio waters into the main stream [Qiu, 2001], and this is the source of the cooler fresher water and the OI *Ostreococcus* in our samples. The correlations between OI and temperature and salinity appear to support this view. In order to explore this idea further, we examine the abundances of both clades in T/S space, shown in figure 5-6. In this figure it is clear that OI are most closely associated with cooler, less saline waters with an Oyashio T/S signature, whereas OII are found in a warmer, saltier Kuroshio water mass. The highest abundances of OI coincide exactly with the Oyashio portion of T/S space, and lie on a mixing line between the Oyashio and Kuroshio water masses. This appears to support the hypothesis that OI is in fact transported into the open ocean Kuroshio front when Oyashio waters are entrained further upstream. As the Oyashio water mass is transported along the front, it is gradually mixed with the Kuroshio water, and as a result, OI and OII cells are mingled together. By visual inspection of the data, we estimate a length scale of co-occurence of roughly 30 - 50km from the *Ostreococcus* clade abundance data. This suggests that a physical mechanism acting at the mesoscale, or possibly sub-mesoscale, is likely to be driving the mixing of the water masses containing the two clades.

Given that *Ostreococcus* clades OI and OII appear to be associated with coastal and oceanic water masses, respectively, we examine the patterns in their distributions along a salinity gradient. This also allows us to simplify our interpretation of the data somewhat, by eliminating the complex spatial structures in the study region due to complex mesoscale and submesoscale circulation, in particular the warm filament north of the main stream of the Kuroshio. Figure 5-7 shows the abundances of both clades plotted against salinity. Although the two clades are present along a salinity gradient between the two water masses, neither clade appears to follow a linear mixing line between the characteristic salinities for the Oyashio and Kuroshio water masses. As might be expected, they are not acting as passive tracers. OII shows quite a striking increase in abundance at salinities between 34 and 34.2, with decreased abundance at higher and lower salinities. OI abundances remain high at salinities below $\sim$ 34 and decrease sharply above that value. However, figure 5-7

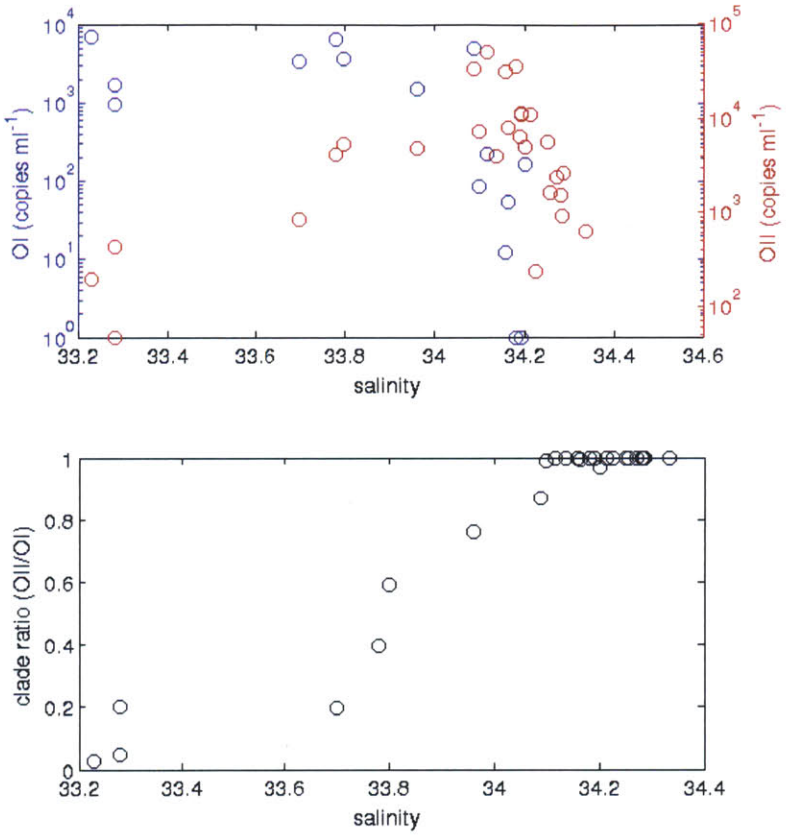

Figure 5-7: Top panel: abundances of *Ostreococcus* clades OI and OII plotted against salinity. Bottom panel: the ratio of the two clades (OII/OI) plotted against salinity. Note the different axes for OI and OII abundances in the top panel.

also shows that the ratio of the two clades does appear to follow a mixing line between the Kuroshio and Oyashio salinity end-members. If neither clade is a passive tracer, both clades must be reacting to environmental conditions along the mixing line in a similar way in order to explain the distributions of both their abundances and the ratio of their abundances.

5.5.3 Reaction-diffusion model of *Ostreococcus* dynamics

The observed distributions of the *Ostreococcus* clades can be interpreted as being, on the one hand, driven by a mixing of water masses containing either population, and on the other hand by active growth in the frontal zone. The observed abundances for the 2 clades do not support a simple mixing relationship, however, the ratio of the two clades does follow a linear mixing relationship between their two representative salinity end-members. We suggest that this is the result of both clades either growing or being removed at the same rate in the frontal region. Here we propose to use a simple diffusion-reaction model to test the hypothesis that the distribution of both clades can be explained by a combination of mixing and positive net growth in the frontal zone. We aim to show that the alternative scenarios, where there is only mixing acting on their distributions, or there is a net sink of both clades in the frontal zone, do not fit our observations. We present a highly idealized system: either side of the front, the abundance of both clades is set to a constant background value, X_n^o, and at the front, the abundance of both clades is set by the mixing of those end-member populations and local growth. In equation 1, below, we represent the time rate of the change of both clades at the front as a balance between a diffusive mixing process and biological net growth.

$$\frac{\partial X_n}{\partial t} = \kappa \frac{\partial^2 X_n}{\partial x^2} + \mu_{NET} X_n \tag{5.1}$$

for n=1,2, and where X_n represents the abundance of Ostreococcus (X_1 is OI, the coastal clade and X_2 is OII, the oceanic clade), κ is the mixing coefficient and μ_{NET} is the net biological growth rate, incorporating both growth and mortality. However, given the spatial complexity of our system, and the strong evidence, presented above, that both *Ostreococcus* clades are associated with a characteristic water mass, we cast the model in salinity space, described by the following equation:

$$\frac{\partial X_n}{\partial t} = \kappa_S \frac{\partial^2 X_n}{\partial S^2} + (\mu - m) X_n \tag{5.2}$$

We scale κ_S, the diffusivity in salinity space, using the following scaling:

$$\kappa_S \sim \kappa \frac{\Delta S^2}{\Delta L^2}$$

This relies on the assumption that $\frac{\Delta S}{\Delta L}$ is constant. We estimate ΔS and ΔL from the

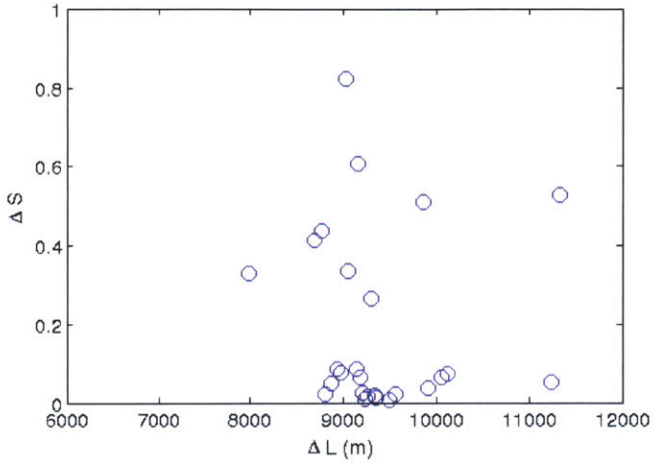

Figure 5-8: Absolute values of the salinity gradients between adjacent stations plotted against the distance between stations. These values are used to approximate a diffusivity scaled into salinity space.

data by calculating the difference in salinity and the distance between each neighbouring sample station (shown in figure 5-8). From this we obtain a range of estimates for $\frac{\Delta S^2}{\Delta L^2}$. We approximate κ, the horizontal diffusivity in this region to be O(10^4) m^2 s^{-1} (Zhurbas and Sang Oh [2003], R. Abernathey (pers. comm)). This results in a wide range of values for κ_S, ranging from 10^{-9} s^{-1} to 10^{-5} s^{-1}. However, the majority of the data shows a small salinity gradient (<0.2) between stations, so we base our estimate of κ_S on those sets of points. Using this more limited set of data, we estimate a value of κ_S that falls between 10^{-9} and 10^{-7} s^{-1}. The boundary conditions set the background abundance of the two clades at either salinity extreme. S_{min} represents the Oyashio water mass and is set to 33.2, and S_{max} represents the Kuroshio water mass and is set to 34.4. The boundary conditions for the system are as follows:

Table 5.2: Model parameters.

Parameter	Exp 1	Exp 2	Exp 3	Units	Description
X_1^o	100	5000	5000	copies/ml	Abundance of X_1 at S_{min}
X_2^o	100	5000	5000	copies/ml	Abundance of X_2 at S_{max}
μ	0.9	0	0	day^{-1}	Growth rate
m	0.1	0	0.1	day^{-1}	Mortality rate
κ_S	0.5 x 10^{-7}			s^{-1}	Diffusivity scaled into salinity space

$$X_1(S_{min}) = X_1^o;$$

$$X_1(S_{max}) = 0;$$

$$X_2(S_{min}) = 0;$$

$$X_2(S_{max}) = X_2^o;$$

We examine three possible configurations of the system: $\mu_{NET} > 0$ (experiment 1), $\mu_{NET} = 0$ (experiment 2) and $\mu_{NET} < 0$ (experiment 3), reflecting the hypotheses described above. For each case, we vary only μ_{NET} and X^o which are both set to be the same for both clades. To keep the experiment as simple as possible, in each case we assume the growth rate to be constant across the domain. Experiment 1 represents the case where both clades are being mixed away from a source region at the boundary, and are actively growing. In experiment 2, we consider the case where there is zero net growth, so the clade distributions are set only by mixing. This represents the case where biological sources and sinks are tightly coupled, or where the clades are acting entirely passively. Experiment 3 is the case where mortality is greater than growth. We include this case because it is entirely conceivable for a species mixed out of its ideal habitat to have a negative μ_{NET} (analogous to the *immigrant* types discussed in Chapter 3). Given the highly dynamic nature of the environment at the front, we examine transient solutions of the model for each experiment. We set the initial abundances of X_1 and X_2 are set to be zero everywhere but S_{min} and S_{max} respectively. We run the model for 10 days, as this is broadly consistent with the

transit time from a coastal region to our study area. We list the parameters used in each experiment in table 5.2. We assign higher boundary condition values to both clades for experiments 2 and 3, as it is clear from the clade abundance data that they must have a high abundance somewhere in the domain in order to generate the observed abundances. The values assigned for the boundary conditions for each experiment, however, are consistent with the data, as abundances for both clades range from O(10^2) to O(10^3) at their respective salinity endmembers.

We show the results of these experiments in figures 5-9, 5-10 and 5-11. In each case, our results are a good fit to the clade ratio, but experiment 1, qualitatively, appears to reproduce a pattern similar to the observed pattern in the abundances of both clades. This supports the idea that the distributions of both *Ostreococcus* clades are the result of mixing from two end-member water masses coupled with a positive net growth of both clades in the region between S_{min} and S_{max}. The results of experiments 2 and 3 reveal that there would need to be a large abundance of both clades at their associated end-member salinities in order to approach their observed abundances in the intermediate salinity region. Of course, these results are highly dependent on the choice of parameters and the duration of the model run. We recognise that although we can make informed decisions about the value for the biological parameters (μ and m), the value of the diffusivity is much harder to define, especially within the framework of a model set up in salinity space. We are also aware that given a system where $\kappa_S = \kappa_S(x)$, we may find that it is possible to produce similar results, but this is beyond the scope of this study. Despite these limitations, we believe that these simple models do help guide our understanding of the system, and that they provide support to the hypothesis that both positive net growth and mixing are needed to produce the observed *Ostreococcus* clade distributions.

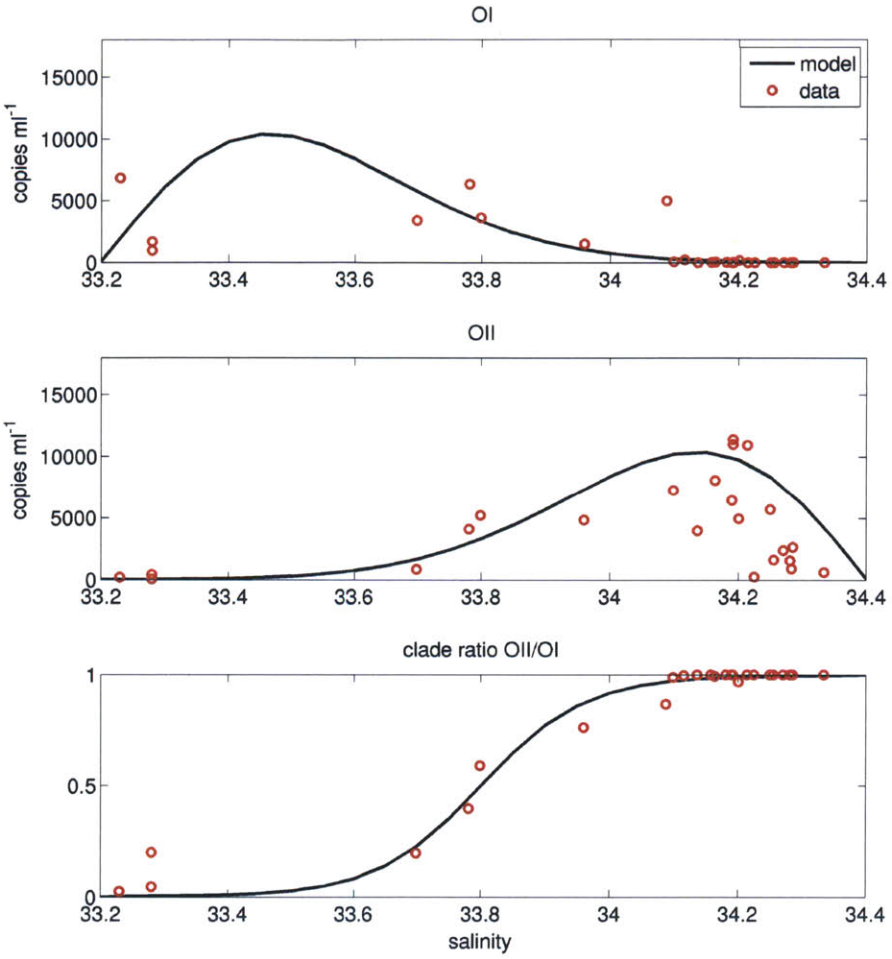

Figure 5-9: The solid black line shows the solution of experiment 1, where $\mu_{NET} > 0$. The observed *Ostreococcus* abundances are shown as open red circles. The top panel shows the result for modelled X_1 (OI analog), X_2 (OII analog) is shown in the middle panel, and the ratio of the two clades, X_2/X_1 is shown in the bottom panel.

5.6 Conclusions

We have a conducted a study of the distributions of distinct *Ostreococcus* clades across the Kuroshio Extension Front, and found that both clades co-occur in more than half of our samples, all taken at the sea surface. Figure 5-12 shows a conceptual model of the processes

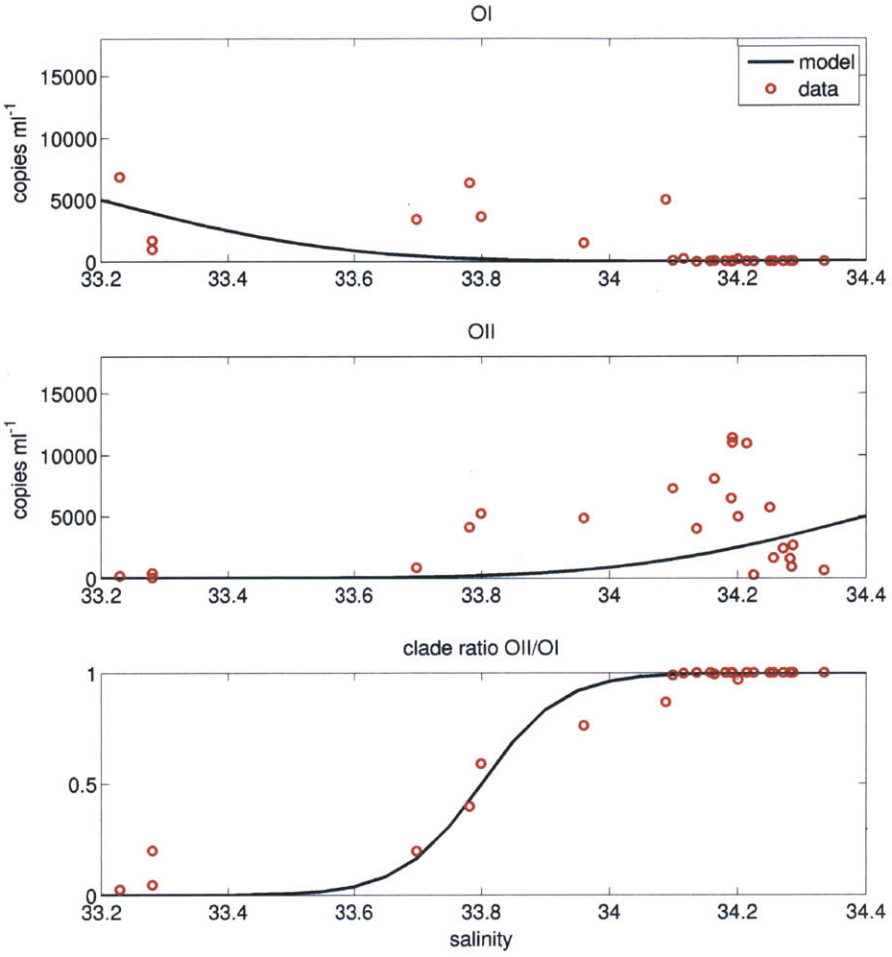

Figure 5-10: As for figure 5-9, but for experiment 2 where $\mu_{NET} = 0$.

acting in the study region to shape the distributions of the two clades. There is clear evidence that the coastal-adapted OI clade is transported into the Kuroshio main stream along with parcels of Oyashio waters that are entrained further upstream. The stations where the two clades co-occur lie on a mixing line between Kuroshio and Oyashio waters in T/S space. It is less clear what the source of the OII clade to the surface at the front is, as this clade is generally associated with the DCM in subtropical waters. It is conceivable that it

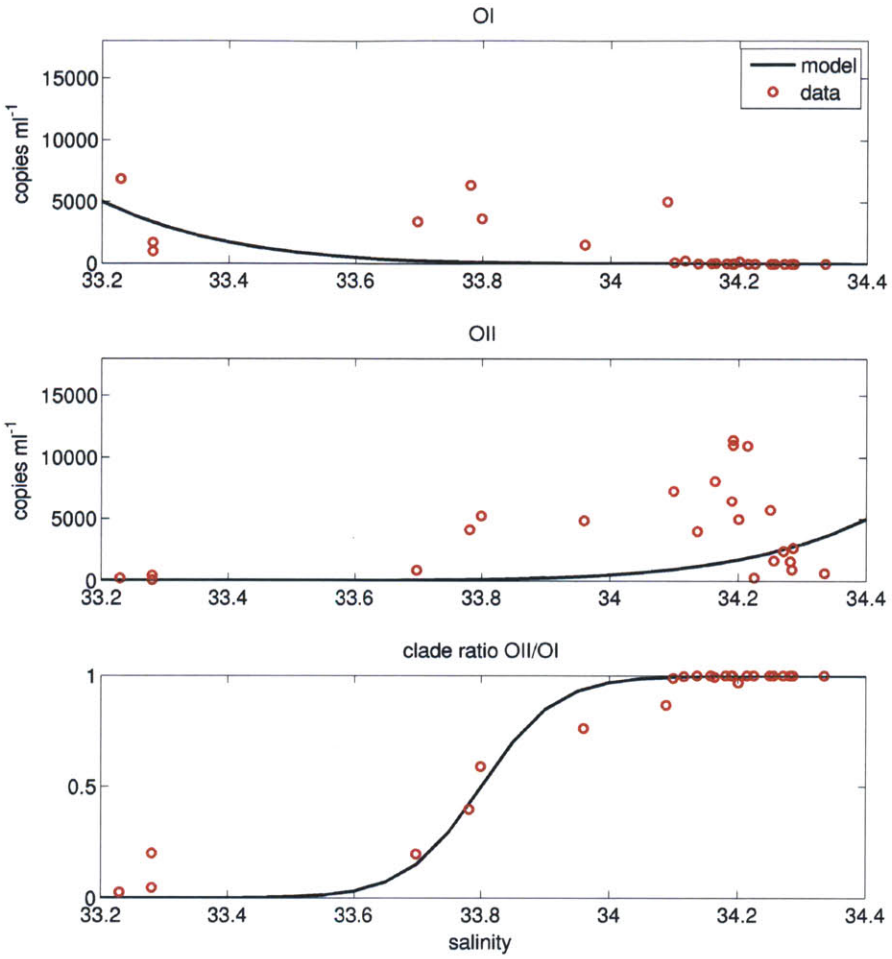

Figure 5-11: As for figure 5-9, but for experiment 3 where $\mu_{NET} < 0$.

may be advected along isopycnals by the frontal circulation, but without any data on its vertical distribution, this remains unclear. However, it appears that the OII clade was advected to the north of the Kuroshio Front within a warm filament clearly visible in high resolution SST data from the time of the cruise. Our results illustrate the complexity of the controls on phytoplankton community structure across a western boundary current front. Although we have shown that the observed *Ostreococcus* clade distributions are driven primarily by

the mixing of their "home" water masses into a favourable environment for growth of both clades at the front, we are still left with many open questions. Possibly the most important of these is whether or not both clades can be said to be co-existing at the front. Our simple model suggests that both clades would need to have a positive net growth rate to explain their observed abundances, but we lack direct measurements of their growth rates.

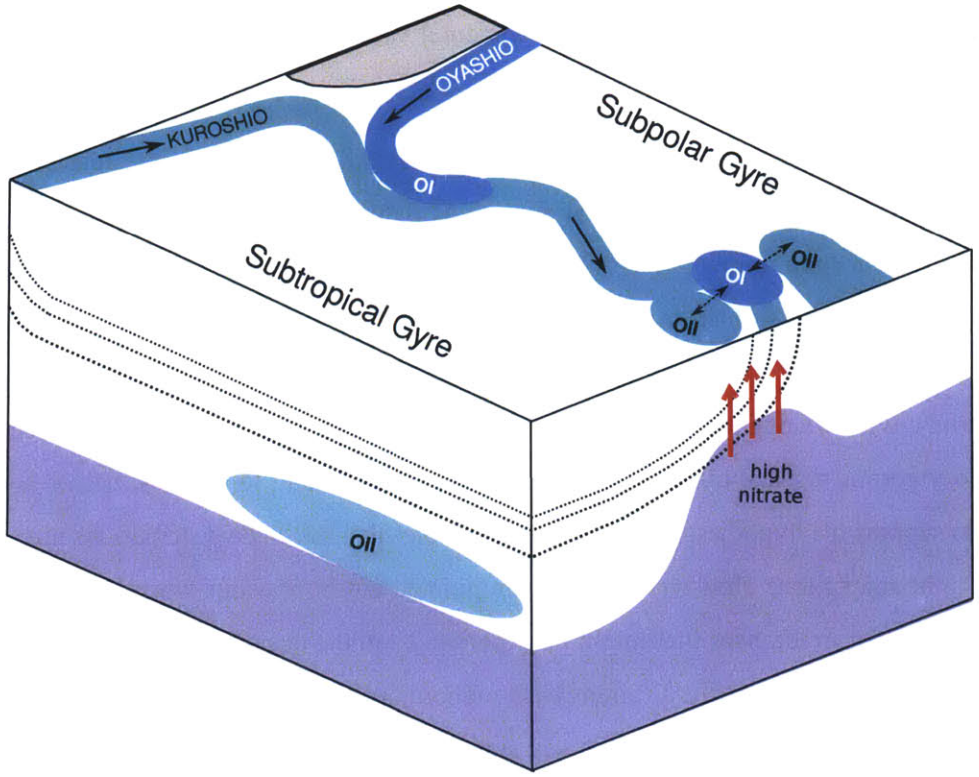

Figure 5-12: Schematic of processes occuring in frontal zone shaping the distribution of the *Ostreococcus* clades.

These observations are surprisingly well aligned with the model predictions on the controls of diversity hotspots outlined in Chapter 3, where we outline the necessary conditions for the formation of a phytoplankton diversity hotspot. Specifically, we show that diversity hotspots arise where the following three conditions are satisfied: 1). a confluence of populations; 2). an enhanced nutrient supply; and 3). elevated environmental variability. We

find that all of these conditions are satisfied in our study region. We have shown that it is a region of high *Ostreococcus* diversity, as both clades are present. The Kuroshio jet acts to create a region of confluence for both clades by entraining Oyashio waters, and there is an enhanced local nutrient supply driven by the frontal dynamics. Finally, the complexity of the mesoscale circulation in the region represents a source of environmental variability. Thus we have shown that in region with a confluence of populations, an enhanced nutrient supply and a high level of environmental variability, we find a high diversity of *Ostreococcus*.

Having completed this preliminary work, avenues of future study are clear. Extending the sampling to cover the vertical as well as the horizontal distributions of different organisms will help unravel some of our unanswered questions about the source of OII *Ostreococcus* to the surface frontal zone. More extensive surveys along the length of the front would uncover the extent of the co-occurence of the two clades along the front. In this study, we have only collected samples at the sea surface, in a region known to be subject to vigorous vertical circulations. As a result, it is difficult to say whether or not our results support the hypothesis from laboratory studies that the clade distributions are set by their light adaptation. However, as has been pointed out in previous work [Demir-Hilton et al., 2011], at irradiances that might be experienced in the ocean, the growth rates of the two clades are not markedly different in the laboratory studies. We find that both clades are abundant in large numbers at the sea surface, and although they may be transported there by the vertical circulation, it appears that both are able to thrive in similar conditions. Further sampling, incorporating depth profiles may help to explain the presence of the OII clade at the sea surface in our results.

We believe that this is the first study where molecular techniques for identifying organisms within the phytoplankton community have been combined with a high resolution survey of the hydrography and dynamics of a western boundary current front. Although we have concentrated on only one species in this study, we believe that similar studies could be undertaken which explore a wider range of organisms within the phytoplankton. This

represents an exciting new development in the study of phytoplankton ecology. Given the drive to understand patterns of biodiversity in the oceans, and previous work showing that highly dynamic regions of the ocean are hotspots of diversity, we believe that this type of study will be invaluable in gaining a deeper understanding of the controls on patterns of diversity in the ocean.

Chapter 6

Summary and Future Directions

6.1 Overview

In conducting the research that makes up this thesis, I have sought to understand how features of physical ocean circulation interact with phytoplankton ecological processes to shape the observed community structure. More specifically, I have tried to build up an understanding of how large scale lateral dispersal and vertical motions on finer scales, together, can influence community structure and biodiversity.

In Chapter 2, I explore the role of model resolution in influencing the solution of a complex marine ecosystem model. Interpretations of the numerical simulations suggest that although changes in ocean physics at the large scale do drive regional changes in bulk ecosystem properties such as phytoplankton biomass and primary production, they do not result in any fundamental shift in dominant phytoplankton functional groups or phenotypes. It appears, with this diverse ecosystem model anyway, that the individual phenotypes that make up the community are not modified by this increase in resolution.

In Chapter 3, I diagnose the role of the physical circulation in generating patterns of phytoplankton diversity. I find a large increase in the levels of modelled phytoplankton diversity with increased physical resolution. This increase in local diversity can be attributed to a combination of factors, fundamentally controlled by the physical circulation. I con-

centrate particularly on "hotspots" of diversity associated with the most dynamic regions of the ocean, and show that they are sustained through a combination of lateral dispersal and local environmental conditions.

In Chapter 4, I present the results of a fine-scale biogeochemical survey of the Kuroshio Extension Front. I collected fine scale data on the distributions of dissolved inorganic nutrients, phytoplankton pigments, nucleic acids, picophytoplankton and microphytoplankton. I found that the frontal circulation did appear to generate patchy distributions in dissolved nutrients, but that the overall picture suggests that the front acts as a barrier between two distinct phytoplankton populations.

In Chapter 5, I focus on a small subset of the data from the Kuroshio Extension Front, exploring how the physical circulation of the front shapes the distributions of two genetically distinct clades of the picoeukaryote, *Ostreococcus*, and how this fits into the larger scale hydrography of the region. I show that both clades are brought together and mixed by the large scale horizontal circulation. A somewhat different result from the previous chapter. Both clades appear to be stimulated by small scale local nutrient supply in the study region.

In this section, I present an integrative overview of the findings of my thesis, and tie together the main conceptual strands of the work. I concentrate particularly on discussing those parts of the reseach related to hotspots of phytoplankton diversity and the phytoplankton community structure in western boundary current regions. Finally, I set out some ideas for extending the work in the "Future Directions" section.

6.2 Drivers of Diversity in Western Boundary Current Regions

Although the work in this thesis can be broadly split into a modelling section and an observational section, there are many conceptual links between both parts. Ultimately, these all lead back to the main theme of the thesis, which is to explore the role of ocean physics in

influencing phytoplankton community ecology. I believe that the most compelling results of the thesis research relate to the physical controls on community structure and diversity at western boundary current fronts. Results from my modeling work showed that increased dispersal, resulting from faster current velocities in the higher resolution model, increased levels of phytoplankton diversity across the whole of the model domain. The biggest increases in diversity, however, could not simply be explained by increased dispersal. We identified diversity "hotspots" associated with western boundary currents and coastal upwelling regions. Diversity in these hotspots was due to dispersal and the confluence of different seed populations, but also an enhanced nutrient supply. This work prompts further questions: Are the patterns of diversity in the model results realistic? Do the predicted hotspots of phytoplankton diversity really exist in the oceans? These remain very much open questions, as there are very few observations of phytoplankton diversity to draw from to test the hypotheses generated by the model.

In the second part of the thesis, I present and discuss the biogeochemical and ecological data that I collected across the Kuroshio Front. In essence, this represents a set of data taken from one of the predicted hotspots of phytoplankton diversity. In many respects it is a unique data set, which, when taken together with the physical data also collected during the cruise, gives a very complete view of the physical, chemical, biological and ecological picture of the region during the sampling period. I showed that there are clear links between the hydrography and the phytoplankton community, that some organisms are associated with specific water masses and that there are signatures of small scale mixing between these water masses at the frontal scale. Although the microscopy and flow cytometry data did not give any clear answer to the question of whether or not we were truly observing a diversity hotspot, the qPCR determination of the *Ostreococcus* clades clearly showed that this was a region where both clades of that species were present and appeared, surprisingly, to be thriving. This is at least some indication that we could expect to see a peak in phytoplankton diversity with more targeted sampling also extending further to the north and south of the frontal zone. A few previous studies also support the existence of a diversity hotspot in the

Kuroshio Extension region [Honjo and Okada, 1974] and other frontal zones [Ribalet et al., 2010, Taylor et al., 2012].

Taken together, the simulations and observations presented in Chapters 3 and 5 help to build up a picture of how large scale patterns of dispersal interact with smaller scale vertical dynamics in an energetic western boundary current front to shape the observed community. In my analysis of the distributions of *Ostreococcus* and the observed hydrography, I have been able to show that we are seeing the confluence of two different populations, associated with different water masses. Estimates of the vertical velocities at the front, measurements of turbulent microstructure made by Nagai et al. [2012] clearly suggest the potential for an enhanced nutrient supply to the surface mixed layer. This is supported by my estimates of the nitrate flux divergence along two of the transects sampled. The complex structures in the SST fields of the study region highlight high levels of environmental variability. Thus I can show that all three of the criterion for sustaining hotspots of biodiversity in the model are suported by the observations. Clearly there are limitations in the data set from the Kuroshio Front. I was unable to make estimates of rates of primary production, which could have confirmed whether or not the stations inferred to have higher nutrient fluxes were also supporting higher rates of production. It would also have been helpful to have collected data along longer transects extending further into the subtropical gyre to the south of the front, and the subpolar gyre to the north. This would have yielded useful information on the constituents of the "end-member" populations of phytoplankton, and aided in determining the level of mixing between populations at the front. However, despite these limitations, tantalizing correspondences between the simulations and the observations suggests that this is a topic worthy of further investigation.

6.3 Future Directions

This is an exciting time to study phytoplankton community ecology. Advances in automated sampling devices which can identify picoplankton functional groups by continu-

ous flow cytometry (FlowCytobot, Olson et al. [2003]; CytoSub, Thyssen et al. [2008]; SeaFlow, Swalwell et al. [2011]), microplankton functional groups using imaging (Imaging FlowCytobot, Olson and Sosik [2007]) and individual phenotypes using genomic techniques (Environmental Sample Processor, Scholin et al. [2009]) promise to broaden the field and allow for more targeted studies of particular microbial groups and species. Paired with simultaneous measurements of the physical properties of the water column, these kinds of instruments will make it possible to deepen our understanding of the linkages between phytoplankton ecology and ocean physics. I believe that my work linking targeted genomics with detailed hydrography represents a proof of concept for similar such studies exploring links between ocean dynamics and phytoplankton ecology.

Several questions either remain unanswered, or have been prompted by this work. I discussed in detail the factors that sustain hotspots of phytoplankton diversity in our ecosystem model, but it is certainly not clear whether or not these exist in reality, though my data and that of others suggests it to be the case [e.g Honjo and Okada, 1974]. Is it possible to infer μ_{NET} of either the phytoplankton community or individual functional groups or phenotypes from observations? Previous work using satellite-derived chlorophyll fields and geostrophic velocities has shown that this may be possible at least for phytoplankton biomass as a whole [Jönsson et al., 2010]. This method would not translate directly to shipboard measurements, but work is currently underway to infer phytoplankton growth rates from SeaFlow data [Sosik et al., 2003, Ribalet et al., in prep]. Below, I briefly outline a proposal to explore these questions in more detail using observations across the North Pacific. Data collected during the TARA Oceans expedition may also help answer some of these questions about patterns of phytoplankton diversity [Karsenti et al., 2011]. A more general set of questions, perhaps, relates to ecosystem stability and biodiversity. If ecosystem stability is dependent on biodiversity, is stability affected if the community is dominated by immigrant phenotypes (with negative net growth) or locally-adapted phenotypes (with positive net growth)? If we can get a better grasp on these questions, we may be better equipped to understand how phytoplankton communities will be affected (or not)

by climate change.

6.3.1 Observing Diversity Hotspots

In this thesis and elsewhere, predictions have been made concerning patterns of phytoplankton diversity in the global ocean (e.g. Barton et al. [2010]). There is relatively little data on patterns of phytoplankton diversity in the oceans, and to date, there has not been a study specifically addressing the question of diversity hotspots. As part of a planned post-doctoral research project, I propose to conduct such a study, directly testing the hypothesis that regions of high phytoplankton diversity are associated with highly dynamic regions of the oceans. Recent advances in underway flow cytometry make it possible to measure the abundance and time rate of change of cells and estimate cell division rates and loss rates in situ for some important phytoplankton functional groups (e.g Prochlorococcus, Synechococcus and picoeukaryotes) at high spatial resolution [Swalwell et al., 2011, Ribalet et al., in prep]. In combination with molecular tools to quantify microbial diversity and targeted, higher resolution, sampling of the physical and chemical properties of transition regions, I believe that the modeling work described in Chapter 3 can be used to act as a bridge between theory and observations of phytoplankton ecology in the open ocean. Combining these state-of-the-art observational and modeling tools, it is now possible to start to disentangle the relative contributions of net biological growth and dispersal to the observed standing stocks. Using an integrated approach, in collaboration with members of the Armbrust Lab at the University of Washington, I propose to test the following hypotheses using data already collected with SeaFlow, and by collected new datasets in relevant locations (e.g. Gulf Stream, Kuroshio Extension):

Hypothesis 1: Levels of phytoplankton diversity are elevated in western boundary current regions.

I will analyze existing SeaFlow flow cytometry data collected from transects that cross both frontal and gyre regions (shown as cruise tracks overlain on model-predicted patterns

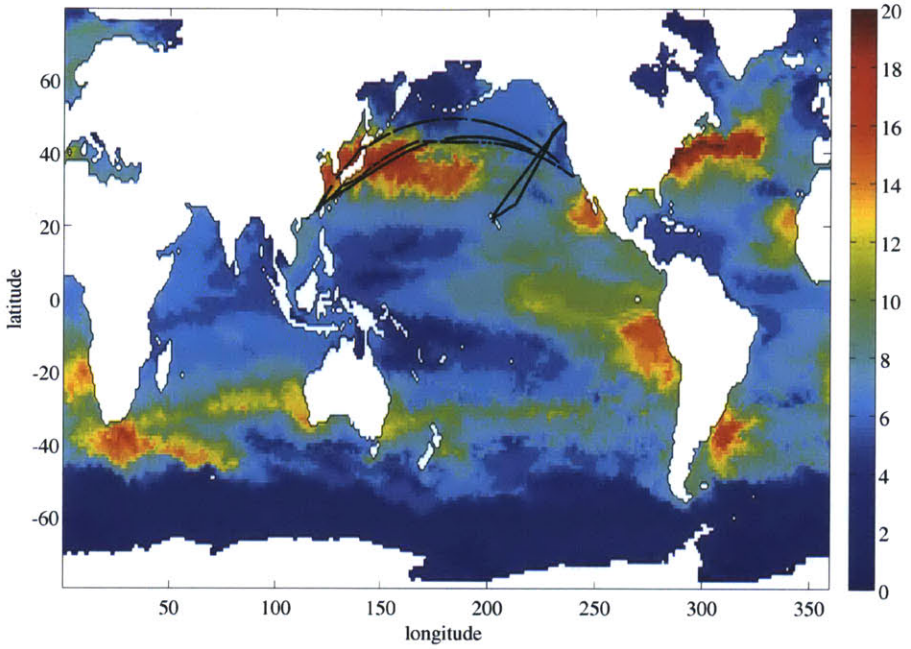

Figure 6-1: Phytoplankton diversity predicted by a global ecosystem model (annual mean). Diversity is defined as the number of modeled phytoplankton types with a biomass exceeding 0.001% of the total phytoplankton biomass in each grid cell. The solid black lines show the cruise tracks for which SeaFlow data is already available.

of diversity in figure 6-1), areas predicted to cut across a diversity hotspot region. Diversity will be determined using both the cytometric diversity index [Li, 1997] and DNA-based identification of species (e.g. 18s rDNA). Using statistical analyses of the phytoplankton community data, I will explore how the hotspot community composition compares to that found either side and upstream/downstream of them, and look for distinct communities within and in the vicinity of the hotspots. Based on my thesis work, I hypothesize that we will find distinct regions of elevated diversity associated with the Kuroshio Front. Using concurrent measurements of environmental parameters (T, S, nutrients, SeaFlow and DNA) I will explore how the biological, chemical and physical components of the system interact to shape the observed patterns of diversity.

Hypothesis 2: There is a shift in the balance between dispersal and net growth controls on diversity as we travel downstream along a front

Following on from the work outlined above, I also plan to explicitly address the role of dispersal in setting patterns of diversity. Using SeaFlow, coupled to a growth rate model, it is now possible to determine the time rate of change of phytoplankton biomass and the gross growth rate of phytoplankton from in situ data [Ribalet et al., in prep]. The sum of grazing and lysis loss terms and the advective and diffusive source/sink of biomass makes up the residual. I plan to work on refining this method to estimate both the losses due to grazing and the physical contribution to the observed cell abundances. I will use complementary shipboard ADCP (where available) and remote sensing data (SSH, derived geostrophic velocities) to provide context on the dynamical environment of the sample regions, as well as identifying source waters for different communities using T/S water mass properties. We predict a shift in the balance between transport and net growth as we travel downstream along a front, and as we move away from the coast in an upwelling zone.

6.4 Closing

Phytoplankton play a crucial role not only in global biogeochemical cycles and climate, but also as the base of the marine food chain. Biodiversity is an important factor in determining the stability and efficiency of the oceanic ecosystem that we rely on for more than just food [Worm et al., 2006]. In this thesis I have shown that physical processes are important not only in controlling levels of primary production and phytoplankton biomass, but also in setting patterns of phytoplankton diversity. Although my modelling work suggests that small scale physical dynamics may not play a role in determining the dominant phenotypes in a given region, they do set rates of species dispersal and, as a result, biodiversity. In some regions, dispersal may in fact be the main driver of diversity (e.g. the subtropical gyres), whereas in others, the local environmental conditions can support high levels of diversity (e.g. coastal upwelling zones), but that in the most diverse regions of the ocean

dispersal and local conditions interact to support a diverse community. In light of these results, I argue that if we are to fully understand what drives patterns of biodiversity in phytoplankton, and how the phytoplankton community may respond to climate change, it is essential to take an integrated approach which combines an appreciation of the physical environment with community ecology.

Bibliography

M. Adjou, J. Bendtsen, and R. K. Modeling the influence from ocean transport, mixing and grazing on phytoplankton diversity. *Ecological Modelling*, 225:19–27, 2012. doi: 10.1016/j.ecolmodel.2011.11.005.

C. M. Aiken and S. A. Navarrete. Environmental fluctuations and asymmetrical dispersal: generalized stability theory for studying metapopulation persistence and marine protected areas. *Marine Ecology Progress Series*, 428:77–88, 2011. doi: 10.3354/meps09079.

C. M. Aiken, S. A. Navarrete, M. I. Castillo, and J. C. Castilla. Along-shore larval dispersal kernels in a numerical ocean model of the central Chilean coast. *Marine Ecology Progress Series*, 339, 13–24 2007.

T. Anderson. Plankton functional type modelling: running before we can walk? *Journal of Plankton Research*, 27(11):1073–1081, 2005.

R. A. Armstrong. Grazing Limitation and Nutrient Limitation in Marine Ecosystems: Steady State Solutions of an Ecosystem Model with Multiple Food Chains. *Limnology & Oceanography*, 39(3):597–608, 1994.

M. E. Baird, P. G. Timko, J. H. Middleton, T. J. Mullaney, D. R. Cox, and I. M. Suthers. Biological Properties across the Tasman Front off southeast Australia. *Deep-Sea Research I*, 55:1438–1455, 2008.

A. D. Barton, S. Dutkiewicz, G. Flierl, J. Bragg, and M. J. Follows. Patterns of diversity in marine phytoplankton. *Science (New York, N.Y.)*, 327(5972):1509–11, Mar. 2010. ISSN 1095-9203. doi: 10.1126/science.1184961.

C. Benitez-Nelson, R. Bidigare, T. Dickey, M. Landry, C. Leonard, S. Brown, F. Nencioli, Y. Rii, K. Maiti, J. Becker, et al. Mesoscale eddies drive increased silica export in the subtropical pacific ocean. *Science*, 316(5827):1017–1021, 2007.

A. Bower and M. S. Lozier. A closer look at particle exchange in the Gulf Stream. *Journal of Physical Oceanography*, 24(6):1399–1418, 1994.

A. S. Bower, H. T. Rossby, and J. L. Lillibridge. Gulf Stream - Barrier or Blender? *Journal of Physical Oceanography*, 15(1):24–32, 1985.

A. Bracco, A. Provenzale, and I. Scheuring. Mesoscale Vortices and the Paradox of the Plankton. *Proceedings of the Royal Society B*, 267(1454):1795–1800, 2000.

S. Brown, M. Landry, K. Selph, E. Jin Yang, Y. Rii, and R. Bidigare. Diatoms in the desert: Plankton community response to a mesoscale eddy in the subtropical north pacific. *Deep Sea Research Part II: Topical Studies in Oceanography*, 55(10):1321–1333, 2008.

M. W. Cadotte. Dispersal and species diversity: a meta-analysis. *The American Naturalist*, 167(6):913–924, 2006.

K. K. Cavender-Bares, D. M. Karl, and S. W. Chisholm. Nutrient gradients in the western North Atlantic Ocean: Relationship to microbial community structure and comparison to patterns in the Pacific Ocean. *Deep-Sea Research I*, 48:2373–2395, 2001.

P. Cermeño and P. G. Falkowski. Controls on diatom biogeography in the ocean. *Science*, 325(5947):1539–1541, 2009. doi: 10.1126/science.1174159.

P. Cermeño, S. Dutkiewicz, R. P. Harris, M. Follows, O. Schofield, and P. Falkowski. The role of nutricline depth in regulating the ocean carbon cycle. *PNAS*, 105(51):20344–20349, 2008. doi: 10.1073/pnas.0811302106.

F. Chai, R. Dugdale, T. Peng, F. Wilkerson, and R. Barber. One-dimensional ecosystem model of the equatorial pacific upwelling system. part i: model development and silicon and nitrogen cycle. *Deep Sea Research Part II: Topical Studies in Oceanography*, 49 (13):2713–2745, 2002.

A. T. Chan. Comparative physiological study of marine diatoms and dinoflagellates in relation to irradiance and cell size. 1. Growth under continuous light. *Journal of Phycology*, 14:396–402, 1978.

M. J. Chrétiennot-Dinet, C. Courties, A. Vaquer, J. Neveux, H. Claustre, J. Lautier, and M. C. Machado. A new marine picoeukaryote: *Ostreococcus tauri* gen et sp. nov. (Chlorophya, Prasinophyceae). *Phycologia*, 34:285–292, 1995.

P. Countway and D. Caron. Abundance and distribution of *Ostreococcus* sp. in the San Pedro Channel, California, as revealed by quantitative PCR. *Applied and environmental microbiology*, 72(4):2496–2506, 2006.

R. K. Cowen, K. M. M. Lwiza, S. Sponaugle, C. B. Paris, and D. B. Olson. Connectivity of marine populations: open or closed? *Science*, 287(5454):857–859, 2000. doi: 10.1126/science.287.5454.857.

R. K. Cowen, C. B. Paris, and A. Srinivasan. Scaling of connectivity in marine populations. *Science*, 311(5760):522–527, 2006.

J. Cullen, P. Franks, D. Karl, and A. Longhurst. Physical influences on marine ecosystem dynamics. *The Sea*, 12:297–336, 2002.

G. Danabasoglu, J. McWilliams, P. Gent, et al. The role of mesoscale tracer transports in the global ocean circulation. *Science-AAAS-Weekly Paper Edition-including Guide to Scientific Information*, 264(5162):1123–1125, 1994.

E. D'Asaro, C. Lee, L. Rainville, R. Harcourt, and L. Thomas. Enhanced turbulence and energy dissipation at ocean fronts. *Science*, 332(6027):318–322, 2011.

E. Demir-Hilton, S. Sudek, M. L. Cuvelier, C. L. Gentemann, J. P. Zehr, and A. Z. Worden. Global distribution patterns of distinct clades of the photosynthetic picoeukaryote *Ostreococcus*. *ISME Journal*, 5:1095–1107, 2011.

T. Dickey. The emergence of concurrent high-resolution physical and bio-optical measurements in the upper ocean and their applications. *Rev. Geophys*, 29(3):383–413, 1991.

T. D. Dickey, F. Nenciolia, V. S. Kuwahara, C. Leonard, W. Black, Y. M. Rii, R. R. Bidigare, and Q. Zhang. Physical and bio-optical observations of oceanic cyclones west of the island of Hawaii. *Deep-Sea Research II*, 55:1195–1217, 2008.

S. Doney. Major challenges confronting marine biogeochemical modeling. *Global Biogeochemical Cycles*, 13(3):705–714, 1999.

F. d'Ovidio, S. De Monte, S. Alvain, Y. Dandonneau, and M. Lévy. Fluid dynamical niches of phytoplankton types. *PNAS*, 109(23):18366 – 18370, 2010. doi: 10.1073/pnas.1004620107.

H. Ducklow. Biogeochemical provinces: towards a JGOFS synthesis. *Ocean Biogeochemistry*, pages 3–17, 2003.

S. Dutkiewicz, M. J. Follows, and J. G. Bragg. Modeling the coupling of ocean ecology and biogeochemistry. *Global Biogeochemical Cycles*, 23, 2009. doi: 10.1029/2008GB003405.

C. S. Ewart, M. K. Meyers, E. Wallner, D. J. McGillicuddy, and C. A. Carlson. Microbial dynamics in cyclonic and anticyclonic mode-water eddies in the northwestern sargasso sea. *Deep-Sea Research II*, 55(10-13):1334–1347, 2008.

P. G. Falkowski. The Role of Photosynthesis in global biogeochemical cycles. *Photosynthesis Research*, 39(3):235–258, 1994.

P. G. Falkowski and J. A. Raven. *Aquatic Photosynthesis*. Princeton University Press, second edition edition, 2007.

P. G. Falkowski, D. Ziemann, Z. Kolber, and P. K. Bienfang. Role of eddy pumping in enhancing primary production in the ocean. 1991.

C. Field, M. Behrenfeld, J. Randerson, and P. Falkowski. Primary production of the biosphere: integrating terrestrial and oceanic components. *Science*, 281(5374):237–240, 1998.

G. Flierl and C. S. Davis. Biological Effects of Gulf Stream Meandering. *Journal of Marine Research*, 51(3):529–560, 1993.

M. Follows and S. Dutkiewicz. Modeling diverse communities of marine microbes. *Annual Review of Marine Science*, 3:427–451, 2011.

M. J. Follows and J. C. Marshall. Eddy driven exchange at ocean fronts. *Ocean Modelling*, 102(5):5–9, 1994.

M. J. Follows, S. Dutkiewicz, S. Grant, and S. W. Chisholm. Emergent Biogeography of Microbial Communities in a Model Ocean. *Science*, 315:1843–1846, 2007.

P. Gent and J. Mcwilliams. Isopycnal mixing in ocean circulation models. *Journal of Physical Oceanography*, 20(1):150–155, 1990.

B. Gilbert. Joint consequences of dispersal and niche overlap on local diversity and resource use. *Journal of Ecology*, 100:287–296, 2012.

W. Gregg, P. Ginoux, P. Schopf, and N. Casey. Phytoplankton and iron: validation of a global three-dimensional ocean biogeochemical model. *Deep Sea Research Part II: Topical Studies in Oceanography*, 50(22):3143–3169, 2003.

L. Guillou, W. Eikrem, M. Chrétiennot-Dinet, F. Le Gall, R. Massana, K. Romari, C. Pedrós-Alió, and D. Vaulot. Diversity of picoplanktonic prasinophytes assessed by direct nuclear SSU rDNA sequencing of environmental samples and novel isolates retrieved from oceanic and coastal marine ecosystems. *Protist*, 155(2):193–214, 2004.

I. Hewson, J. A. Steele, D. G. Capone, and J. A. Fuhrman. Temporal and spatial scales of variation in bacterioplankton assemblages of oligotrophic surface waters. *Marine Ecology Progress Series*, 311:66–77, 2006.

R. D. Holt. Population dynamics in two-patch environments: some anomalous consequences of an optimal habitat distribution. *Theoretical Population Ecology*, 28(2):181–208, 1985.

S. Honjo and H. Okada. Community structure of coccolithophores in the photic layer of the mid-Pacific. *Micropaleontology*, pages 209–230, 1974.

S. B. Hooker, L. Van Heukelem, C. S. Thomas, H. Claustre, J. Ras, R. Barlow, H. Sessions, L. Schluter, J. Perl, C. Trees, V. Stuart, E. Head, L. Clementson, J. Fishwick, C. Llewellyn, and J. Aiken. The Second SeaWiFS HPLC Analysis Round-Robin Experiment (SeaHARRE-2). *NASA Tech Memo 2005-212785*, 2005.

G. Hutchinson. The paradox of the plankton. *The American Naturalist*, (882):137–145, 1961.

J. Ishizaka, H. Kiyosawa, K. Ishida, K. Ishikawa, and M. Takahashi. Meridional distribution and carbon biomass od autotrophic picoplankton in the Central North Pacific Ocean during Late Northern Summer 1990. *Deep-Sea Research I*, 41(11/12):1745–1766, 1994.

S. Jeffrey, R. Mantoura, and W. S, editors. *Phytoplankton Pigments in Oceanography: Guidelines to Modern Methods.* UNESCO, 2005.

Z. Johnson, E. Zinser, A. Coe, N. McNulty, E. Woodward, and S. Chisholm. Niche partitioning among *Prochlorococcus* ecotypes along ocean-scale environmental gradients. *Science*, 311(5768):1737–1740, 2006.

B. Jönsson, J. Salisbury, and A. Mahadevan. Large variability in continental shelf production of phytoplankton carbon revealed by satellite. *Biogeosciences Discussions*, 7(6): 8953–8978, 2010.

H. Kaneko, I. Yasuda, K. Komatsu, and S. Itoh. Observations of the structure of turbulent mixing across the kuroshio. *Geophysical Research Letters*, 39(15):L15602, 2012.

E. Karsenti, S. Acinas, P. Bork, C. Bowler, C. De Vargas, J. Raes, M. Sullivan, D. Arendt, F. Benzoni, J. Claverie, et al. A holistic approach to marine eco-systems biology. *PLoS biology*, 9(10):e1001177, 2011.

T. Kataoka, Y. Hodoki, K. Suzuki, H. Saito, and S. Higashi. Tempo-spatial patterns of bacterial community composition in the western North Pacific Ocean. *Journal of Marine Systems*, 77:197–207, 2009. doi: 10.1016/j.jmarsys.2008.12.006.

H. Kawai and S. I. Saitoh. Secondary fronts, warm tongues and warm streamers of the Kuroshio Extension System. *Deep-Sea Research*, 33:1487–1507, 1986.

P. Kilham and R. E. Hecky. Comparative Ecology of Marine and Freshwater Phytoplankton. *Limnology and Oceanography*, 33(4):776–795, 1988.

P. Klein and G. Lapeyre. The Oceanic Vertical Pump Induced by Mesoscale and Submesoscale Turbulence. *Annual Review of Marine Science*, 1:351–375, 2009.

R. Lande. Statistics and partitioning of species diversity, and similarity among multiple communities. *Oikos*, 76(1):5–13, 1996.

G. Lapeyre and P. Klein. Impact of small-scale elongated filaments on the oceanic vertical pump. *Journal of Marine Research*, 64:835–851, 2006.

W. Large, J. McWilliams, and S. Doney. Oceanic vertical mixing: A review and a model with a nonlocal boundary layer parameterization. *Reviews of Geophysics*, 32(4):363–403, 1994.

S. A. Levin and R. T. Paine. Disturbance, Patch Formation, and Community Structure. *PNAS*, 71(7):2744–2747, 1974.

M. Lévy. The modulation of biological production by oceanic mesoscale turbulence. In *Transport and Mixing in Geophysical Flows*, volume 744, page 219, 2008.

M. Lévy, L. Mémery, and G. Madec. The onset of a bloom after deep winter convection in the northwestern mediterranean sea: mesoscale process study with a primitive equation model. *Journal of marine systems*, 16(1):7–21, 1998.

M. Lévy, P. Klein, and A.-M. Tréguier. Impact of sub-mesoscale physics on production and subduction of phytoplankton in an oligotrophic regime. *Journal of Marine Research*, 59: 535–565, 2001.

M. Lévy, P. Klein, a. M. Tréguier, D. Iovino, G. Madec, S. Masson, and K. Takahashi. Modifications of gyre circulation by sub-mesoscale physics. *Ocean Modelling*, (1-2): 1–15, 2010. ISSN 14635003. doi: 10.1016/j.ocemod.2010.04.001.

W. K. W. Li. Cytometric diversity in marine ultraphytoplankton. *Limnology and Oceanography*, 42(5):874–880, 1997.

W. K. W. Li, P. M. Dickie, and B. D. Irwin. Biomass and production of bacteria and phytoplankton during the spring bloom in the western North Atlantic Ocean. *Deep Sea Research Part II*, 40(1-2):307–327, 1993.

J. L. Lillibridge, G. Hitchcock, T. Rossby, E. Lessard, M. Mork, and L. Golmen. Entrainment and Mixing of Shelf/Slope Waters in the Near-Surface Gulf Stream. *Journal of Geophysical Research*, 95(C8):13065–13087, 1990.

I. D. Lima, D. B. Olson, and S. C. Doney. Biological response to frontal dynamics and mesoscale variability in oligotrophic environments: Biological production and community structure. *Journal of Geophysical Research*, 107(C8), 2002. doi: 10.1029/2000JC000393.

M. Loreau and N. Mouquet. Immigration and the maintenance of local species diversity. *The American Naturalist*, 154(4):427–440, 1999.

R. H. MacArthur and E. O. Wilson. *The Theory of Island Biogeography*. Princeton University Press, 1967.

A. Mahadevan and D. Archer. Modeling the impact of fronts and mesoscale circulation on the nutrient supply and biogeochemistry of the upper ocean. *Journal of Geophysical Research*, 105(C1):1209–1225, 2000.

A. Mahadevan, E. DAsaro, C. Lee, and M. Perry. Eddy-Driven Stratification Initiates North Atlantic Spring Phytoplankton Blooms. *Science*, 337(6090):54–58, 2012.

R. Malmstrom, A. Coe, G. C. Kettler, A. C. Martiny, J. Frias-Lopez, E. R. Zinser, and S. W. Chisholm. Temporal dynamics of *Prochlorococcus* ecotypes in the atlantic and pacific oceans. *ISME J*, 4:1252–1264, 2010. doi: 10.1038/ismej.2010.60.

E. Marañòn, P. M. Holligan, M. Varela, B. Mouriño, and A. J. Bale. Basin-scale variability of phytoplankton biomass, production and growth in the Atlantic Ocean. *Deep Sea Research Part I*, 47(5):825–857, 2000.

R. Margalef. *Perspectives in Ecological Theory*. University of Chicago Press, 1968.

R. Margalef. Life-forms of phytoplankton as survival alternatives in an unstable environment. *Oceanologica Acta*, 1(4), 1978.

J. Marshall, C. Hill, L. Perelman, and A. Adcroft. Hydrostatic, quasi-hydrostatic, and nonhydrostatic ocean modeling. *Journal of Geophysical Research*, 1997.

A. P. Martin, K. J. Richards, A. Bracco, and A. Provenzale. Patchy productivity in the open ocean. *Global Biogeochemical Cycles*, 16(2):9–1–9–9, 2002. ISSN 1944-9224. doi: 10.1029/2001GB001449.

B. Matthiessen and H. Hillebrand. Dispersal frequency affects local biomass production by controlling local diversity. *Ecology Letters*, 9:652–662, 2006.

D. McGillicuddy, R. Johnson, D. Siegel, A. Michaels, N. Bates, and A. Knap. Mesoscale variations of biogeochemical properties in the Sargasso Sea. *Journal of Geophysical Research*, 104(13):381, 1999.

D. McGillicuddy, L. Anderson, S. Doney, and M. Maltrud. Eddy-driven sources and sinks of nutrients in the upper ocean: Results from a 0.1 resolution model of the North Atlantic. *Global Biogeochemical Cycles*, 17(2):1035, 2003.

D. J. McGillicuddy, L. A. Anderson, N. R. Bates, T. Bibby, K. O. Buesseler, C. A. Carlson, C. S. Davis, C. Ewart, P. G. Falkowski, S. A. Goldthwait, D. A. Hansell, W. J. Jenkins, R. Johnson, V. K. Kosnyrev, J. R. Ledwell, Q. P. Li, D. A. Siegel, and D. K. Steinberg. Eddy/wind interactions stimulate extraordinary mid-ocean plankton blooms. *Science*, 316:1021–1026, 2007.

D. Menemenlis, J. Campin, P. Heimbach, C. Hill, T. Lee, A. Nguyen, M. Schodlok, and H. Zhang. ECCO2: High resolution global ocean and sea ice data synthesis. *Mercator Ocean Quarterly Newsletter*, (31):13–21, 2008.

G. Monterey and S. Levitus. Seasonal variability of mixed layer depth for the world ocean. *NOAA Atlas NESDIS 14*, 1997.

T. Nagai, H. Yamazaki, and D. Kamykowski. A lagrangian photoresponse model coupled with 2nd-order turbulence closure. *Marine Ecology Progress Series*, 265:17–30, 2003.

T. Nagai, A. Tandon, H. Yamazaki, and M. J. Doubell. Evidence of enhanced turbulent dissipation in the frontogenetic Kuroshio Front thermocline. *Geophysical Research Letters*, 36, 2009. doi: 10.1029/2009GL038832.

T. Nagai, A. Tandon, H. Yamazaki, M. J. Doubell, and S. Gallagher. Direct observations of microscale turbulence and thermohaline structure in the Kuroshio Front. *Journal of Geophysical Research*, 117(C08013), 2012. doi: 10.1029/2011JC007228.

T. Odate, M. Yanada, L. V. Castillo, and Y. Maita. Distribution of cyanobacteria and other picoplankton in the Western North Pacific Ocean, Summer 1989. *Journal of the Oceanographical Society of Japan*, 46:184–189, 1990.

R. Olson and H. Sosik. A submersible imaging-in-flow instrument to analyze nano-and microplankton: Imaging FlowCytobot. *Limnol. Oceanogr. Methods*, 5:195–203, 2007.

R. Olson, A. Shalapyonok, and H. Sosik. An automated submersible flow cytometer for analyzing pico-and nanophytoplankton: Flowcytobot. *Deep Sea Research Part I: Oceanographic Research Papers*, 50(2):301–315, 2003.

R. J. Olson, S. W. Chisholm, E. R. Zettler, M. A. Altabet, and J. A. Dusenberry. Spatial and temporal distributions of prochlorophyte picoplankton in the north-atlantic ocean. *Deep Sea Research Part A - Oceanographic Research Papers*, 37:1033–1051, 1990a.

R. J. Olson, S. W. Chisholm, E. R. Zettler, and E. V. Armburst. Pigments, size and distribution of *Synechococcus* in the north atlantic and pacific oceans. *Limnology and Oceanography*, 35:45–58, 1990b.

A. Oschlies and V. Garçon. Eddy-induced enhancement of primary production in a model of the north atlantic ocean. *Nature*, 394(6690):266–269, 1998.

A. R. Palmer and R. R. Strathman. Scale of disperal in varying environments and its implications for life histories of marine invertebrates. *Oecologia*, 48:308–318, 1981.

J. L. Pelegri, G. T. Csanady, and A. Martins. The North Atlantic Nutrient Stream. *J. Oceanogr.*, 52:275–299, 1996.

C. Perruche, P. Riviere, G. Lapeure, X. Carton, and P. Pondaven. Effects of surface quasigeostrophic turbulence on phytoplankton competition and co-existence. *Journal of Marine Research*, 69:105–135, 2011.

J. Pinot, J. Tintore, and D. Wang. A study of the omega equation for diagnosing vertical motions at ocean fronts. *Journal of marine research*, 54(2):239–259, 1996.

R. T. Pollard and L. A. Regier. Large variations in potential vorticity at small scales in the upper ocean. *Nature*, 348:227–229, 1990.

L. R. Pomeroy. The oceans food web, a changing paradigm. *Bioscience*, 24:499–504, 1974.

A. E. F. Prowe, M. Pahlow, S. Dutkiewicz, M. Follows, and A. Oschlies. Top-down control of marine phytoplankton diversity in a global ecosystem model. *Progr. Oceanogr.*, 2011. doi: 10.1016/j.pocean.2011.11.016.

A. E. F. Prowe, M. Pahlow, and A. Oschlies. Controls on the diversity-productivity relationship in a marine ecosystem model. *Ecological Modelling*, 225:167–176, 2012.

H. R. Pulliam. Sources, sinks and population regulation. *The American Naturalist*, 132(5): 652–661, 1988.

B. Qiu. *Encyclopedia of Ocean Sciences*, chapter Kuroshio and Oyashio currents, pages 1413–1425. Academic Press, 2001.

C. L. Quéré, S. P. Harrison, I. C. Prentice, E. T. Buitenhuis, O. Aumont, L. Bopp, H. Claustre, L. C. D. Cunha, R. Geider, X. Giraud, C. Klaas, K. E. Kohfeld, L. Legendre, M. Manizza, T. Platt, R. B. Rivkin, S. Sathyendranath, J. Uitz, A. J. Watson, and D. Wolf-Gladrow. Ecosystem dynamics based on plankton functional types for global ocean biogeochemistry models. *Global Change Biology*, 11(11):2016–2040, 2005.

F. Ribalet, A. Marchetti, K. Hubbard, K. Brown, C. Durkin, R. Morales, M. Robert, J. Swalwell, P. Tortell, and E. Armbrust. Unveiling a phytoplankton hotspot at a narrow boundary between coastal and offshore waters. *Proceedings of the National Academy of Sciences*, 107(38):16571–16576, 2010. doi: 10.1073/pnas.1005638107.

F. Ribalet, J. Swalwell, C. Ellis, L. Yanjuan, Z. Johnson, and E. Armbrust. Controls of oceanic phytoplankton abundance revealed through particle size distribution dynamics. in prep.

R. Ricklefs. Community diversity: relative roles of local and regional processes. *Science*, 235:167–171, 1987.

Ring Group. Gulf Stream Cold-Core Rings: their physics, chemistry, and biology. *Science*, 212(4499):1091–1100, 1981.

P. Rivière and P. Pondaven. Phytoplankton size classes competitions at sub-mesoscale in a frontal oceanic region. *Journal of Marine Systems*, 60:345–364, 2006.

F. Rodriguez, E. Derelle, L. Guillou, F. Le Gall, D. Vaulot, and H. Moreau. Ecotype diversity in the marine picoeukaryote *Ostreococcus* (Chlorophyta, Prasinophyceae). *Environmental Microbiology*, 7(6):853–859, 2005.

S. Roy, C. Llewellyn, E. Skarstad Egeland, and G. Johnsen. *Phytoplankton Pigments: Characterization, Chemotaxonomy and Applications in Oceanography*. Cambridge University Press, 2011.

D. L. Rudnick and J. R. Luyten. Intensive surveys of the Azores Front: 1. Tracers and dynamics. *Journal of Geophysical Research*, 101(C1):923–939, 1996.

C. M. Sakamoto. Influence of Rossby waves on nutrient dynamics and the plankton community structure in the North Pacific subtropical gyre, 2004. ISSN 0148-0227.

R. Schlitzer. Ocean Data View. *http://odv.awi.de*, 2012.

C. Scholin, G. Doucette, S. Jensen, B. Roman, D. Pargett, R. Marin III, C. Preston, W. Jones, J. Feldman, C. Everlove, et al. Remote detection of marine microbes, small invertebrates, harmful algae, and biotoxins using the environmental sample processor (esp). *Oceanography*, 22(2):158, 2009.

D. Siegel, D. McGillicuddy Jr, and E. Fields. Mesoscale eddies, satellite altimetry, and new production in the Sargasso Sea. *Journal of Geophysical Research*, 104(C6):13359–13, 1999.

B. Sinha, E. T. Buitenhuis, C. Le Quere, and T. R. Anderson. Comparison of the emergent behaviour of a complex ecosystem model in two ocean general circulation models. *Progress in Oceanography*, 84:204–224, 2010.

C. Six, Z. F. Finkel, F. Rodriguez, D. Marie, F. Partensky, and D. A. Campbell. Contrasting photoacclimation costs in ecotypes of the marine eukaryotic picoplankter *Ostreococcus*. *Limnol. Oceanogr.*, 53(1):255–265, 2008.

H. Sosik, R. Olson, M. Neubert, A. Shalapyonok, and A. Solow. Growth rates of coastal phytoplankton from time-series measurements with a submersible flow cytometer. *Limnology and oceanography*, pages 1756–1765, 2003.

A. Sournia. Pelagic biogeography and fronts. *Progress in Oceanography*, 34:109–120, 1994.

S. Spall and K. Richards. A numerical model of mesoscale frontal instabilities and plankton dynamicsi. model formulation and initial experiments. *Deep Sea Research Part I: Oceanographic Research Papers*, 47(7):1261–1301, 2000.

V. H. Strass, A. C. Naveira Garabato, R. T. Pollard, H. I. Fischer, I. Hense, J. T. Allen, J. F. Read, H. Leach, and V. Smetacek. Mesoscale frontal dynamics: shaping the environment of primary production in the Antarctic Circumpolar Current. *Deep-Sea Research II*, 49: 3735–3769, 2002.

I. N. Sukhanova. *Phytoplankton Manual*, chapter Settling without the inverted microcope. United Nations Educational, Scientific and Cultural Organization, Paris, 1978.

J. Swalwell, F. Ribalet, and E. Armbrust. Seaflow: A novel underway flow-cytometer for continuous observations of phytoplankton in the ocean. *Limnol. Oceanogr. Methods*, 9: 466–477, 2011.

G. A. Tarran, M. V. Zubkov, M. A. Sleigh, P. H. Burkill, and M. Yallop. Microbial community structure and standing stocks in the NE Atlantic in June and July of 1996. *Deep-Sea Research II*, 48:963–985, 2001.

A. G. Taylor, R. Goericke, M. R. Landry, K. E. Selph, D. A. Wick, and M. J. Roadman. Sharp gradients in phytoplankton community structure across a frontal zone in the California Current Ecosystem. *Journal of Plankton Research*, 34(9):778–789, 2012.

L. Thomas and C. Lee. Intensification of ocean fronts by down-front winds. *Journal of Physical Oceanography*, 35(6):1086–1102, 2005.

L. Thomas, A. Tandon, and A. Mahadevan. Submesoscale processes and dynamics. *Ocean Modeling in an Eddying Regime, Geophys. Monogr. Ser*, 177:17–38, 2008.

M. Thyssen, G. Tarran, M. Zubkov, R. Holland, G. Grégori, P. Burkill, and M. Denis. The emergence of automated high-frequency flow cytometry: revealing temporal and spatial phytoplankton variability. *Journal of plankton research*, 30(3):333–343, 2008.

D. Tilman, S. Kilham, and P. Kilham. Phytoplankton community ecology: the role of limiting nutrients. *A.. Rev. Ecol. Syst*, 13:349–372, 1982.

S. Tozzi, O. Schofield, and P. Falkowski. Historical climate change and ocean turbulence as selective agents for two key phytoplankton functional groups. *Marine Ecology Progress Series*, 274:123–132, 2004.

P. Vanormelingen, K. Cottenie, M. E, K. Muylaert, W. Vyverman, and L. De Meester. The relative importance of dispersal and local processes in structuring phytoplankton communities in a set of highly interconnected ponds. *Freshwater Biology*, 53:2170–2183, 2008. doi: 10.111/j.1365-2427.2008.02040.x.

J. A. Veech, K. S. Summerville, T. O. Crist, and J. C. Gering. The additive partitioning of species diversity: recent revival of an old idea. *Oikos*, 99:3–9, 2002.

B. A. Ward, S. Dutkiewicz, O. Jahn, and M. J. Follows. A size-structured food-web model for the global ocean. *Limnology and Oceanography*, 57(6):1877, 2012.

P. Wiebe, E. Hulburt, E. Carpenter, A. E Jahn, G. Knapp, S. Boyd, P. Ortner, and J. Cox. Gulf stream cold core rings: large-scale interaction sites for open ocean plankton communities. In *Deep Sea Research and Oceanographic Abstracts*, volume 23, pages 695–710. Elsevier, 1976.

R. Williams and M. Follows. *Ocean Dynamics and the Carbon Cycle: Principles and Mechanisms*. Cambridge University Press, 2011.

R. G. Williams, V. Roussenov, and M. J. Follows. Nutrient streams and their induction into the mixed layer. *Global Biogeochemical Cycles*, (1):1–18, 2006. ISSN 0886-6236. doi: 10.1029/2005GB002586.

A. Worden and F. Not. Ecology and diversity of picoeukaryotes. *Microbial Ecology of the Oceans, Second Edition*, pages 159–205, 2008.

A. Worden, J. Lee, T. Mock, P. Rouzé, M. Simmons, A. Aerts, A. Allen, M. Cuvelier, E. Derelle, M. Everett, et al. Green evolution and dynamic adaptations revealed by genomes of the marine picoeukaryotes micromonas. *Science*, 324(5924):268–272, 2009.

A. Z. Worden. Picoeukaryote diversity in coastal waters of the Pacific Ocean. *Aquatic Microbial Ecology*, pages 165–175, 2006. ISSN 0948-3055. doi: 10.3354/ame043165.

A. Z. Worden, J. K. Nolan, and B. Palenik. Assessing the dynamics and ecology of marine picophytoplankton: The importance of the eukaryotic component. *Limnol. Oceanogr.*, 49(1):168–179, 2004.

B. Worm, E. Barbier, N. Beaumont, J. Duffy, C. Folke, B. Halpern, J. Jackson, H. Lotze, F. Micheli, S. Palumbi, et al. Impacts of biodiversity loss on ocean ecosystem services. *science*, 314(5800):787–790, 2006.

C. Wunsch and P. Heimbach. Practical global oceanic state estimation. *Physica D*, 230: 197–208, 2007.

T. Yamamoto, A. Taniguchi, and S. Nishizawa. Microplankton distribution at an oceanic front formed in the Sanriku Waters off Northeast Japan. *Bulletin of Plankton Society of Japan*, 28(2):111–120, 1981.

T. Yamamoto, S. Nishizawa, and T. Taniguchi. Formation and retention mechanisms of phytoplankton peak abundance at the Kuroshio front. *Journal of Plankton Research*, 10 (6):1113–1130, 1988.

H. Yamazaki, I. Iwamatsu, D. Hasegawa, and T. Nagai. Chlorophyll Patches Observed during Summer in the Main Stream of the Kuroshio. *Atmosphere-Ocean*, 47(4):299–307, 2009. doi: 10.3137/OC306.2009.

J. A. Yoder, S. G. Ackleson, R. Barber, P. Flament, and W. M. Balch. A line in the sea. *Nature*, 371:689–692, 1994.

F. Zhu, R. Massana, F. Not, D. Marie, and D. Vaulot. Mapping of picoeucaryotes in marine ecosystems with quantitative PCR of the 18S rRNA gene. *FEMS Microbiology Ecology*, 52(1):79–92, 2006.

V. Zhurbas and I. Sang Oh. Lateral diffusivity and Lagrangian scales in the Pacific Ocean as derived from drifter data. *Journal of Geophysical Research*, 108(C5), 2003. doi: 10.1029/2002JC001596.